Mechanochromic Fluorescent Probe Molecules for Damage Detection in Aerospace Polymers and Composites

Ryan E Toivola

A dissertation submitted in partial fulfillment of the requirements for the degree of

Doctor of Philosophy

University of Washington

2013

Reading Committee:

Brian Flinn, Chair

Alex Jen

Christine Luscombe

Program Authorized to Offer Degree:

Materials Science & Engineering

University of Washington

Abstract

Mechanochromic Fluorescent Probe Molecules for Damage Detection in Aerospace Polymers and Composites

Ryan E Toivola

Chair of the Supervisory Committee:
Dr. Brian Flinn
Materials Science & Engineering

The detection of damage in aerospace composites can be improved by incorporation of mechanochromic fluorescent probe molecules into the polymers used in composite parts. This study focuses on a novel series of mechanochromic probes, AJNDE15 and AJNDE17, which are incorporated in structural epoxy resin DGEBA-DETA.

Chapter 1 details the characterization of the DGEBA-DETA epoxy system used in this study. The important characteristics of DGEBA-DETA's response to mechanical loading will be discussed within the larger field of glassy amorphous polymer deformation. The mechanical,

thermal, and chemical properties of DGEBA-DETA relevant to this work will be measured using standardized techniques and instrumentation.

Chapters 2 and 3 focus on the mechanochromic probes AJNDE15 and AJNDE17 in the DGEBA-DETA system. Chapter 2 presents research designed to identify the mechanism through which the probes display mechanochromism. The possible mechanochromic mechanisms are introduced in a literature review. Research on these probes in DGEBA-DETA will be presented and discussed with respect to the possible mechanisms, and the mechanism that best fits the results will be identified as a mechanochemical reaction.

Chapter 3 continues the analysis of the mechanochromism of the probes in DGEBA-DETA. The kinetics of the mechanochromic reaction will be studied and compared with the current understanding of glassy polymer deformation. Possible models for the molecular interactions responsible for mechanochromism in this system will be put forward. Research will be presented to evaluate the mechanochromism kinetics and for comparison with the behavior predicted by the models.

TABLE OF CONTENTS

INTRODUCTION

In this section, the motivation for the current study is introduced – detection of barely visible impact damage in aerospace polymers and composites using mechanochromic fluorescent probes. Impact damage in polymers and composites will be introduced, fluorescence imaging and sensing techniques in polymers and polymer composites will be presented, and a short review of relevant fluorescence mechanics will be shown. The research approach presented in this study will be outlined as well.

1. BARELY VISIBLE IMPACT DAMAGE IN POLYMER COMPOSITES

Composite materials have found widespread use in the aerospace and commercial aircraft industry because of their many advantages in stiffness, strength, and weight when compared to metals. One area in which composite parts do not perform as well as monolithic metal structures, however, is in impact damage resistance and detection. Low-energy or low-velocity impact events in metal parts are generally considered not serious because any impact that causes significant damage will form a dent on the part surface, and will be easily detected in visual inspection. In composite parts, however, impact events can cause sub-surface damage and delaminations, which can reduce part performance, especially compressive strength (1; 2; 3). The damaged sub-surface areas are often much larger than the impacted surface area. To further complicate matters, impact events - especially low-velocity impacts such as collisions with ground vehicles or runway debris on takeoff or landing - do not always leave an easily visible mark on the surface of a composite part. Such impact events and the damage they cause are termed Barely Visible Impact Damage (BVID) (2; 4). Because BVID is so difficult to detect in composites, current industry practice allows BVID to exist on in-service parts and accounts for

its mechanical property degradation in safety factor calculations. As a result, many structural parts are heavier than strictly required, making them less fuel-efficient. A method for rapidly finding, assessing, and repairing BVID would reduce the required margins of safety and correspondingly save weight and fuel.

1.1 Ultrasonic NDE methods

Of the currently available NDE methods, those using ultrasonics have enjoyed the most success in analyzing composite structures (5). These test methods involve propagating mechanical waves through the part to be tested. The waves displace particles of the material as they travel through the medium, with typical wave characteristics like amplitude, frequency, and propagation velocity. Polymer composites as a wave propagating medium are highly complex, being generally heterogeneous, anisotropic, and found in thin-plate geometries. The most useful practice for composite has been to restrict wave frequencies to the point where the material can be treated as homogeneous.

To explore polymer composite material properties a standard technique is to use a transducer to send an ultrasonic wave pulse through the thickness of the composite part. Test methods are defined by how the signal is detected – if a transducer opposite the sending transducer on the opposite side of the part is used, this is called through-thickness transmission or "pitch-catch." If the first transducer also receives the signal, this is called the "pulse-echo" method (5; 6).

These techniques have had success measuring part thickness (6), void content (7), various anisotropic moduli (8), and in the identification of delaminations and disbonding in polymer composite structures (6; 9; 10). The most successful technique is called C-scanning, which plots the amplitude of returning pulses against position in the part. Signal scattering is very high in

regions of damage, resulting in a high contrast in pulse amplitude. Figure 1 shows an example of ultrasonic C-scanning detecting a simulated delamination (1; 10).

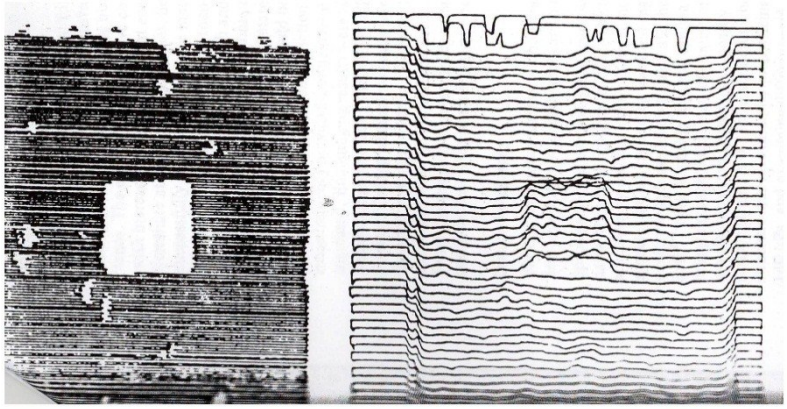

Figure 1: Ultrasonic C-scan of delamination damage. From (10).

Ultrasonic C-scanning can detect delaminations and disbonds quite effectively, but it has some serious drawbacks. The test is time consuming and not suitable for routine inspections of very large parts. In addition, ultrasonic scanning detects density changes and therefore has difficulty finding microcracks in the resin and 'kiss-bonds' (where two bonded surfaces are in intimate contact but for some reason the bond between them is weaker than expected). Another drawback of ultrasonic C-scanning is its lack of in-service part inspection capability. Investigation of used or damaged parts usually requires removal of the part from the structure. Part removal incorporates more significant downtime losses into any structure, and may not even be feasible as more complex part geometries and bonding strategies are developed.

1.2 Project motivation and organization

The motivation for this research project is to contribute to the development of a complementary technique to the accurate but time-consuming ultrasonic C-scan technique - a method for fast, accurate BVID detection that can be performed during routine aircraft service. Such a method

could both quickly establish whether a more extensive inspection is necessary, and guide such inspection efforts when they do occur. The ability to consistently, accurately, and in a timely fashion detect and diagnose BVID could mean that part designers would not have to account for its presence, leading to significant weight savings in future designs.

The approach to this problem is to functionalize the coatings, topcoats, and resins that are already applied to the surface of the aircraft. Composite aircraft parts have a structural reinforced epoxy matrix, which is then sprayed with a compatible primer, painted with the airline logo, and sprayed with a protective topcoat. Coatings, primers, and resins that can change in some optically detectable manner due to the stress or deformation caused by BVID would be very useful. Currently, fluorescent molecules have been discovered or designed whose fluorescent behaviors change in response to external stimuli such as stress or deformation; we have chosen to attempt to incorporate these dyes into existing aircraft polymers to create a fluorescent sensor or "witness" coating or resin for BVID detection.

This report discusses research conducted as part of a project funded by the Boeing Company #BL8DL, which is a collaborative effort between the Boeing Company, the Flinn research group in the Materials Science & Engineering Department at the University of Washington, and the Jen research group in the Materials Science & Engineering and Chemistry Departments at the University of Washington. The Jen group is responsible for design, synthesis, and characterization of probe molecules. The Flinn group is responsible for incorporation of probe molecules into aerospace polymers, fabrication and testing of test specimens, and characterization of probe responses to various external conditions.

2. FLUORESCENCE, MECHANOCHROMISM AND RATIOMETRY

In this section a brief introduction to fluorescent probe molecules and their use as sensors in solid polymeric materials will be outlined. Specific attention will be paid to a specific type of probe sensor system called ratiometry and the probe features necessary for its use, and to mechanochromic probes, which are sensitive to mechanical force, deformation, or damage.

2.1 Fluorescence

Fluorescence is an energy transfer mechanism in which a molecule absorbs a photon of some energy level and, after some internal energy conversions, emits a photon of lower energy. The wavelengths at which absorption and emission occur, and the efficiency of the absorption and emission events, are determined by the molecule's energy gap and charge transfer characteristics. Both of these are in turn affected by the molecule's local environment.

When a photon of energy $E = h\upsilon$ is incident upon a molecule in its ground energy state S_0, if the molecule has an appropriate energy distribution, the molecule can absorb the photon and be promoted to a higher energy state S_2. This state is energetically unstable, and a number of energy releasing transitions take place rapidly. The molecule often decays via thermal or electronic rearrangements to some intermediate energy state S_1, from which the molecule can emit a photon of (typically) lower energy than the one it absorbed, a process summarized in Eqn. 1 (11).

$$S_0 + h\upsilon_2 \rightarrow S_2 \rightarrow S_1 \rightarrow h\upsilon_1 + S_0 \qquad \mathbf{1}$$

This emission is called photoluminescence. There are several types of photoluminescence – the one this work will focus on is fluorescence. A Jablonski energy diagram showing these transitions is presented in Figure 2 (12).

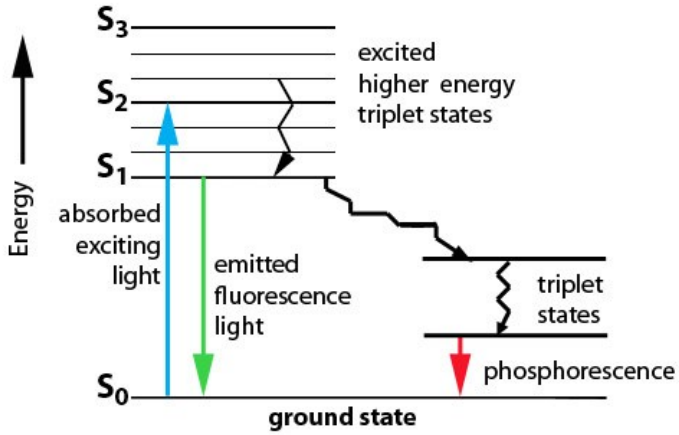

Figure 2: Jablonski Diagram of Photon Absorption and Fluorescent Emission. From (12).

While in the excited state S_1 the molecule can also interact with other molecules in various ways. Two well-documented mechanisms are Forster and Dexter energy transfer methods (13). In Forster energy transfer, the absorbing molecule develops a dipole moment which can induce an opposite dipole in a nearby molecule. This transition can take place when the distance between molecules is up to 10nm. Dexter energy transfer occurs when the excited molecule collides with another molecule. The overlapping molecular orbitals allow transfer of energy between the two. This method requires a much closer distance between the two molecules – one nanometer or less.

2.2 Fluorescent ratiometric probes

The concept of using fluorescent molecules as sensors is quite widespread, having applications in biology and environmental science among many other fields. It is relevant to this study that fluorescent probe molecules have been used quite often in the last 20 years to investigate a

variety of properties of solid polymers. Researchers have identified or designed molecules whose fluorescent behavior is sensitive to temperature (14), pressure (15), and pH level (16) in solid polymers. Reference (17) is an excellent review of this work before 1990, while reference (18) is an updated review from 2010. The fundamental technique involves a fluorescent probe molecule which emits differently under different local conditions within the solid polymer matrix.

Simple fluorescent sensors are quite useful for detecting the presence or absence of a quenching environmental condition by turning 'ON' or 'OFF', but it is often not possible to gather quantitative information from this type of sensor. Fluorescence intensity measurements can depend on factors like local probe concentration, testing geometry, and excitation light source strength as well as the environmental condition of interest. These other factors often make probe fluorescence intensity an unreliable quantitative measurement for the environmental condition, as the change cannot be made a monotonic, one-to-one function of the environmental condition alone. To combat these problems, fluorescent sensors called ratiometric probes have been developed which can quantitatively measure the change in an environmental condition. The shift in a probe's maximum fluorescent emission wavelength or change in emission intensity due to an environmental condition can be compared with some other feature which is independent of the environmental condition of interest. If both emission features vary identically with changes in concentration or testing procedure, then the ratio is independent of these variables and can often produce a monotonic, one-to-one curve with the changes in theenvironmental condition of interest.

Ratiometric probes have been used for many years to sense pH and the presence or absence of various quenching species. One such probe, Indo-1, has become widely used in flow cytometry as an indicator of the presence of calcium (19). In an environment free of calcium, Indo-1's emission spectrum has a maximum at ~485nm. A calcium ion can bind to an Indo-1 molecule, changing the maximum fluorescence emission of that molecule to ~400nm. Increasing calcium concentration causes more molecules to be bound and increased emission at 400nm. Figure 3 shows the changing emission spectrum of Indo-1 fluorescent emission due to 338nm excitation as calcium concentration increases (20).

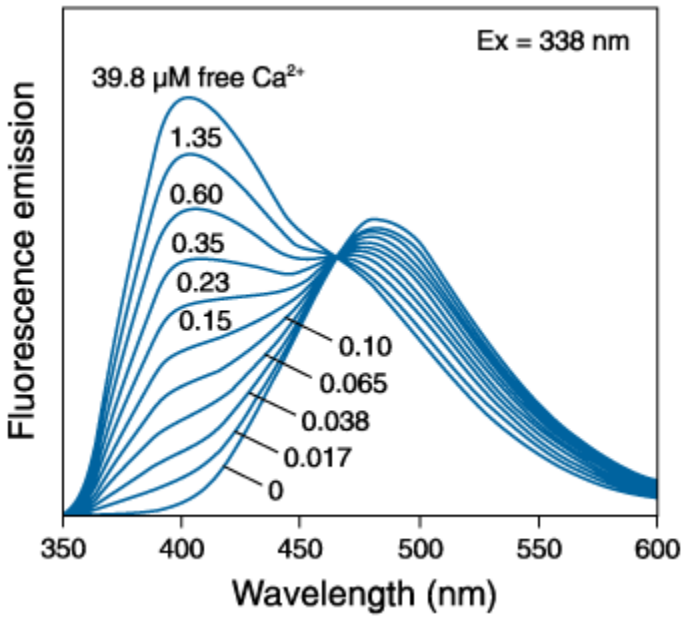

Figure 3: Spectra of Indo-1 calcium indicator probe molecule in solutions with varying calcium concentration. From (20).

The ratio of 485nm emission to 400nm emission can be used to develop calibration curves which allow extremely accurate quantification of the concentration of calcium in a liquid solution.

A more specific subset of ratiometric probe molecules is the dual-emission ratiometric probe. In these probes, two emitting species are present, one or both of which are sensitive to the quantity

to be sensed. Sensors of this type have been developed to determine pH and detect the concentration of tryptophan and DNA proteins. These sensors generally display one of two mechanisms – either a reaction takes place where one fluorescent species changes to another fluorescent species due to the presence of the sensing quantity (Indo-1 is an example), or one species' fluorescence is increasingly quenched by the presence of the sensing quantity while another species' fluorescence is unchanged. In these probes, the ratio of the emission intensities of the two fluorescent species is widely used as the sensing variable for the desired quantity.

An example of the reaction type dual emission ratiometric probe is PYMPON, a pH probe developed to detect the pH of a solution. A protonation reaction at a pyridine ring on the

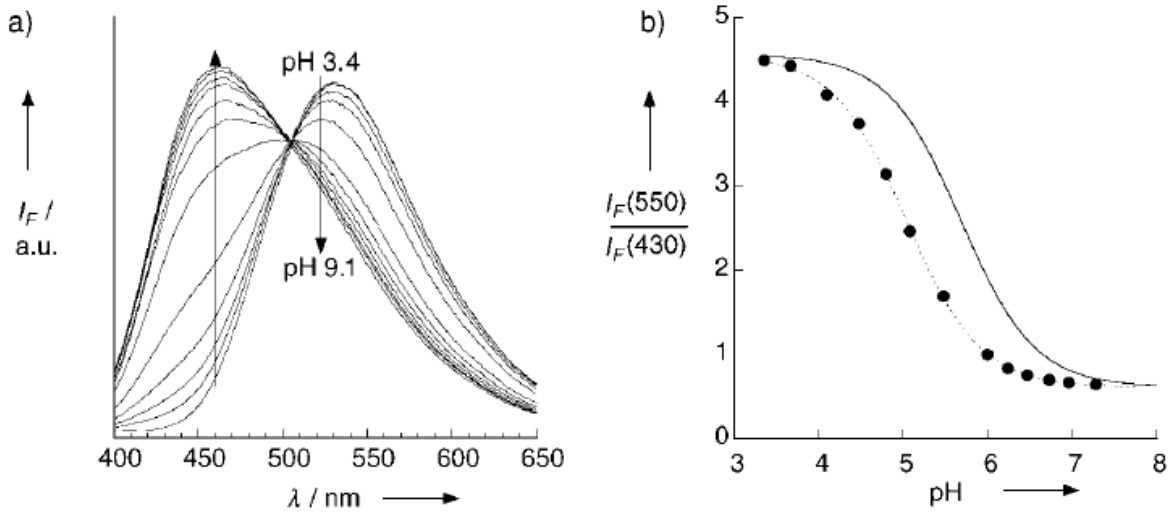

Figure 4: Ratiometric pH probe PYMPON behavior with increasing pH - a) emission spectra and b) ratio of emission peaks. From (21).

molecule causes a shift from a species emitting at 550nm to one at 430nm as pH increases. The ratio of 550nm to 430nm emission changes monotonically and one-to-one with pH, making PYMPON a useful pH sensor. Figure 4a shows the spectral change of PYMPON as pH increases, while Figure 4b shows the change in the ratios of the two peaks as pH increases (21).

An example of the quenching-type dual-emission ratiometric probe has been developed by Zhu et.al. which combines graphene oxide with CdTe quantum dots to produce a ratiometric probe sensitive to iron concentrations. The presense of iron has little effect on the fluorescence of graphene oxide, but is a strong quencher for CdTe quantum dot fluorescence. The combination of these two effects creates a very sensitive ratiometric system which uses the ratio of the fluorescent emission of the two species as a measurement of Fe^{2+}/Fe^{3+} concentration. Figure 5 shows the change in emission spectra of the hybrid probe, with the ratio of the probe emission intensities in the inset (22).

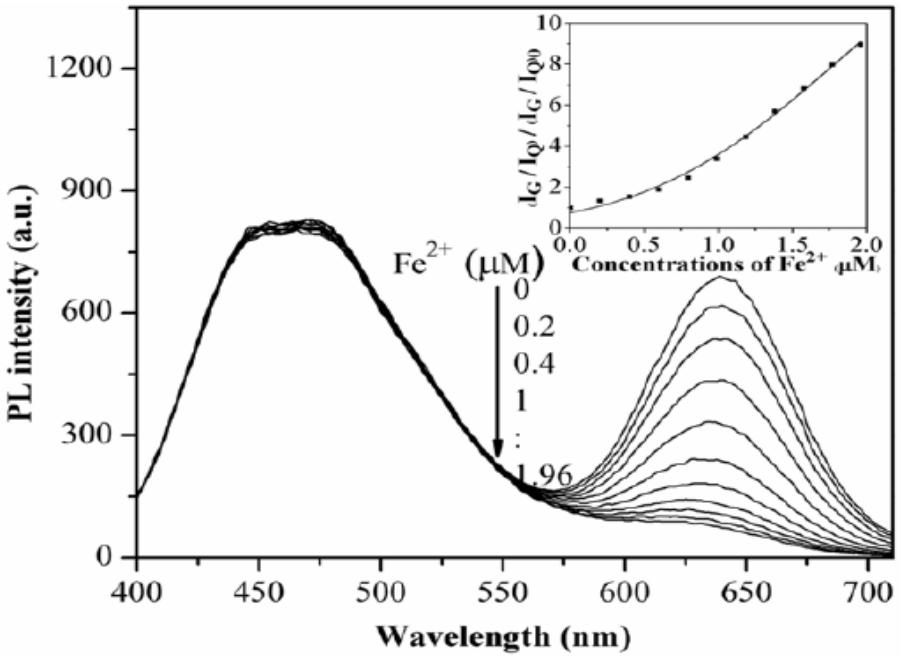

Figure 5: Graphene oxide-quantum dot hybrid dual emission ratiometric probe emission with increasing Fe concentration. inset - ratio of emission intensities. From (22).

In dual emission ratiometric probes, a measurement of the quantity to be sensed is often calibrated using the ratio of the two emission peak intensities. A plot of this intensity ratio, as in Figure 4b and the inset of Figure 5, is called a modified Stern-Volmer plot. The quantity plotted

is often the ratio of the peak intensities normalized by the ratio when no quencher is present. With quantities gathered into a simple arrangement, the modified Stern Volmer relationship is

$$\frac{I_0^a I^b}{I^a I_0^b} - 1 = k_q * \tau_0 * [Q] \quad \textbf{2}$$

Where I_0s are the initial intensities of fluorescent species *a* and *b*, Is are the intensities at a given quencher concentration, k_q is the Stern-Volmer quenching coefficient, τ_0 is the fluorescent lifetime, and [Q] is the concentration of quenching species (23).

2.3 Fluorescent mechanochromic probes

Mechanochromism is a term that defines a color change in a material due to mechanical grinding, crushing, milling, pressure, or sonification (24). In this study the term will be used to describe a change in fluorescent behavior of a probe molecule – that is, a change in the absorbance, excitation or emission of light by a probe in response to mechanical stimulus. Mechanochromism in polymers is a phenomenon that has been identified and studied only relatively recently; the first papers discussing mechanochromism in poly(diacetylene) and poly(3-alkylthiophene) began appearing in the late 1980s (25; 26). Current research has identified polymer systems with intrinsic mechanochromic behavior as well as polymers with mechanochromic probe molecules incorporated in a variety of ways. Chapter 2 will present a more in-depth review of mechanochromic polymer systems.

3. RESEARCH PLAN

The overall project's goals are to develop a system of aerospace resins and coatings suitable for detecting mechanical and thermal damage to aerospace composite parts.

The project has recently developed a series of probe molecules that show mechanochromic response to deformation in a solid epoxy polymer system. Two of these probes, labeled AJNDE15 and AJNDE17, will be studied extensively in this research study. The goal of this particular research is to understand fully the behavior of these probe molecules in the epoxy system. Specifically, this dissertation will present efforts to identify the activation mechanism for the probe mechanochromic response; quantify the kinetics of the mechanochromism; and put forward a model for the molecular interactions that govern the probes' mechanochromic response.

3.1 Document organization

The preceding sections have introduced the project motivation – improving the detection capability of damage in aerospace composites; the approach – functionalize aerospace polymers with mechanochromic fluorescent probe molecules; and the goals of this dissertation – to understand the mechanochromic response of probe molecules AJNDE15 and AJNDE17 in epoxy.

The rest of the document will be organized into 3 chapters. Chapter 1 will present the epoxy system in which mechanochromism will be studied, and show relevant research describing the characterization of this system. Chapter 2 will discuss the mechanisms by which mechanochromism could occur, and present research that attempts to identify the mechanism by which AJNDE15 and AJNDE17 display mechanochromism. Chapter 3 will present research into the kinetics of the mechanochromic response, and discuss possible models to explain the molecular interactions responsible for the mechanochromism.

CHAPTER 1

CHARACTERIZATION OF EPOXY POLYMER SYSTEM

1. INTRODUCTION

In this section the epoxy and curing agent used to produce the structural matrix in this research will be identified and discussed. The relevant mechanical, optical, and thermal properties will be presented, as well as the responses these properties display in relation to the variables most important to this study.

1.1 Epoxy and curing agent

1.1.1 Epoxy - DGEBA

The epoxy used for this study is Di-Glycidyl Ether of Bisphenol-A (DGEBA), a basic epoxide that is often used as a model epoxy system. DGEBA has 2 reactive epoxide sites and few opportunities for competing reactions available along its main chain. The main chain's benzene rings add stiffness to the network structure, improving its mechanical properties. Figure 6 has a

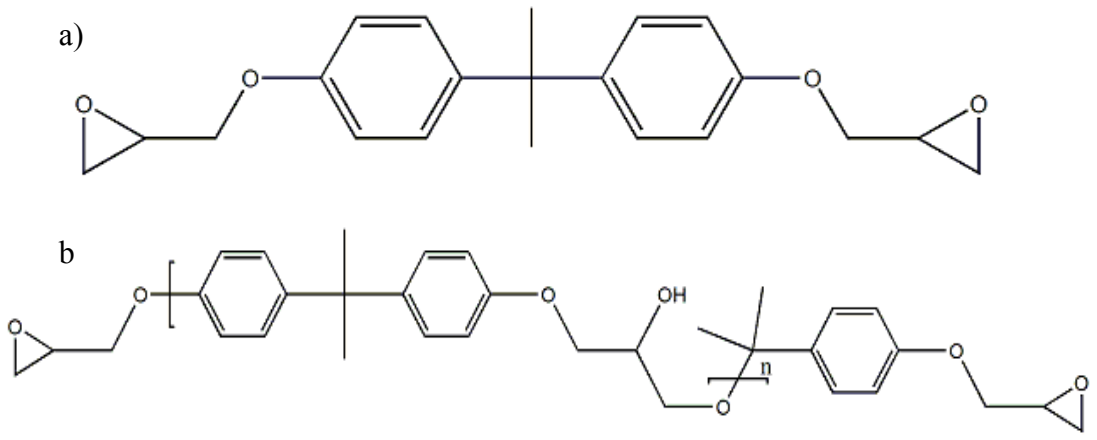

Figure 6: a) DGEBA molecule, ideal structure. b) DGEBA commercial structure.

chemical diagram of the DGEBA structure, while Table 1 gives its relevant properties.

For this study, the DGEBA used comes from two sources - Epon 828 (Shell Chemical Co., local distributor Miller-Stephenson) and DER 330 (Dow Chemical Co.). In commercial form, DGEBA has some impurities that are shown as repeat units in Figure 6b.

Table 1: DGEBA Properties.

Molecular weight, ideal (g/mol)	340
EEW*, ideal (g/mol)	170
Molecular weight, commercial (g/mol)	354-384
EEW*, commercial (g/mol)	177-192
Viscosity, cps (25 deg C)	11000 – 15000
Density, g/c.c. **	1.2-1.3

* = epoxide equivalent weight. **=approx. amine-cured properties.

1.1.2 Curing agent - DETA

Diethylene Triamine (DETA) is a commonly used curing agent for epoxides. It has 5 amino hydrogens, 4 primary and 1 secondary, available to form bonds with epoxide groups. DETA's chemical structure is shown in Figure 7, with relevant properties given in Table 2.

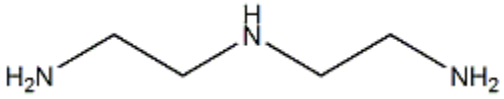

Figure 7: DETA chemical structure.

For this study, the DETA used is Epikure 3223 (Shell Chemical Co., local dist. Miller-Stephenson). It is used as received.

Table 2: DETA properties.

Molecular weight (g/mol)	103.5
Wt. per amino H (g/mol)	20.7
Viscosity, cps (20 deg C)	10
Density, g/cc	0.95

1.2 Curing of DGEBA-DETA

There are four main curing reactions for epoxide-amine polymerization. The first is a ring-opening reaction in which the epoxide reacts with a primary amino hydrogen to form a partially crosslinked site with a secondary amine still available for bonding, and an –OH group. The epoxide can also react with a secondary amino hydrogen to form a fully crosslinked site with two hydroxyl groups remaining. A third reaction is the etherification reaction of epoxide and –OH groups. This reaction is less desirable because the crosslink site is not as rigid with only two bonds; etherification generally occurs only at high temperature and can be avoided with careful cure control. The fourth reaction, epoxide homopolymerization, is also undesirable because it produces a less than ideal crosslink site. Homopolymerization also requires high temperatures and an excess of epoxides, and can be avoided with care. Figure 8 summarizes these reactions.

The cure reaction of epoxy is highly exothermic and forms a 3-dimensional network of crosslink sites. The reaction proceeds rapidly until a gelation point when the network becomes rigid enough that unreacted epoxides and amino hydrogens can no longer easily reach one another. At this point, the glass transition temperature of the bulk sample is set. Curing after this point is controlled by diffusion and is much slower than the rapid autocatalytic reaction before the

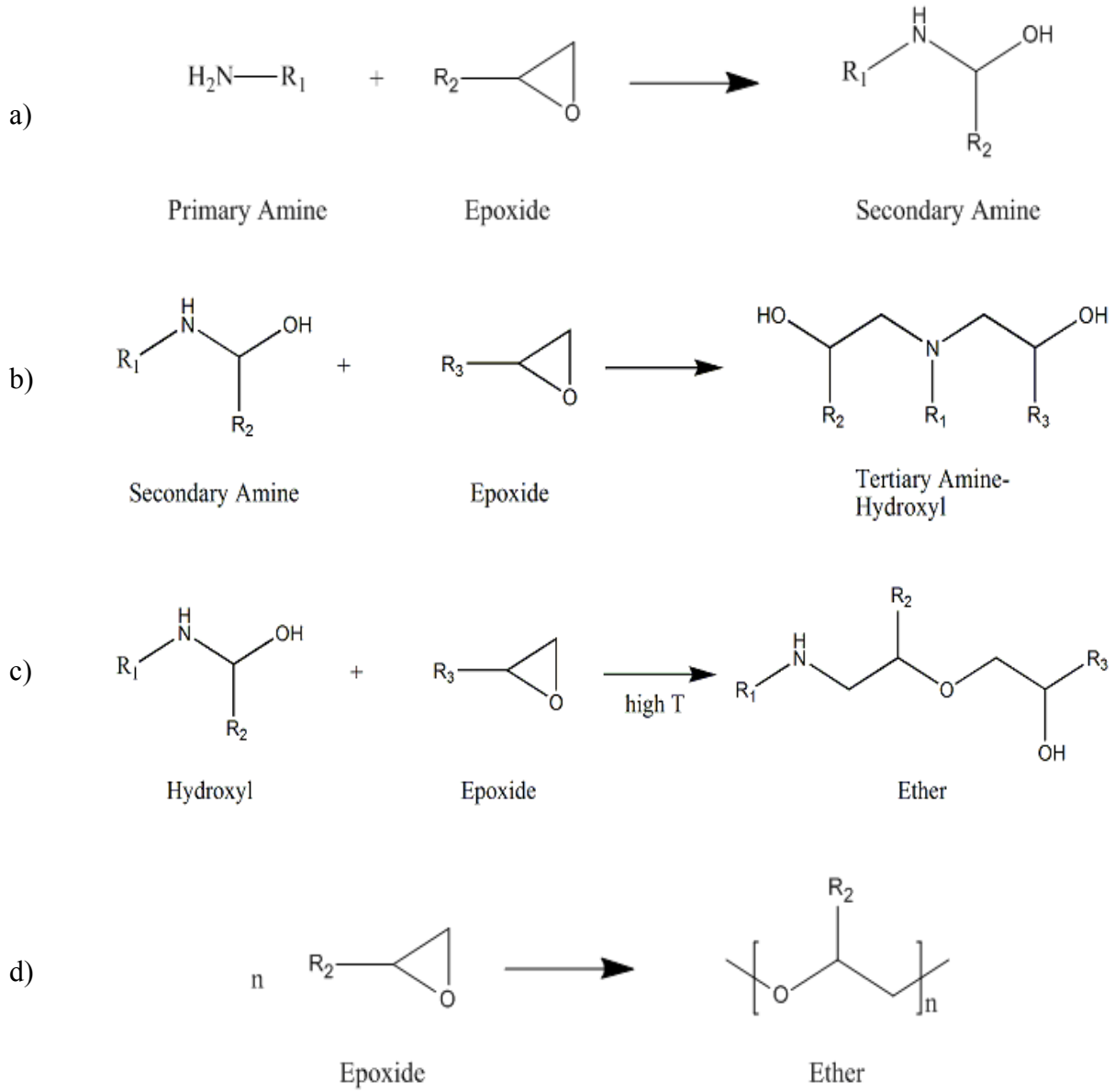

Figure 8: Reactions involved in curing of epoxy with amines. a)primary amine with epoxide. b) secondary amine with epoxide. c) etherification. d) homopolymerization.

gelation point. Samples may or may not be fully cured when this T_g is developed; in fact, T_g is very often lower than $T_{g\infty}$, the ultimate glass transition temperature reached when an epoxy network is completely cured.

1.3 Room temperature cured DGEBA-DETA

DGEBA-DETA can be cured at a wide range of temperatures, with corresponding variation in network structure and cure extent. For this study we have cured DGEBA-DETA at room temperature to avoid potential temperature related complications with mechanochromic probe molecules. The cure takes 24 hours. At room temperature DGEBA-DETA does not reach its full cure extent; that is, every epoxide molecule is not reacted with an available amino hydrogen site. Because of this, the glass transition of RT DGEBA-DETA is much lower than the ultimate glass transition. There is also a significant percentage of crosslinks that are not completely fulfilled. This has ramifications which will be discussed as they become relevant.

In an effort to learn more about the behavior of the mechanochromic probes in DGEBA-DETA this project initially studies the change in response of the probes to changes in the bulk epoxy. The most important of these for the overall project goal is the probe response to mechanical deformation. We will use fluorescent measurements to evaluate our probe molecules. To properly attribute changes in the fluorescent spectra we measure to probe behavior, we must first understand the mechanical behavior of DGEBA-DETA itself. This will be reviewed in section 1.4. The optical properties of DGEBA-DETA, and any changes due to mechanical deformation, will be quantified to help us properly attribute changes in fluorescence to probe behavior.

To understand the fundamental mechanism by which our probes activate, however, more information must be gathered. Two other conditions that are easily applied that can contribute a

great deal of information are the temperature exposure after curing and the stoichiometry of the pre-cured mixture. The amine-to-epoxide ratio χ is a simple variable to change that can cause a wide range of different thermal properties in the bulk polymer. Temperature exposure can cause increased curing and can enhance molecular chain motion, as well as any reaction kinetics that are temperature-dependent. More details on these will be presented as they become relevant.

1.4 Mechanical deformation of epoxy polymers

In this section a review of the mechanical properties of epoxy that are relevant to this study will be presented. Discussion will focus on the stress-strain behavior of epoxy in the glassy state, which is the most important temperature region for the application.

Researchers have studied the response of epoxy polymers to mechanical deformation in great detail since the 1950s. Their mechanical behavior is best understood by first dividing the behavior by temperature – the response is much different when above the glass transition temperature (T_g) than it is when below. In this study, mechanical deformations are performed at room temperature, which is below the T_g of room-temperature cured DGEBA-DETA (see section 2.2.1). Under these conditions, epoxy exhibits behavior similar to glassy amorphous polymers with only small differences (27; 28; 29). This discussion will present the response of glassy amorphous polymers to mechanical loading, and point out areas where epoxy differs from these responses.

The stress-strain curve is a good starting point for discussion of the response of glassy amorphous polymers below T_g. A generic stress-strain curve for glassy amorphous polymers in mechanical deformation is given in Figure 9.

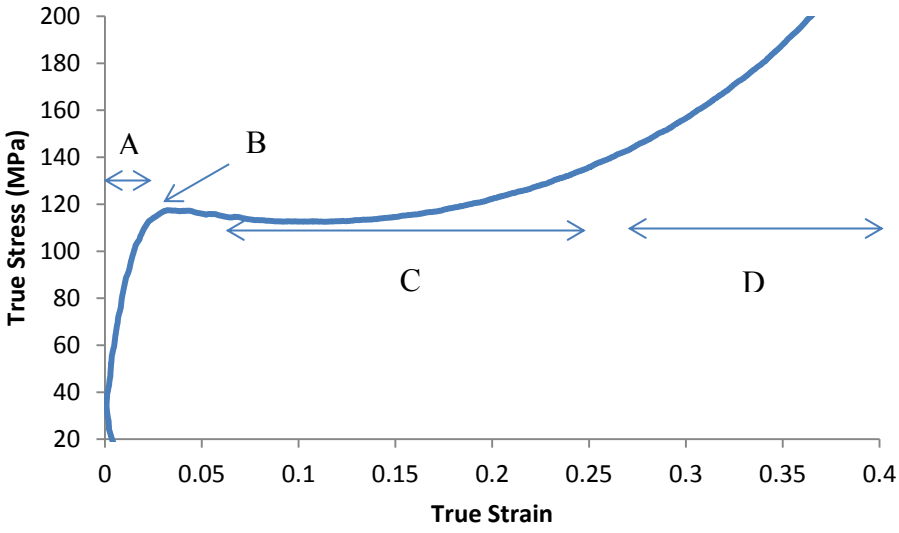

Figure 9: Example stress-strain plot of glassy polymer in compression.

This curve is consistently displayed by samples in both tension and compression, and for various strain states, with small differences that will be discussed. The predominant features are identified in the plot – the elastic region (A), the yield strength (B), the post-yield or strain softening region (C), and the strain hardening region (D). The responses in these regions at the molecular and polymer chain level are of interest to this study, and the current understanding of these phenomena is discussed below.

1.4.1 Elastic deformation

The initial response of a glassy amorphous polymer to a mechanical load is linear elastic, like many materials. The elastic modulus E characterizes this response. Most glassy amorphous polymers have modulus values of 2-4 GPa when tested at temperatures well below T_g. This value is independent of the rigidity of the polymer repeat unit, degree of crosslinking, or entanglement frequency, and is two orders of magnitude below the observed resistance to stretching of a covalent C-C bond. The modulus of a glassy amorphous polymer has been shown to depend strongly on the density of the polymer, however (30; 31). These observations have led

researchers to the conclusion that the resistance to deformation in the elastic region comes primarily from secondary intermolecular interactions between chains such as Van der Waals interactions, and not from stretching of primary bonds (30; 31).

The elastic deformation ends at the yield point ($\varepsilon_{yield,}$ σ_{yield}) of the glassy amorphous polymer. For most glassy polymers σ_{yield} can reach a maximum of appromimately 150MPa, and varies with the testing temperature's proximity respect to T_g. Comparison of σ_{yield} with the theoretical fracture strength of a C-C bond within the polymer chain shows that glassy polymers yield at stresses much lower than required to break a C-C bond. Again, this is evidence that the elastic deformation of glassy polymers is 'dominated by the deformation of secondary bonds' (30).

1.4.2 Yielding and post-yield behavior

After the polymer has been loaded with a stress above σ_{yield}, inelastic deformation begins. The strain produced after ε_{yield} persists after the load is removed, while the elastic strains are instantaneously recovered. We shall refer to the strain after the yield point as deformation strain, ε_{def}. These strains can occur at constant volume, or can be accompanied by small increases in volume, depending on the mechanism by which they develop. The two most important processes responsible for polymer inelastic deformation are yielding and craze formation. The type of process involved depends heavily on the structure of the polymer at the molecular level. Figure 10 shows a plot of the process involved in plastic deformation of crosslinked polystyrene – crazing or yielding - for various levels of crosslinking (ν, the x-axis) (32).

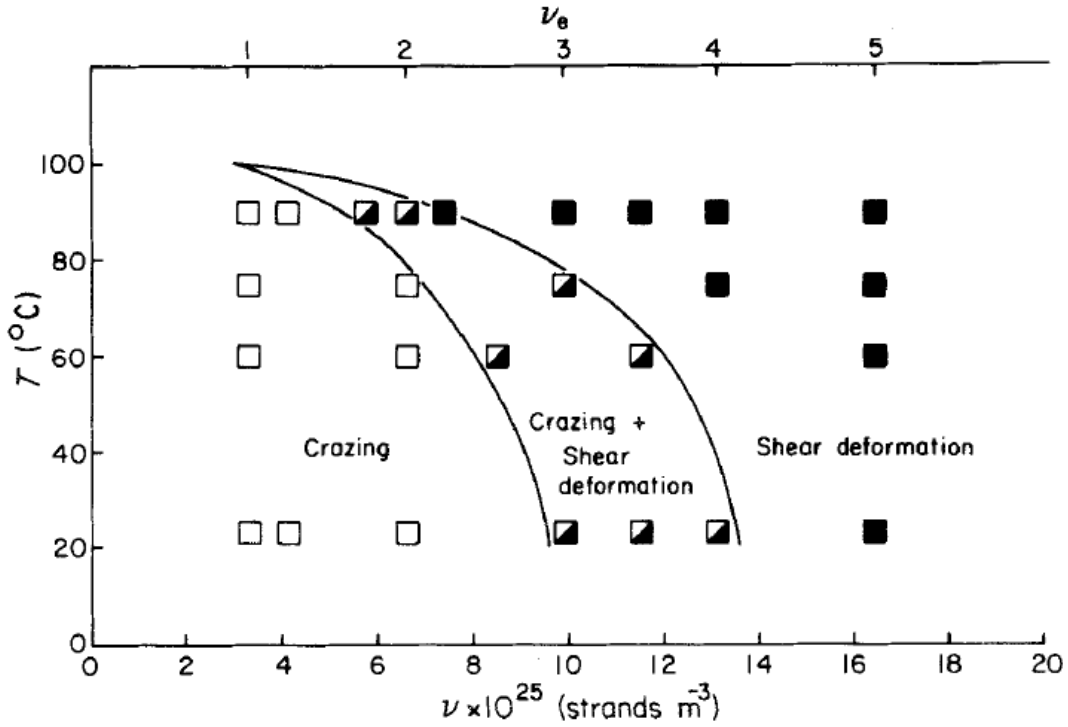

Figure 10: Determination of inelastic deformation process in crosslinked/entangled polystyrene. From (32).

Samples deform exclusively via crazing at low crosslinking, and exclusively via yielding at high crosslinking. In epoxies, the crosslink density is generally so high that it must be reduced in some way to allow yielding to occur before fracture (32; 33). Crazing processes therefore will not be considered further in this work.

In metals and crystalline materials, yielding occurs via nucleation, growth, and motion of dislocations. The dislocation framework was not attractive to resarchers attempting to model polymer yielding at first; the prevailing theory for many years was that coiled structures within the chains were straightening in response to load (34; 35). However, many experiments have shown that in glassy polymers below T_g, chain uncoiling is the dominant process only at the very last stages of deformation, during strain hardening. The current understanding of plastic deformation shows that ε_{def} is produced by the nucleation and motion of short-scale shear

defects, referred to variously as ‘local shears’ (34), plastic shear defects (PSDs) (36), deformation zones (DZs) (33), or shear transformations (STs) (34).

Imaging of shear defects in polymers has not been as successful as dislocation imaging in metals;

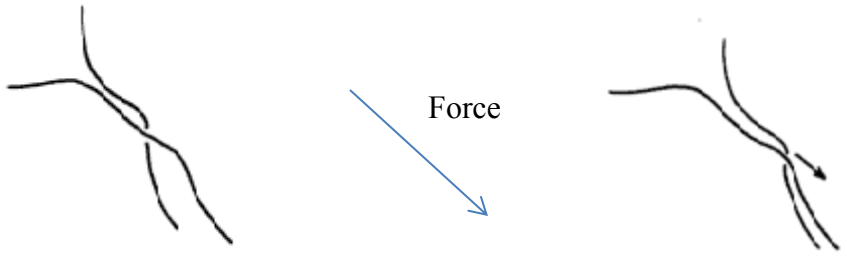

Figure 11: Sketch of shear deformation in adjacent polymer chains. From (27).

however, theoretical studies and computer simulations of disordered structures have produced an accurate picture of their development and motion under stress. Figure 11 has an image of the rearrangement of polymer chains in shear. The ‘permanent’ nature of the shape change associated with plastic deformation suggests that some secondary bonding which was present in the initial conformation has re-formed in the post yielding conformation.

A visualization of shear defect motion in loading is in the inset of Figure 12 (34). Localized regions of high shear can both expand during loading, and change position relative to the bulk polymer. Both processes are based in movement of chains relative to one another, called intermolecular motion in this work.

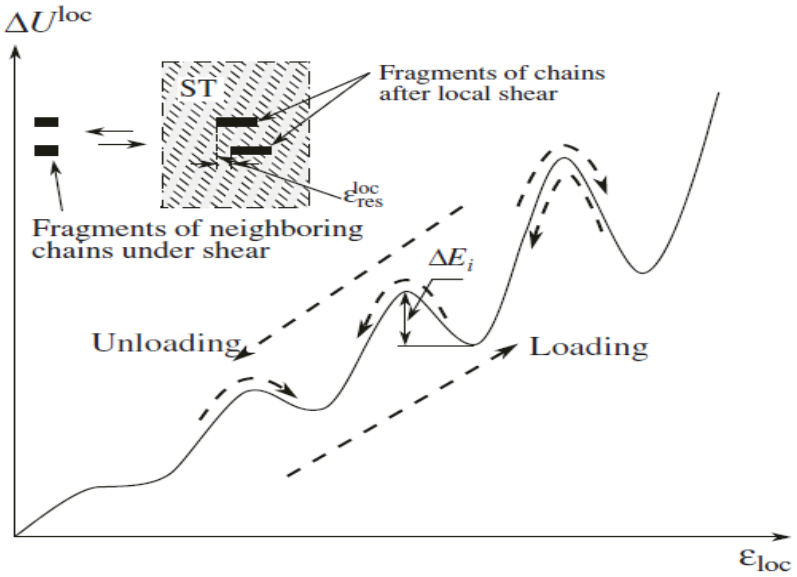

Figure 12: Shear Transformations (STs) motion under loading. From (34).

1.4.3 Unloading and recovery

It is well-known that after yielding, if the load on a sample is removed, the sample returns to a state of no stress via a path with the same slope as the elastic modulus, but to a point of non-zero strain ε_{def}. Figure 13 has an example of the loading and unloading of polystyrene tested in uniaxial compression, with arrows pointing out the value of ε_{def} after unloading.

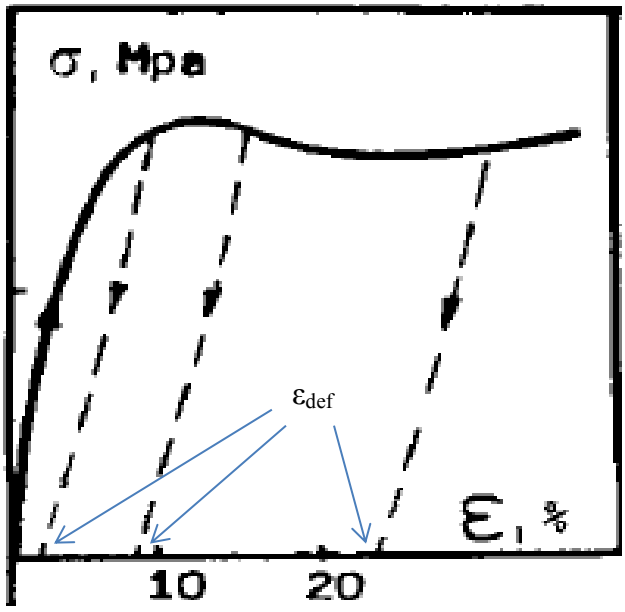

Figure 13: Loading and unloading stress-strain curves of polystyrene in uniaxial compression. From (36).

The strain remaining after unloading, ε_{def}, is a more complicated quantity in glassy polymers than it is in metallic or other crystalline materials. In metals, careful heating of a deformed sample can return it to its original ductility by annihilation of dislocations (37). But the dimension change is permanent below the melting point of the metal. In polymers, however, samples can conditionally recover some or all of the change in dimension they have experienced as well depending on the amount of deformation and the temperature and duration of the heat treatment after deformation. The quantity ε_{def} in polymers consists of the sum of two types of strain, called anelastic strain (ε_{an}) and plastic strain (ε_{pl}), as in Eqn. 3.

$$\varepsilon_{def} = \varepsilon_{an} + \varepsilon_{pl} \qquad 3$$

Current understanding of plastic deformation in glassy polymers holds that ε_{an} results from the nucleation and growth of shear defects. After some deformation, ε_{pl} begins to occur when a sufficient concentration of shear defects has been produced. The shear defects coalesce and annihilate, allowing secondary bonds to form between chains at their new positions. The

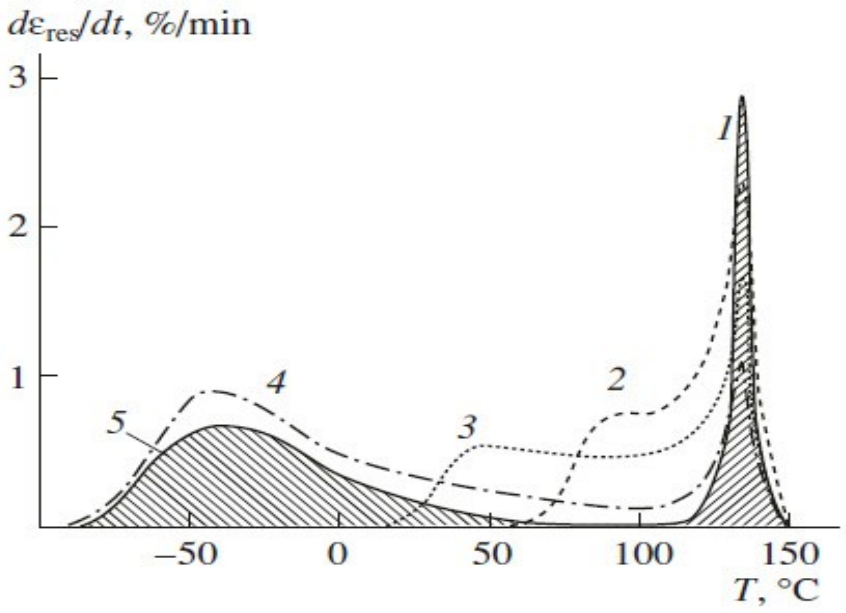

Figure 14: strain recovery curves for glassy amine cured epoxy. curve 1) ε_{def} =.04. curve 2) ε_{def} = .11. curve 3) ε_{def} = .09. curve 4) ε_{def} = .12 curve 5) ε_{def} = .045. From (36).

recovery behavior of glassy polymers illustrates this more clearly. Figure 14 shows the strain recovery of samples of amine-cured epoxy during a temperature scan after varying levels of ε_{def}.

Samples clearly shows two different recovery events – one that occurs below T_g, and one that occurs above T_g (140°C for the system in Figure 14). The low temperature recovery is the recovery of ε_{an}, which can occur at times as low as 1hr when thermal exposure is within (T_g - 20°C). Recovery of ε_{pl}, due to the formation of new secondary bonds, is not possible until samples are heated above T_g, analogous with the re-melting of deformed metals.

Based on the magnitudes of recovery events, the progress of ε_{an} and ε_{pl} have been tracked in the glassy amorphous polymer PMMA (38). Figure 15 shows the quantities of elastic strain (ε_{el}), ε_{an}, and ε_{pl} as the total strain ε_{def} increases. The stress strain curve is also plotted in the figure for

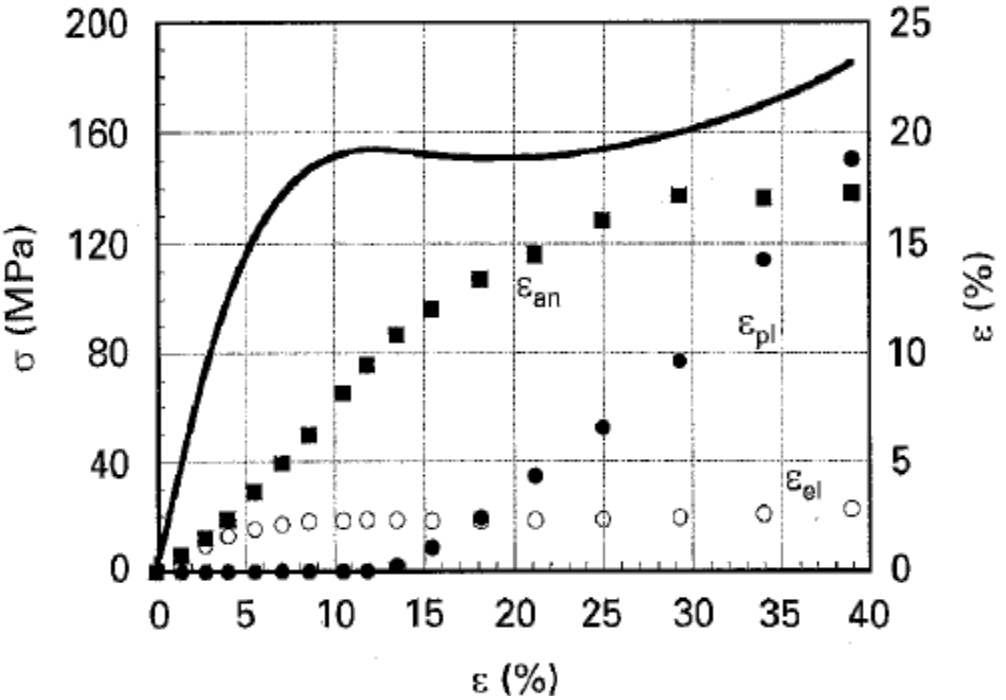

Figure 15: Components of ε_{def} during deformation of PMMA. Open circles – ε_{el}. Closed squares – ε_{an}. Closed circles – ε_{pl}. From (38).

comparison.

The components of strain show differing behavior as loading progresses. The anelastic strain ε_{an} begins growing almost simultaneously with loading, and grows during elastic deformation, yielding, and post-yielding; it reaches a maximum at approximately the onset of strain hardening. The plastic strain ε_{pl}, however, does not begin to appear until just after ε_{yield} and then grows linearly through post yield deformation and strain hardening, presumably continuing to increase until failure.

1.4.4 Yielding, post-yielding, and energy considerations

The stress-strain curve in Figure 13 demonstrates that the dimension change of a glassy polymer sample deformed past ε_{yield} is 'permanent.' This means that work has been done on the sample,

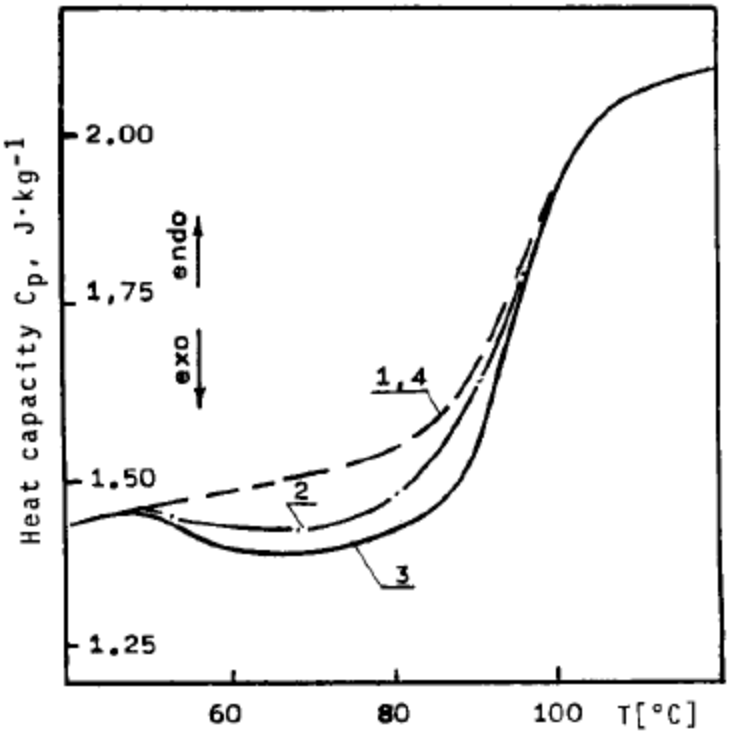

Figure 16: DSC curves of polystyrene - 1) undeformed. 2) ε= .10 3) ε= .20 4) hydrostatic pressure 10kbar. From (36).

and a consideration of the yield behavior in terms of energy naturally follows. Studies of samples before and after deformation using differential scanning calorimetry (DSC) and deformation calorimetry have produced very informative results (27; 29; 34; 36).

Figure 16 shows a DSC scan of samples of undeformed atactic polystyrene (a-PS), a-PS after deformation in uniaxial tension, and a-PS after exposure to hydrostatic pressure of 10kbar (36).

The increasing strain in the samples causes an increase in the exotherm given off by the sample when heated. This indicates a buildup of energy within the sample through some mechanism. The exotherm increases with increasing strain, and the energy is given off at temperatures approaching but below T_g (~90°C for a-PS). Hydrostatic pressure causes no increase in the exotherm.

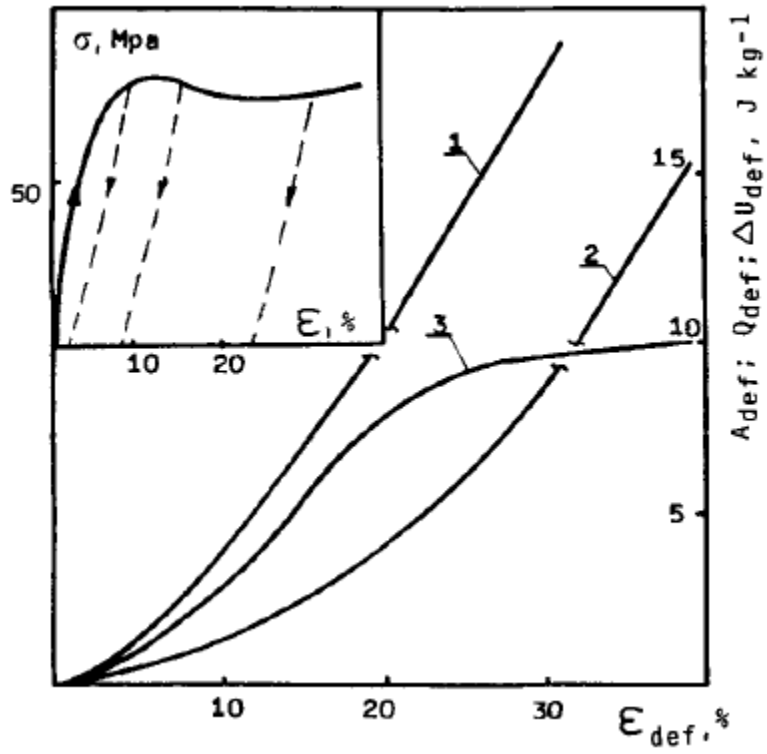

Figure 17: Curves of energy associated with glassy polymer deformation. 1) Mechanical work of deformation. 2) Heat of deformation 3) Internal energy stored by sample. From (36).

Figure 17 shows a plot of the various kinds of energy involved in the deformation of a glassy amorphous polymer, with the stress-strain curve plotted in the inset for reference.

Curve 1 shows the mechanical work of deformation A_{def} (curve 1), determined by the area under the stress strain curve

$$A_{def} = \int_0^{\varepsilon_{def}} \sigma d\varepsilon \qquad \mathbf{4}$$

Curve 2 is the heat of deformation, measured by deformation calorimetry. Curve 3 in Figure 17 shows the amount of energy stored by the sample, ΔU_{def}, the difference between A_{def} and Q_{def}

$$\Delta U_{def} = A_{def} - Q_{def} \qquad \mathbf{5}$$

This quantity agrees very well with exothermic measurements like those in Figure 16. The amount of energy stored in inelastically deformed polymers begins increasing immediately, and reaches a maximum at strains of ε_{def}=.15-.25 after which it remains constant. The behavior of ΔU_{def} as ε_{def} increases compares very well with the behavior of ε_{an} (see Figure 15), as does the observation that liberation of ΔU_{def} appears in DSC measurements at temperatures approaching but below T_g. Many researchers now consider the buildup of ΔU_{def} and the increase in ε_{an} to be indicators of the nucleation and growth of the local shear defects responsible for plastic deformation. The increased disorder immediately surrounding the defect accounts for ΔU_{def} in a manner roughly analogous to strain energy buildup around dislocations in metals (37). Hydrostatic pressure, which applies only dilatational stress components with no shear terms, causes no increase in ΔU_{def}, further supporting the shear defect- ΔU_{def} connection. This hypothesis also suggests that the coalescence of shear defects that occurs at large ε_{def}, which is responsible for producing ε_{pl}, does not cause increased internal energy storage. The

concentration of shear defects has reached the point where coalescence occurs at the same rate as nucleation, making increases in ε_{pl} energy-neutral.

A plot of ΔU_{def} for various materials is shown in Figure 18 (36). Curve 1 in this plot shows the internal energy stored by an amine cured epoxy during deformation. The onset of energy storage does not begin immediately but at some non-zero value ε_{def} ~.05-.10. Epoxy stores the largest amount of energy of the tested glassy polymers, reaching a plateau of ~15 J/kg at the highest ε_{def} shown. The internal energy also does not reach a perfect plateau in epoxy, continuing to increase but more slowly as ε_{def} increases above .30.

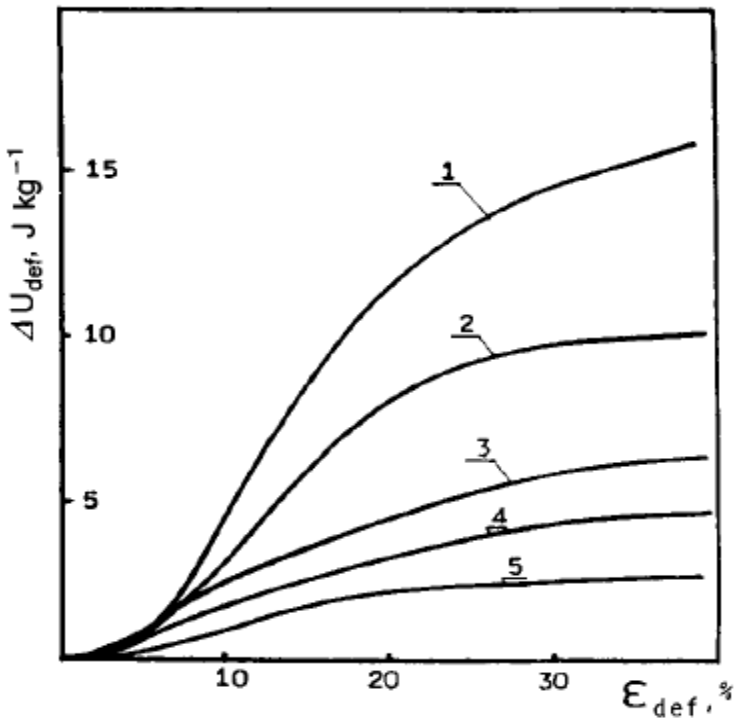

Figure 18: internal stored energy for various polymers. 1) amine-cured epoxy. 2) a-PS. 3) PC. 4) PMMA. 5) a-PET. From (36).

1.4.5 Strain hardening

The earlier model of plastic deformation involved the uncoiling of coiled macromolecular chains. This model is now considered to be inaccurate in the early stages of post yield

deformation, where ε_{def} largely consists of ε_{an} and is associated with nucleation and growth of shear defects between chains rather than chain extension. It is only after significant deformation has already taken place that chains begin to extend and align, bringing the stronger C-C bonds into play in resisting deformation. The coalescence of shear defects and re-formation of secondary bonding between chains also contribute to the increased stiffness.

Experimental data and theoretical studies using a variety of chain-based models have established that the amount of strain hardening experienced in a glassy amorphous polymer increases as the density of crosslinks increases (39; 40; 41). The strain hardening phenomenon is also dependent on the strain state of the sample, with strain hardening occurring at lower strains when samples are loaded in plane strain compression than when loaded in uniaxial compression (42).

1.4.6 Comparison of epoxy to general amorphous glassy polymers

As noted previously, epoxy mechanical deformation is qualitatively very similar to most other glassy amorphous polymers (27; 28; 29). The highly crosslinked network structure plays little role in elastic deformation and yielding, which are dominated by effects from interchain secondary bonding. The large crosslink density of epoxies has one large effect - it increases T_g to very high temperatures for fully cured materials, allowing their mechanical response to remain glassy at higher temperatures than most other glassy amorphous polymers. As discussed in Chapter 1 section 1.4.2, crosslinking determines the plastic deformation process, with highly crosslinked epoxies displaying yielding deformation predominantly. Other subtle effects of crosslinking are to increase ε_{yield} slightly compared to non-crosslinked polymers (33), and to increase the magnitude of strain hardening experienced at high strains (27) (43).

1.5 Summary

When solid epoxy is loaded at a temperature well below its T_g, it responds in a manner very similar to other glassy amorphous polymers. The stress strain curve of epoxy deformation shows four predominant features – the elastic region, the yield point, the post-yield/strain softening region, and the strain hardening region. The elastic region has been associated with the deformation of secondary, Van der Waals-type bonding between polymer chains. Yielding occurs when these secondary bonds begin to break. The post-yield region is characterized by large deformation strains in the sample ε_{def} through yielding, which is currently understood to take place via nucleation and growth of shear defects and motion of chains relative to one another rather than chain alignment or uncoiling. These processes are accompanied by an increase in the anelastic strain ε_{an} beginning at initial loading and reaching a plateau around ε_{def} =.20. After sufficient shear defects have formed, they can coalesce and re-form secondary interchain bonds, which correspond with the plastic strain ε_{pl} beginning after yielding and increasing until failure. DSC scans have measured an increase in stored internal energy ΔU_{def} during yielding, roughly corresponding with shear defect formation and ε_{an}. Recovery of ε_{an} can occur in hours if samples are heated to (T_g -20°C), while temperatures above Tg are required to recover ε_{pl}. The strain hardening region is characterized by major stiffening of the sample response to load, and has been associated with stretching or uncoiling of polymer chains. In many glassy polymers this process does not add ΔU_{def}, however in epoxy it appears to continue increasing slightly as ε_{def} increases into the strain hardening region.

2. CHARACTERIZATION METHODS

In this section the methods used to characterize the DGEBA-DETA system will be presented. The procedure used to cure DGEBA-DETA and the instruments used to characterize the cure process will be introduced. After cure, the methods used to characterize the mechanical, thermal, and optical properties will be presented.

2.1 Characterization of cure

The DGEBA-DETA system is a useful one for this study for many reasons, one of which is that it can be cured at room temperature. This eliminates several problems associated with high-temperature cured systems.

DGEBA and DETA at room temperature are medium- and low-viscosity liquids. To produce samples for continued study, the liquids are mixed at the appropriate stoichiometric ratio until no phase separation is visible. To remove any bubbles introduced during mixing, the liquid mixture is held under vacuum for ~5 minutes, after which the liquid is poured into 63mm aluminum sample weighing dishes for curing. The cure reaction at room temperature is exothermic, but with χ=1 and at the batch sizes involved in this study the reaction causes negligible temperature increase.

Samples were characterized during cure using standard techniques including Differential Scanning Calorimetry (DSC), UV-Visible absorbance spectroscopy, and Fourier Transform Infrared Spectroscopy (FTIR).

2.1.1 Differential Scanning Calorimetry

The standard technique for DSC cure characterization of epoxy is based on the heat of reaction evolved during cure, ΔH_{rxn}. A dynamic DSC scan measures the heat evolved or absorbed by a sample as temperature increases at a controlled rate. After scanning to a temperature sufficient to complete all curing reactions, the DSC's signal can be integrated to measure ΔH_{rxn}

$$\Delta \boldsymbol{H_{rxn}} = \int_{\boldsymbol{T_{onset}}}^{\boldsymbol{T_{completion}}} \frac{\boldsymbol{\partial H}}{\boldsymbol{\partial T}} \qquad \mathbf{6}$$

This is taken as a baseline value, to which samples of variable cure states can be compared. A dynamic DSC measurement identical to the one used to determine ΔH_{rxn} can be performed on partially cured samples to measure the residual heat of reaction, $\Delta H_{res.}$ The final degree of cure, α_{final}, is then that portion of the heat of reaction that is not accounted for in the residual heat of reaction:

$$\alpha_{final} = 1 - \frac{\Delta H_{res}}{\Delta H_{rxn}} \qquad \mathbf{7}$$

The glass transition temperature T_g can also be determined from a dynamic DSC scan. The temperature at which molecular chain motion begins to be thermally allowed is characterized by an inflection point in the heat evolution signal. After partial or full curing, T_g is easily detected by analysis software (44).

To establish ΔH_{rxn}, immediately after mixing, small amounts (5-15mg) of uncured epoxy-amine liquid were weighed and placed in aluminum DSC pans (Netzsch Instruments 6.239.2 – 64.50X). Samples were loaded into a Netzsch DSC-200 with a Netzsch TASC 414/3 controller (Netzsch Instruments, Burlington, MA). Samples were heated in dynamic DSC measurements to 250^{o}C at

a heating rate of 5°C/min under inert gas atmospheres. After the measurement, the samples were cooled with forced air. A second identical DSC measurement was performed to establish $T_{g\infty}$ and ensure no residual cure was present.

Evaluation of samples cured in bulk was performed by sectioning the bulk sample and punching a small disk out of a thin sheet. The disk was placed in a DSC pan and heated, cooled, and heated again as above. The ΔH_{res} was measured by integration as in eqn. 6.

Dynamic DSC data was analyzed using Proteus Thermal Analaysis software (Netzsch Instruments, Burlington, MA).

2.1.2 Fourier Transform Infrared Spectroscopy

To investigate the chemical changes occurring during cure, Fourier Transform Infrared spectroscopy (FTIR) was used. Measurements of DGEBA-DETA during cure were measured with a Bruker Vector 70 FTIR, using a GladiATR diamond ATR accessory (Pike Technologies, Madison, WI). Uncured DGEBA-DETA mixtures were placed on the ATR with a dropper and allowed to cure for 24hr. The FTIR spectrum was collected every 30 min during the cure process. To analyze the spectra, the area under the epoxide's characteristic absorbance peak at 917cm^{-1}, $A_{917}(t)$, was used as a measure of the epoxide groups remaining at a time t. The integrated value was normalized by the initial value of the absorbance integral, which can be related to the degree of cure α(t) in equation **8**:

$$\alpha(t) = 1 - \frac{\int A_{917}(t)}{\int A_{917}^{0}} \qquad \textbf{8}$$

The rate of cure $\frac{d\alpha}{dt}$ for different samples can be compared by observing the slope of the α(t) curve before the onset of diffusion control. The final degree of cure of a sample, $\alpha_{final,}$ can be

determined from the maximum value of $\alpha(t)$ reached during cure. The method has been used successfully to monitor cure reactions and explore the effects of variables such as cure temperature, stoichiometry, and curing agent molecular structure in other works (45; 46; 47).

2.1.3 Absorbance

Absorbance measurements on solid samples were performed on a ThermoScientific Evolution 300 UV-Vis spectrophotometer (Thermo Scientific, Waltham, MA). For liquid samples, plastic cuvettes containing uncured DGEBA-DETA-probe mixture were placed in the UV-Vis absorbance beam path and allowed to cure. Absorbance spectra were collected at appropriate time intervals (every 30 minutes for most mixtures) for the duration of the cure process (24hr for most mixtures). Baseline absorbance was taken on an identical plastic cuvette filled with unmixed DGEBA.

2.2 Characterization of solid epoxy polymer

This section details the characterization of the DGEBA-DETA after curing. The glass transition temperature and relevant mechanical and optical properties will be characterized using DSC, DMA, UV-Vis absorbance, and mechanical deformation techniques. Baseline values for these properties are established for as cured samples with χ=1. The changes in these properties due to variations in thermal exposure , χ, and ε_{def} will be presented.

2.2.1 Glass transition temperature

The glass transition temperature is an extremely important property of a polymer that defines the temperatures where glassy response to loading occurs, along with associated behaviors such as

recovery. The dynamic DSC measurements described in section 2.1.1 give one measurement of $T_{g,}$ but another measurement method is Dynamic Mechanical Analysis (DMA).

DMA is a widely accepted method for determining the glass transition temperature T_g of polymers and polymer composites. The glass transition temperature of a sample was determined using method 1 described in ASTM E1640 (48) – the intersection of tangent lines to the storage modulus E' curve taken above and below the onset of the transition. T_g data can also be measured at the peaks of the loss modulus E''or tan δ curves; T_g from E' data is typically lower than T_g reported from E'' or tan δ data.

Rectangular samples were tested in 3-point bend configuration in a PerkinElmer DMA 7e instrument (PerkinElmer Life and Analytical Sciences, Inc., Waltham, MA). An initial force of 500 mN was applied; force oscillation of 400mN was then conducted at a rate of 1Hz. Temperature was increased at a rate of 5°C/min, and oscillation amplitude was measured. Data was collected and analyzed in Pyris v.6.0.0.33 software.

2.2.2 Mechanical properties

Understanding the mechanical response of DGEBA-DETA to loading is vital to understanding the mechanochromic behavior of probe molecules. Certain defining properties and regions must be established for DGEBA-DETA using uniaxial compression and hydrostatic pressure testing. After deformation, the recovery response of DGEBA-DETA is also tested.

2.2.2.1 Sample preparation

After curing, samples were machined on a low speed saw (Pace Technologies PICO150, Tuscon, AZ) with a wafering blade of low-concentration poly-crystalline diamond, cooled by a water

bath. Samples were machined to form flat square specimens with dimensions approx. 5mm x 5mm x 1mm.

2.2.2.2 Uniaxial Compression Testing

Samples were deformed in compression in an Instron 5500R test frame (Instron, Norwood, MA) at a rate of .1mm/min. For modulus measurements, samples were loaded to slightly past the yield point of the stress strain curve, and then unloaded at .1mm/min. Modulus calculations were performed on the unloading curve to avoid sample alignment variation and the elastic toe region of the stress-strain curve. Yield strength was calculated using the maximum stress level of the stress-strain curve.

For varying ε_{def} testing, samples were loaded to a single value of ε_{def} at .1mm/min before being unloaded rapidly. A single sample was loaded only to one ε_{def} value before subsequent testing, and was not loaded again.

2.2.2.3 Recovery Testing

To evaluate post-yield recovery behavior, a series of samples were tested to varying levels of ε_{def}, approximately every .05 ε_{def}, after which samples were unloaded and their dimensions measured to determine ε_{an} and ε_{pl}. Samples were then placed in a drying oven at 70°C (~T_g + 10°C) to allow recovery processes to occur on a time scale convenient for observation. Sample dimensions were measured at 1hr, 3hr, and 24hr after initial temperature exposure. No additional recovery was observed beyond 1hr of exposure.

2.2.2.4 Hydrostatic Pressure Testing

For hydrostatic pressure testing, samples were machined into prisms approximately 5mmx5mmx7mm. Samples were then loaded with hydrostatic pressure in a cold isostatic press (MTI Corp. CIP-15, Richmond, CA) to varying pressures. Samples were loosely enclosed in aluminum foil and submerged directly in the hydraulic fluid, after which pressure was applied. Three samples were loaded to 77 MPa, 232 MPa, and 349 MPa. After loading samples were removed from the pressure chamber, hydraulic fluid was cleaned from the samples and subsequent testing was carried out.

2.2.3 Optical properties

The mechanochromic response of probe molecules will be measured optically using absorbance, excitation, and fluorescent emission spectroscopy. It is therefore important to measure the behavior of DGEBA-DETA using these techniques to establish responses that are due to the epoxy itself rather than the probe molecule. The techniques and instruments used to perform these characterizing experiments will be presented in this section.

2.2.3.1 Absorbance

For solid samples, absorbance characterization was performed in a similar manner to liquid samples (see Chapter 1 section 2.1.3). Samples were machined just as for mechanical testing and were placed free standing in the beam path. Spectra were compared to baseline spectra taken with no sample in the beam path. Absorbance spectra were often corrected for varying sample thicknesses by offsetting the absorbance at 850nm to 0 A.

2.2.3.2 Excitation and emission

The excitation and emission spectra of solid DGEBA-DETA samples were collected in a Perkin

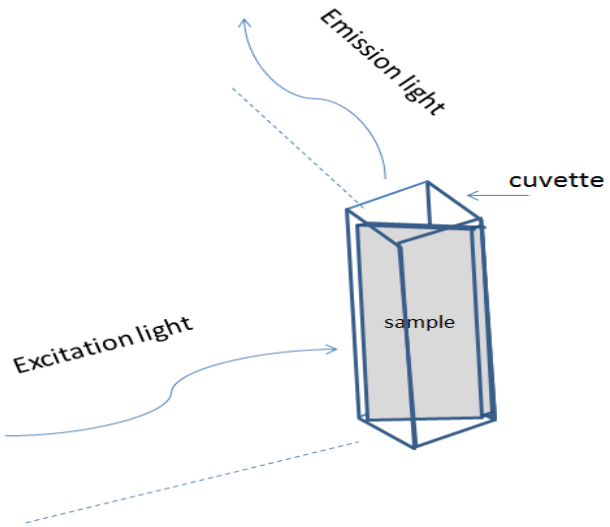

Figure 19: Schematic of solid sample excitation-emission measurements.

Elmer LS-50B Fluorimeter (Perkin Elmer, Waltham, MA). Fluorescence from solid samples was obtained by sectioning samples ~1.0mm thick with appropriate dimensions to fit into 10mm quartz cuvettes at an angle of ~45° to the beam path. Samples were loaded into the cuvette in such a manner that any reflection of the excitation light would occur away from the detector path. Figure 19 has a schematic of the sample alignment.

Excitation and emission spectra were collected iteratively by collecting an initial emission spectrum, then collecting an excitation spectrum corresponding to the peak emission wavelength, then collecting a subsequent emission spectrum corresponding to the peak excitation wavelength. Spectra will be normalized at the peak excitation and emission wavelengths in comparison plots such as the one in Figure 30.

2.2.3.3 In situ emission

Fluorescent emission spectra of samples during in-situ testing and for sample geometries not convenient for fluorimeter testing were collected with a Stellarnet Blue-WAVE UVN miniature spectrometer and Y-type '7-around-1' fiber optic probe (Stellarnet US, Inc., Tampa, FL). Excitation light was carried by 7 exterior optical fibers from an LED single-wavelength source (SL1-LED, Stellarnet US, Inc.) to the illumination site. Emission spectra were collected by a single 600µm optical fiber, within the bundle of exterior fibers. The probe configuration ensures

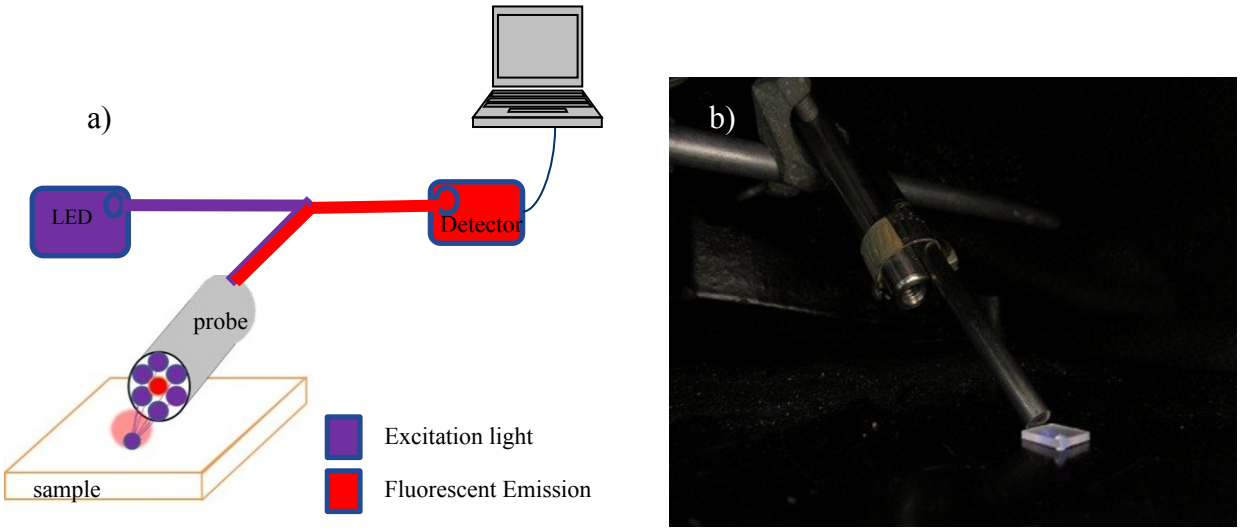

Figure 20: a) spectrometer schematic. b) Image of spectrometer probe tip and sample configuration.

that excitation and emission occur from the same small sample location. The probe tip was held at a 45°angle to the sample surface to minimize excitation light backscatter being detected by the emission probe. A schematic of the setup is shown in Figure 20a, with an image in Figure 20b.

The probe tip and sample area were enclosed in a double layer of thick black cloth to remove ambient light, and spectra were compared to a baseline of the sample with no illumination from the source.

2.2.3.4 Fluorescent Imaging

To display visually the changes in fluorescent response, images of the samples were taken. Images were taken with a Canon PowerShot Elph 100HS camera mounted on a small tripod. Brightfield images were taken against a white background. Fluorescent images were taken in a darkroom against a dark background, using a 15sec shutter exposure. The samples were illuminated by hand with the long wave setting of a UVSL-14P UV Lamp (UVP, Upland, CA).

3. DGEBA-DETA DURING CURE

This section will present the results of characterization of DGEBA-DETA during cure using the techniques presented in Chapter 1 section 2.1. The changes in cure caused by changing the amine-to-epoxide ratio χ will also be presented in this section.

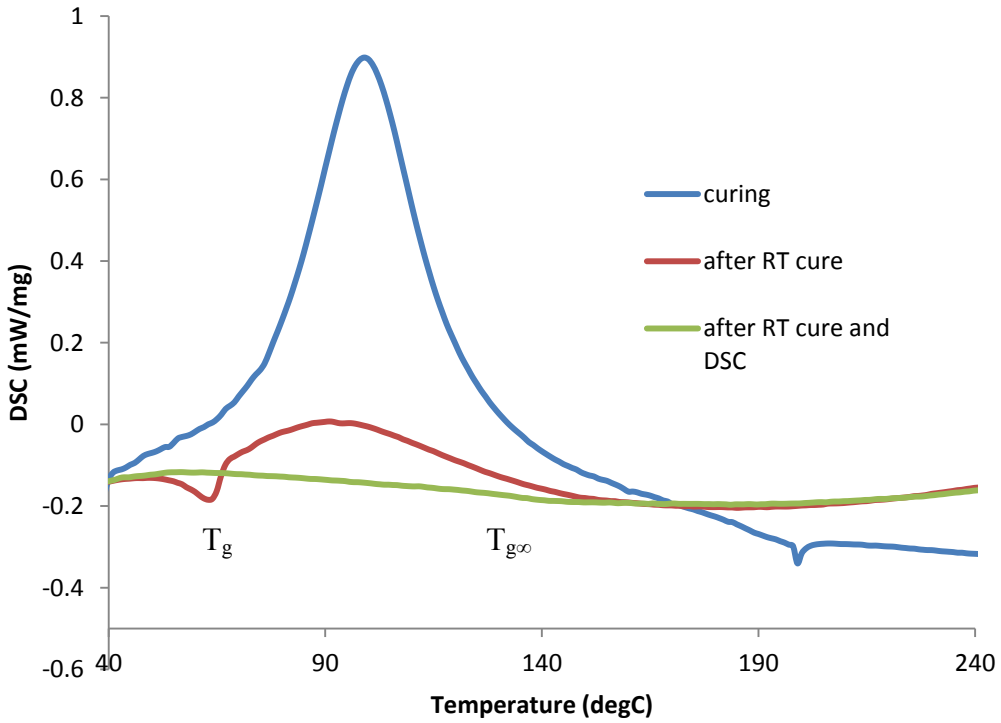

Figure 21: DGEBA-DETA curing exotherm (blue), exotherm after RT cure (red), and after complete cure (green).

3.1 DSC cure characterization

Figure 21 shows the dynamic DSC analysis curves of DGEBA-DETA with χ=1 during heating to 250C, with the curing reaction in blue, the residual reaction after the 24hr RT cure cycle in red, and the curve after the RT cure and DSC heating to 250ºC in green.

The DSC measurement after RT cure shows that this cure cycle does not complete the cure reaction, and the glass transition temperature at 62.6 ± .75ºC is clearly visible. After the first DSC measurement, a second DSC measurement shows no exothermic behavior, and $T_{g\infty}$ of the material is visible at 132ºC. DSC analysis of the areas under the curve allows an approximate estimate of the degree of cure of DGEBA-DETA at α_{final} ~.67 from equation 7.

3.1.1 Effect of stoichiometry

The stoichiometry is one of the most fundamental determining factors in DGEBA-DETA's thermal characteristics. The network structure is highly affected by the amine-to- epoxide ratio

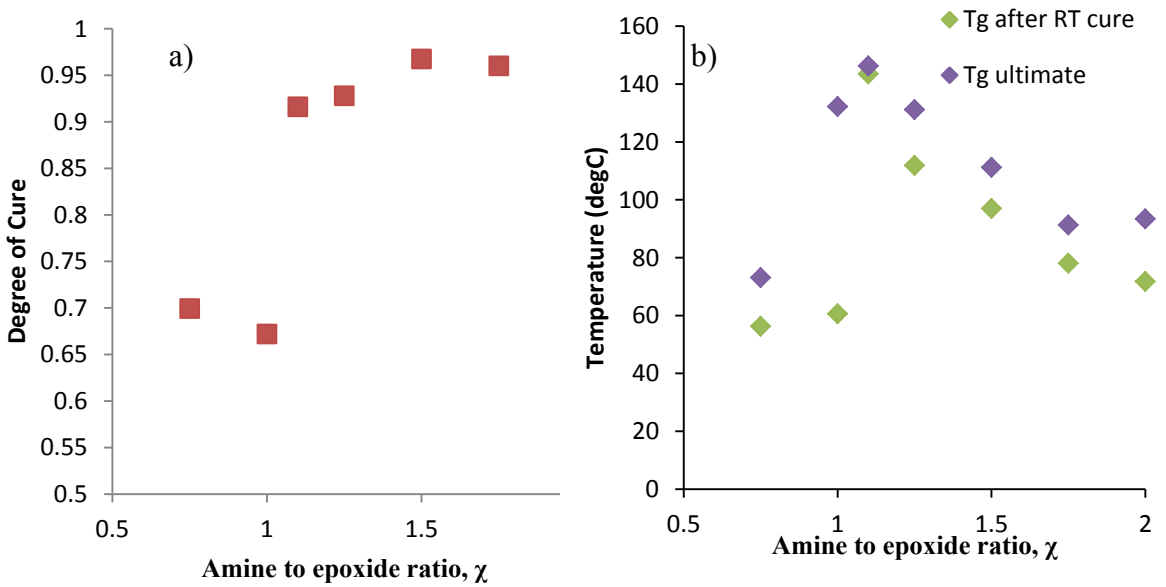

Figure 22: a) Degree of cure for DGEBA-DETA cured at RT with varying χ value. b) Tg and ultimate Tg of RT cured DGEBA-DETA with χ values.

χ, with excess epoxides leaving unreacted or partially reacted epoxide monomers either unbound or partially bound to the network, and excess amines resulting in less-than-optimum crosslinking sites and primary or secondary amines unfulfilled. The effects that changing χ have on DGEBA-DETA are described by Figure 22a and b, which show the α_{final} after RT cure and T_g and $T_{g\infty}$.

Figure 22a shows that room temperature curing of DGEBA-DETA does not result in complete conversion of epoxides at $\chi \leq 1.1$. As amine content increases above $\chi=1.1$, the α_{final} approaches the maximum conversion of 92-97% based on the relative sizes and steric hindrances of DGEBA and DETA (44).

The glass transition data in Figure 22b shows that after room temperature cure, $\chi<1$ samples have a low glass transition which is consistent with the degree of cure they exhibit. After curing is completed by means of a DSC cycle to 250ºC, the ultimate glass transition is exhibited. This is at its highest for samples near the stoichiometric ratio, and decreases for samples with either excess epoxide or excess amine. The large gap between T_g after RT cure and $T_{g\infty}$ for $\chi=1$ suggests a great deal of difference between the RT cure and a completely cured stoichiometric network. This difference can be reasonably attributed to both partially cured epoxide monomers and unfulfilled crosslinks at amino hydrogen reactive sites.

3.1.2 FTIR cure characterization

Figure 23 shows the $\alpha(t)$ curve for DGEBA-DETA with $\chi=1$ during a RT cure. The degree of cure shows behavior typical of autocatalytic reactions, increasing rapidly until gelation sets in and the reaction becomes diffusion controlled.

The degree of cure ultimately reached by this sample is α_{final} =.576, slightly smaller than the DSC measurement of .67. The DSC sample was cured in bulk, where temperatures can be slightly higher due to buildup of heat released from the exotherm; this probably accounts for the

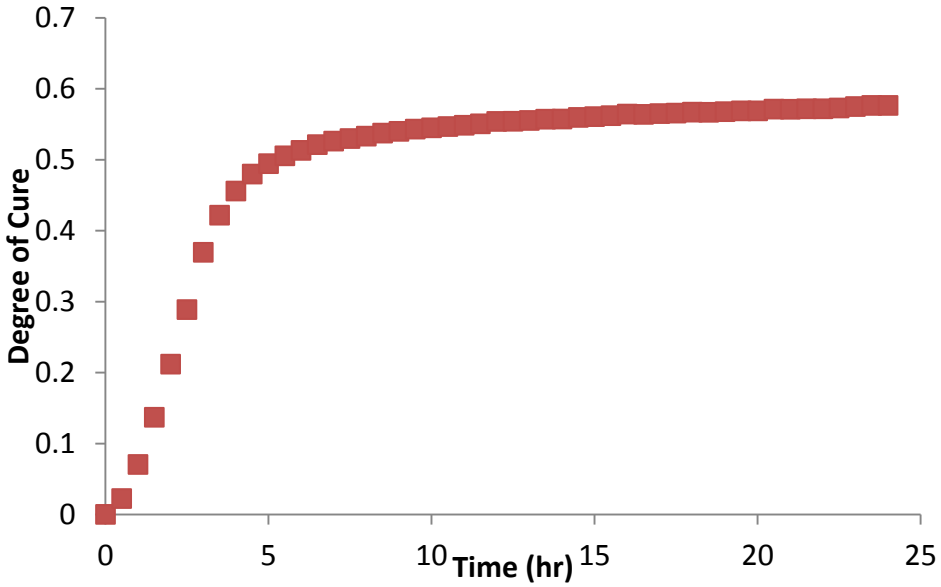

Figure 23: Degree of cure measured by FTIR over time for the curing of DGEBA-DETA with χ=1 at room temperature. The maximum reached is α=.576.

increased α_{final} measured by DSC. Both measurements agree that a significant portion of the epoxide and amine functional groups remain unreacted in RT-cured DGEBA-DETA, and must be considered when discussing deformation processes.

Figure 24a shows α(t) curves for various stoichiometries of DGEBA-DETA. Figure 24b shows the final degree of cure reached by samples with varying χ values. The stoichiometries of the systems are listed in the legend of Figure 24a.

It is clear that increasing χ causes two main effects – an increase in $\frac{d\alpha}{dt}$ and a higher value of α_{final}. These trends are in general agreement with the DSC results presented in Chapter 1 sec. 0. The importance of these results will be discussed more thoroughly as they become relevant.

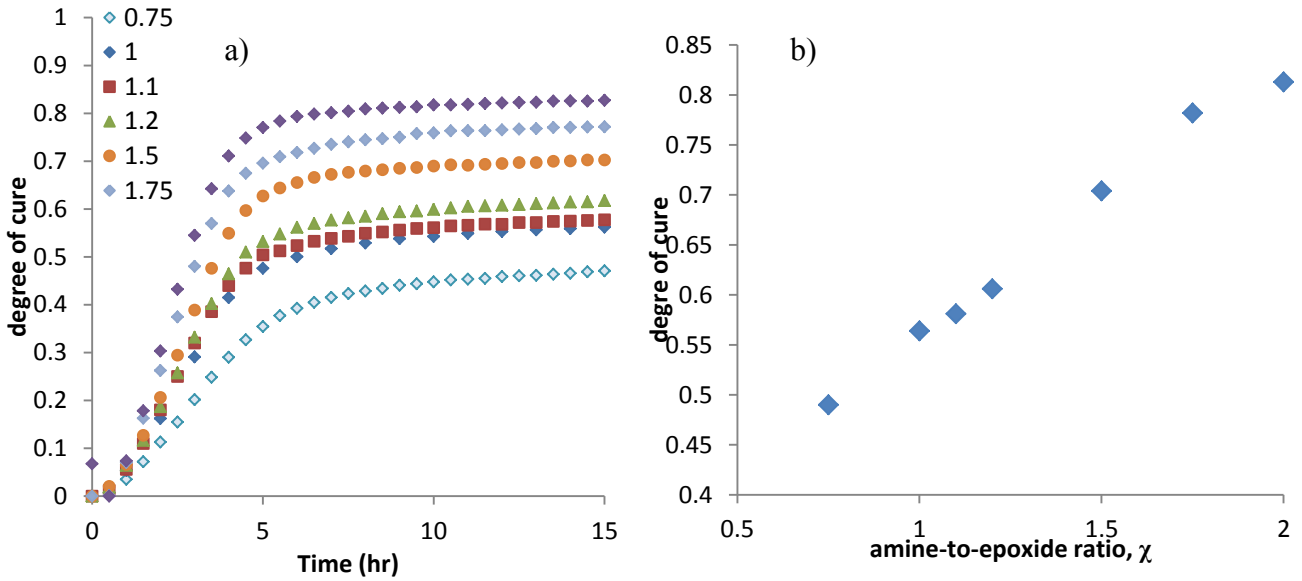

Figure 24: FTIR studies of degree of cure for varying stoichiometries - a) α vs time and b) α_{final} vs χ.

3.1.3 Absorbance during cure

The absorbance of DGEBA-DETA changes very little during the cure process. Figure 25a shows the absorbance spectra at t = 0hr, 10hr, and 20hr into cure. Figure 25b shows the values of the absorbance at 447nm over the course of the cure.

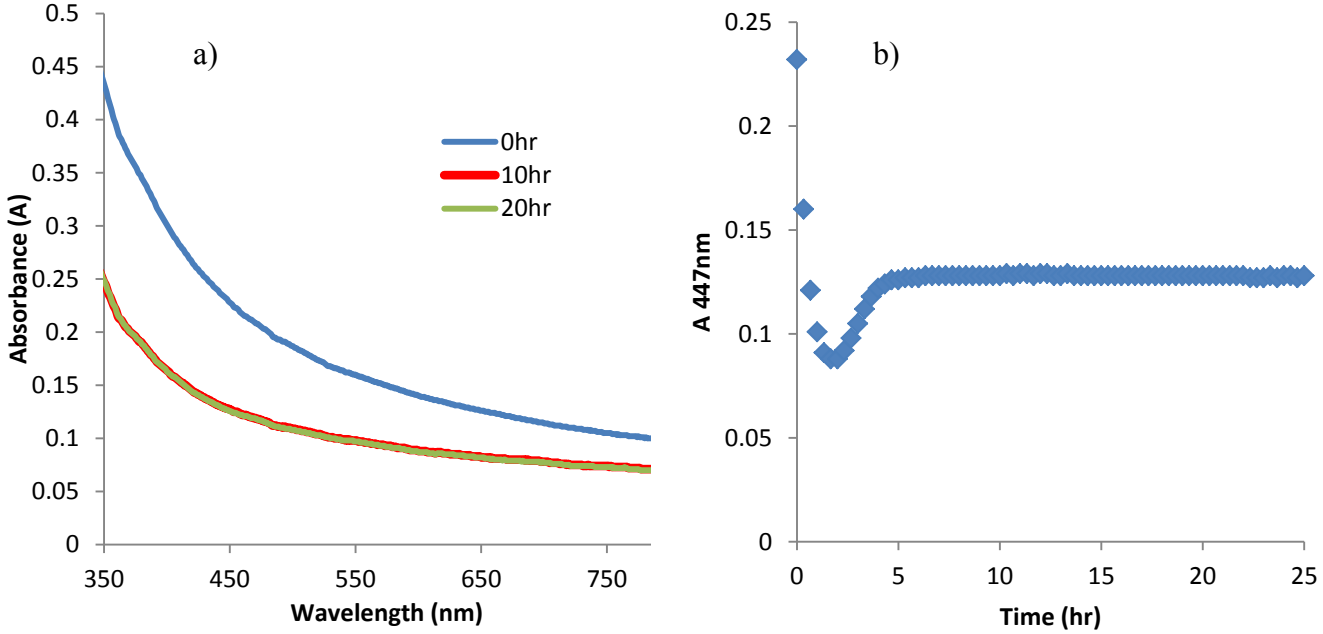

Figure 25: Absorbance of DGEBA-DETA during cure - a) absorbance spectra b) absorbance at 447nm vs time.

The absorbance spectra show low-magnitude, featureless absorbance that is higher in UV wavelengths than in visible. At 447nm, the spectra shows small decrease and increase behavior during the initial stages of cure but remains constant after ~t=5hr. No new absorba nce features are developed during curing. The variation of χ did not produce remarkably different behavior.

3.2 Summary of cure characterization

When DGEBA-DETA is cured at RT it does not reach complete cure at values of χ<1.1. The measured final degree of cure, α_{final}, was calculated to be 0.67 via DSC measurement, and .576 via FTIR measurement for samples with χ=1. DSC analysis showed that that T_g after cure was 63.9°C for χ=1. An increase in α_{final} and T_g was observed when χ was increased, with T_g subsequently decreasing after χ=1.1. FTIR analysis showed that increasing χ produced an increase in α_{final} and increased the rate of reaction $\frac{d\alpha}{dt}$ before the onset of diffusion control. Absorbance measurements during cure showed no development of absorbance features, and a general decrease in absorbance from the initial state until t~3hr after which no changes were observed.

4. SOLID DGEBA-DETA CHARACTERIZATION

The characteristics of DGEBA-DETA after curing into a solid are presented in this section. The glass transition temperature as measured by DMA as well as the mechanical and optical properties of DGEBA-DETA will be shown first, followed by the effects of changing stoichiometric ratio and exposure to heat and deformation on the optical properties.

4.1 Glass transition

Figure 26a shows a typical storage modulus curve measured for DGEBA-DETA cured at room temperature. The DMA measurements determined the glass transition of RT cured DGEBA-DETA to occur at 56.9 deg C. This is in good agreement with the measurements of DSC in presented in Chapter 1 section 3.1. The variation of T_g with χ was also measured with DMA. Figure 26b has a plot of the T_g values measured.

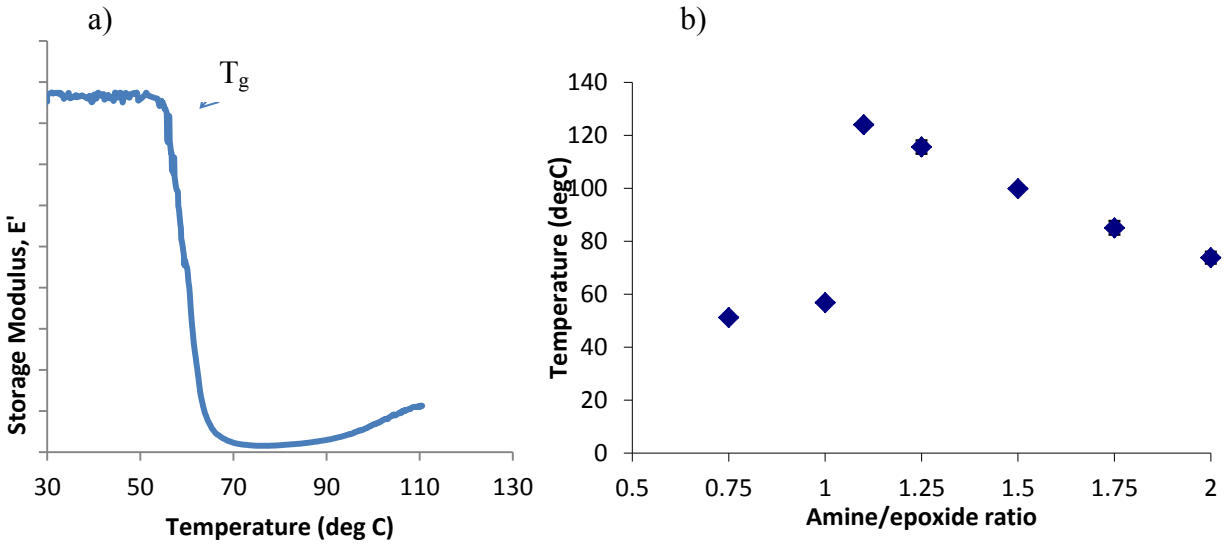

Figure 26: a) typical plot of E' vs T with T_g marked. b) variation of T_g with χ as measured by DMA.

This data also agrees well with the behavior observed in DSC measurements for variation of T_g with χ. As in DSC, the T_g remains low for samples with $\chi<1.1$, increases to the maximum observed T_g at $\chi=1.1$, and decreases as χ increases thereafter.

4.2 Mechanical properties

The mechanical properties of DGEBA-DETA were evaluated in uniaxial compression. Elastic modulus and yield strength were characterized, and deformation behavior after yielding was studied with relaxation measurements.

4.2.1 Elastic modulus, yield strength and strain

Figure 27 shows a typical loading and unloading stress strain curve used for measuring the elastic modulus and yield point of RT cured DGEBA-DETA, with the fitline to the unloading curve displayed, and an arrow highlighting the yield strength.

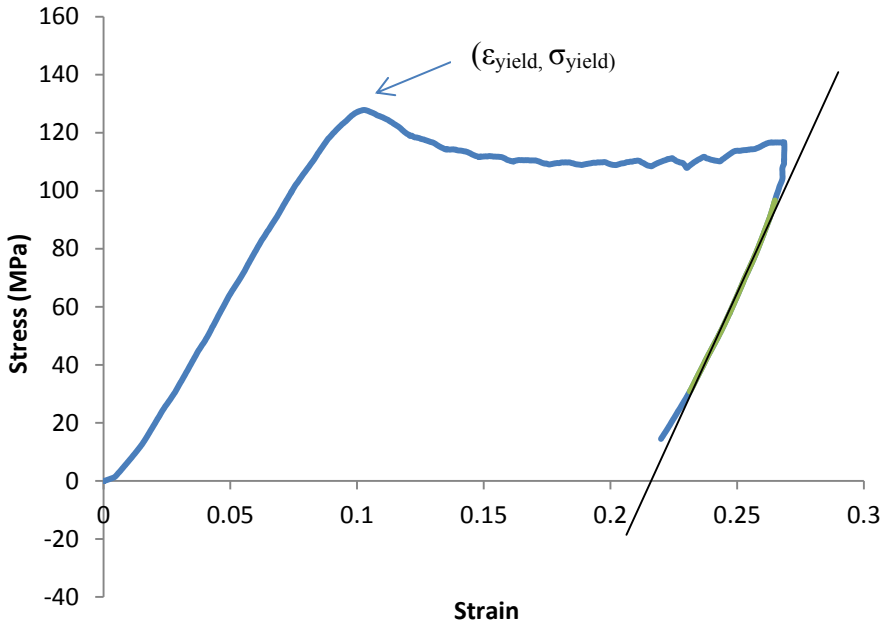

Figure 27: Loading and unloading stress strain curve for RT cured DGEBA-DETA in compression, with line used for calculating elastic modulus and arrow denoting yield strength marked.

Based on an average of 5 samples, the elastic modulus E of RT cured DGEBA-DETA was calculated as 1.619 ± .17 GPa. The yield strength was calculated as 126.7 ± 1.2 MPa, and yielding began at a strain of .115 ± .012. Error is the standard deviation of the data set.

The values of E and σ_{yield} are typical of glassy polymers and agree with theoretical studies suggesting that Van der Waals interactions between chains, not stretching of bonds within a chain, are responsible primarily for the resistance to deformation in the elastic region of the stress strain curve. The measured ε_{yield} is slightly higher than most glassy polymers which is an expected variation attributed to crosslinking.

4.2.2 Strain recovery

Figure 28 shows the data collected during strain recovery study of RT cured DGEBA-DET A deformed to varying true strains. The x-axis shows the ε_{def} of each sample. The y axis displays the amount of ε_{pl} remaining after relaxation, and the amount of ε_{an} that was recovered after heating to T_g +10°C. The error bars are determined from the accuracy of sample dimension measurement, propagated through the true strain calculation.

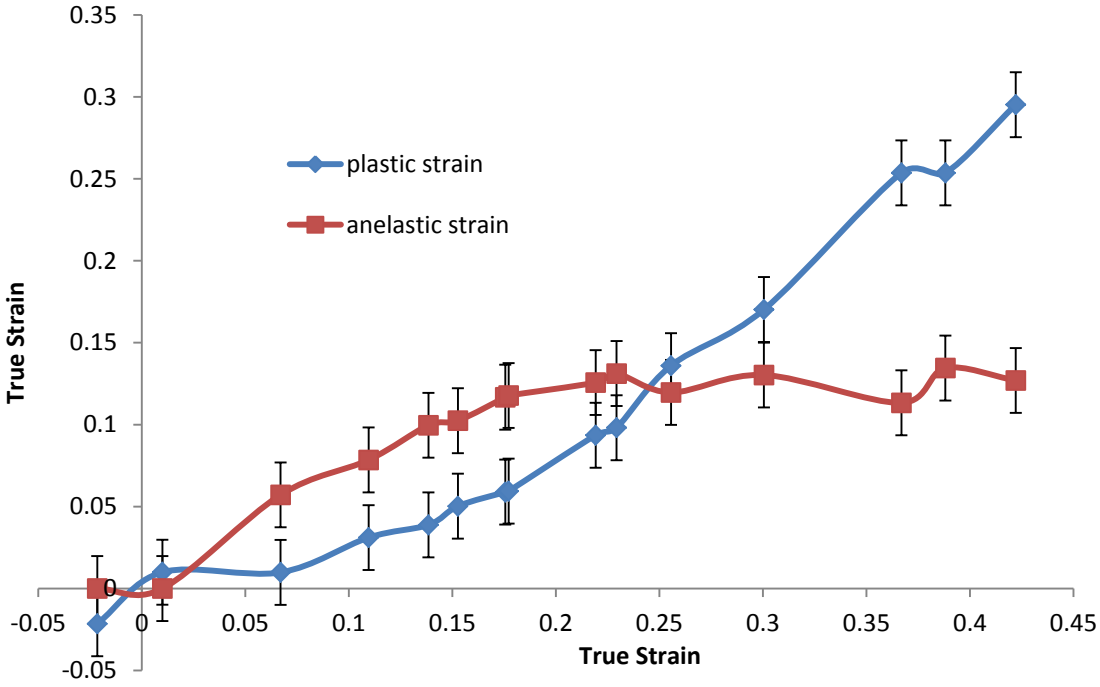

Figure 28: Measured values of ε_{an} and ε_{pl} for varying amounts of ε_{def} in RT cured DGEBA-DETA deformed in uniaxial compression.

As suggested by the study in (38) the anelastic strain reaches a maximum at ε_{def} ~.15 and does not increase further with increasing deformation. The measured deformation is mostly anelastic until plastic deformation begins at ε_{def} ~ .05-.10. Plastic strain increases approximately linearly as deformation increases after ε_{def} ~.10-.15.

4.2.3 DSC of deformed samples

The DSC curve of an undeformed sample of DGEBA-DETA and the curves of samples of varying levels of deformation are shown in Figure 29. These measurements are similar to the ones in Figure 16 (34).

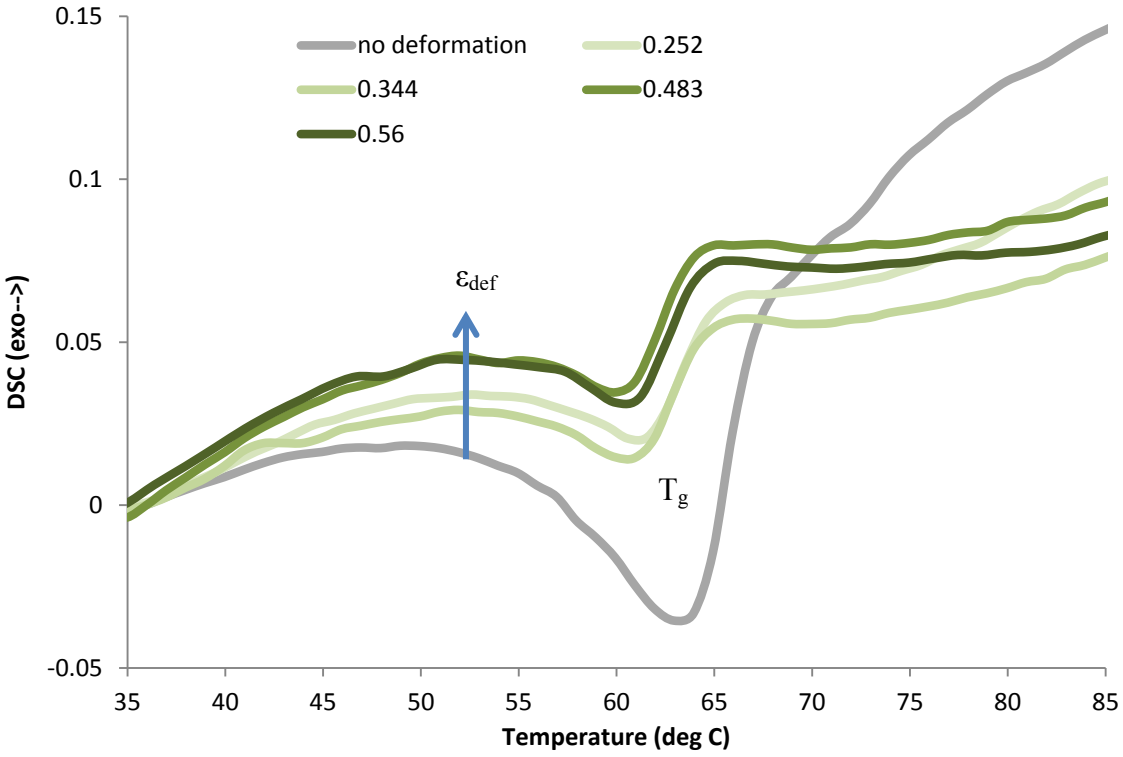

Figure 29: DSC curve near Tg of undeformed and deformed samples of RT cured DGEBA-DETA.

Samples show increasingly exothermic behavior at temperatures immediately below and above T_g as the level of true strain increases. This result agrees with other DSC and deformation calorimetry studies of glassy polymers and of epoxy in particular (34). This behavior has been taken as an indication that deformation increases the internal energy of the epoxy sample in a significant quantity. The exothermic change in samples with deformation is noticeable at temperatures ~ 40°C (T_g - 20°C = 36.9-42.6°C), which is consistent with the temperatures at which ε_{an} recovery becomes significant on a timescale consistent with laboratory work.

4.3 Optical properties

The optical properties including the fluorescent excitation/emission, absorbance, and in-situ fluorescent emission of solid DGEBA-DETA are very important to the study of the mechanochromic behavior of probe molecules in DGEBA. This section presents the results of studies of these properties on solid DGEBA-DETA. In addition, the changes that heat exposure and mechanical deformation can cause in DGEBA-DETA optical behavior are important since these stimuli will be used to evaluate the mechanochromic response in future work.

4.3.1 Excitation and emission spectra

The excitation and emission spectra were collected using the method described in sec. 2.2.3.2. Figure 30 shows the excitation and emission spectra of DGEBA-DETA.

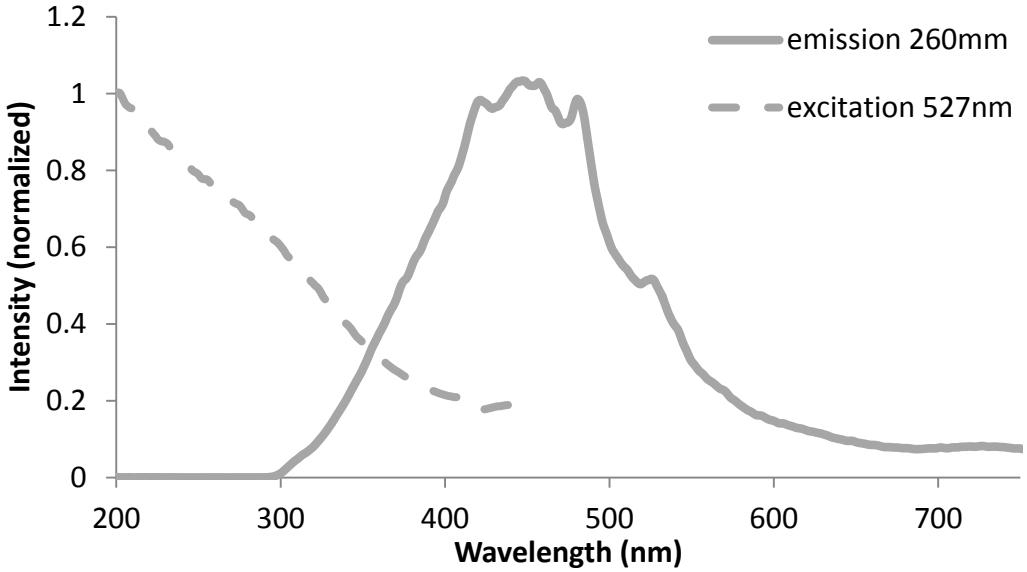

Figure 30: excitation and emission spectra from DGEBA-DETA. Legend has the excitation and emission wavelengths.

The excitation spectrum shows a featureless excitation in the UV wavelengths. Excitation at 260nm causes emission with several peaks in the region between 400 and 500nm (418, 438, 451,

479, 517nm), with very little emission above 550nm. These results will be used as references for the in-situ fluorescent emission studies presented below.

4.3.2 Absorbance

Figure 31 shows the absorbance curve of a DGEBA-DETA sample. The solid DGEBA-DETA absorbance is essentially unchanged from the absorbance during cure, a featureless curve that increases at lower wavelengths (see Figure 25).

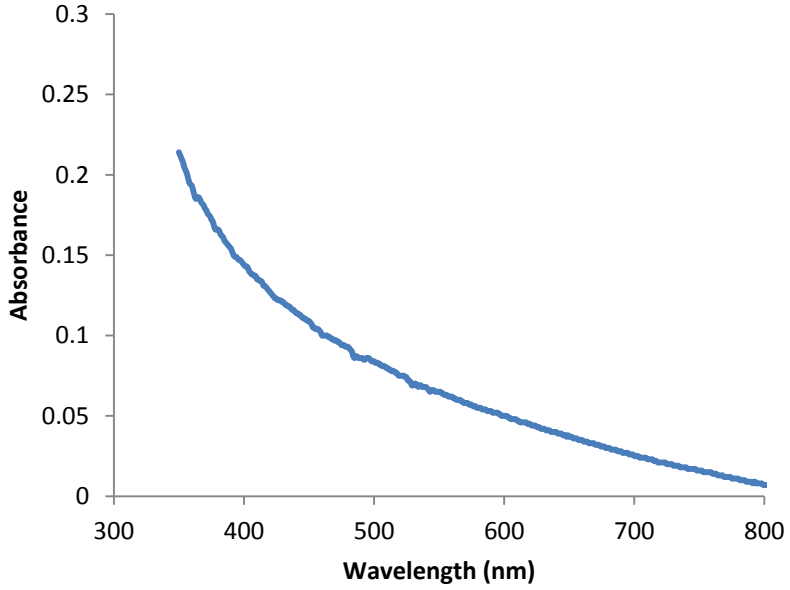

Figure 31: Absorbance of DGEBA-DETA with x=1.

4.3.2.1 Effect of stoichiometry on absorbance

The effect of varying the stoichiometry of DGEBA-DETA on the absorbance is shown in Figure 32 below. The absorbance spectra show an increase in absorbance at ~375nm as χ increases, which is partially obscured by the overall absorbance increase of epoxy at low wavelengths compared to high. This increase is monotonic with increasing amine content.

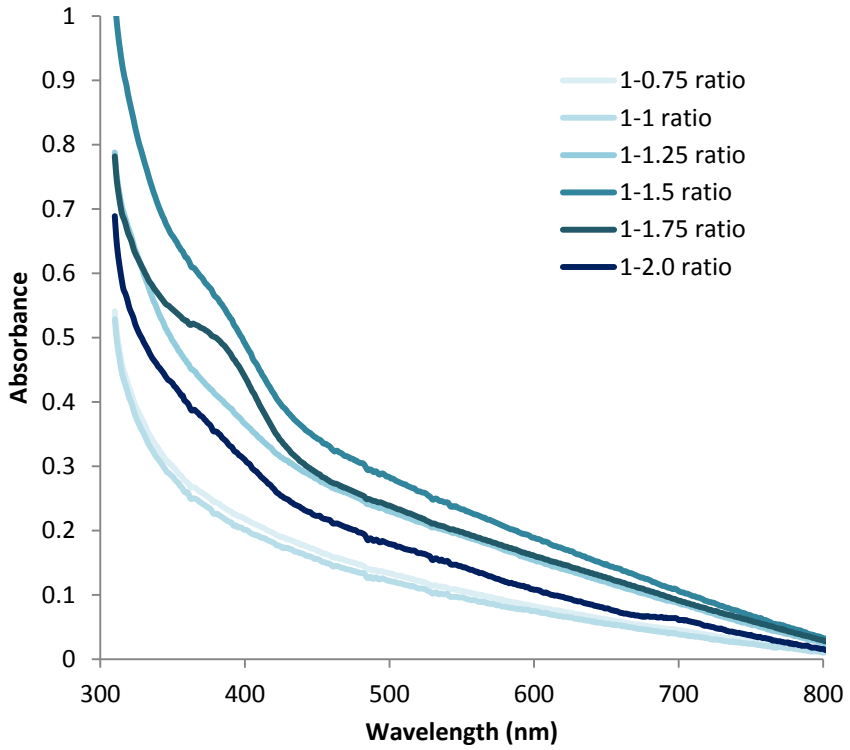

Figure 32: Absorbance of DGEBA-DETA for varying χ.

4.3.2.2 Effect of heat on absorbance

The effect of heat on DGEBA-DETA absorbance is dependent on the amine-to-epoxide ratio as well. Samples with $\chi>1$, which show the absorbance peak at 375nm, show an increase in absorbance after heat exposure to 100°C for 24hr. Figure 33a shows this effect.

Because the peak is overlapping an area where both the bulk sample's absorbance and rate of change of absorbance is changing, quantitative analysis of this change requires some possibly suspect interpretations. Our technique is to fit a line between the upper and lower wavelengths of the absorbance peak, ~436nm and 350nm, and integrate from that line up to the absorbance peak. Figure 33b shows these values before and after heating to 100°C. Negative values show the sigmoidal shape of the curve extending below the linear approximation, while positive values show the peak growing to extend above the line. Samples with $\chi>1$ show an increase in the peak while samples with $\chi<1$ do not show any activity or a decrease in the peak.

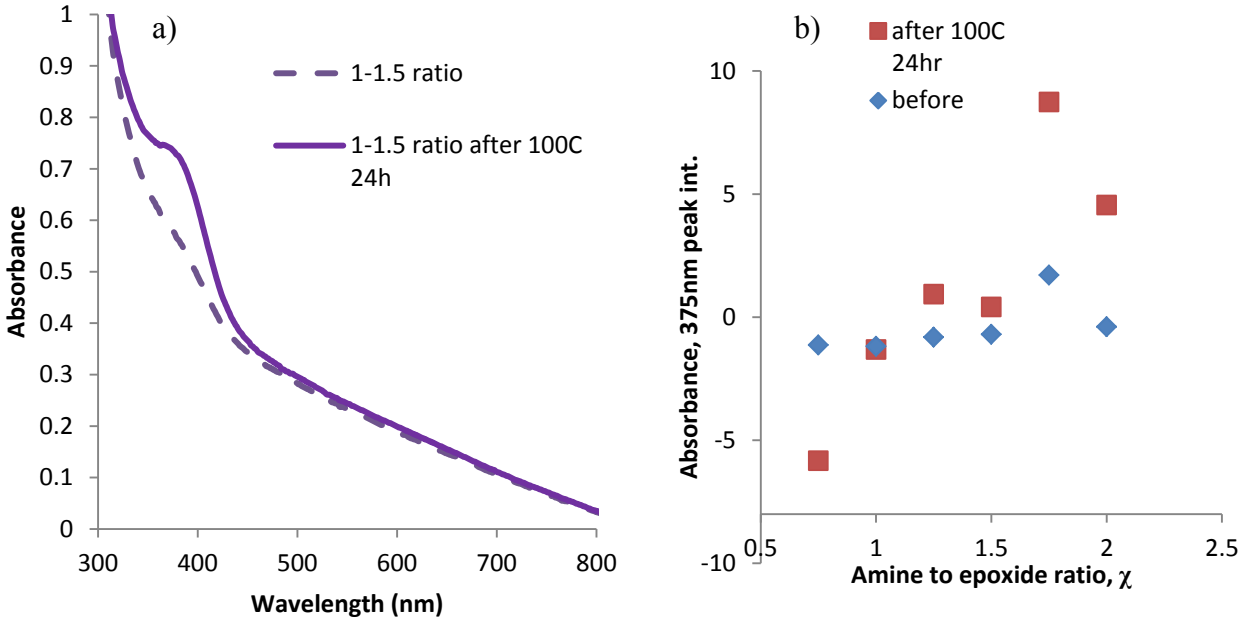

Figure 33: Absorbance change due to heat a) sample with x=1.5. b) integrated absorbance for 377nm peak for varying χ.

4.3.2.3 Effect of uniaxial compression on absorbance

The effect of uniaxial compression to varying levels of ε_{def} on DGEBA-DETA absorbance is shown in Figure 34. The absorbance of DGEBA-DETA is reduced in the UV and visible ranges as compressive strain increases. A possible increase in absorbance can be seen at ~700nm; however this could also simply be the lack of a decrease at this wavelength since the spectra above 700nm track closely with the unstrained spectrum.

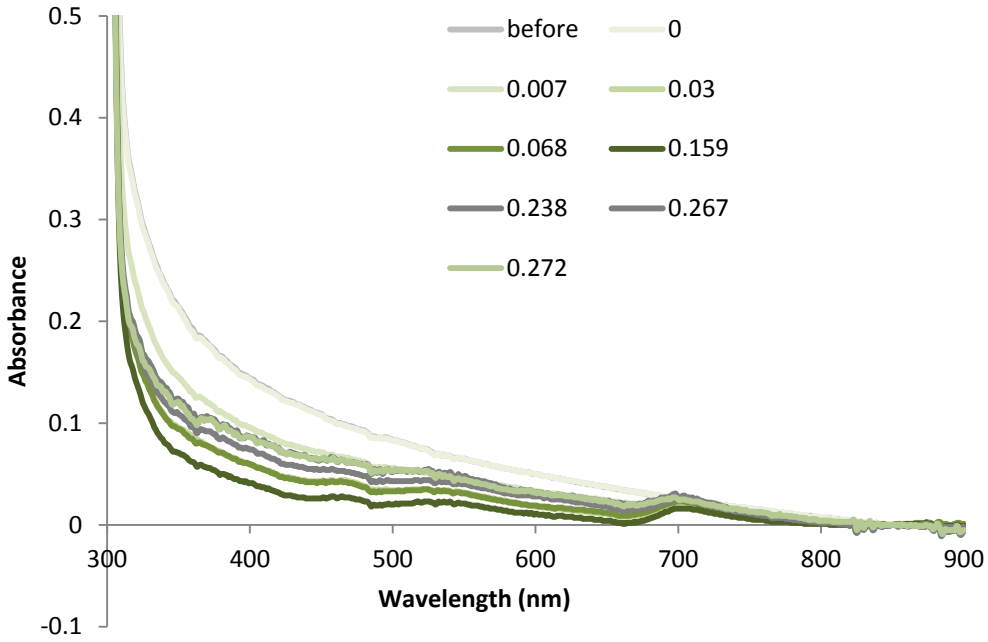

Figure 34: Absorbance spectra of DGEBA-DETA samples compressed to varying $\varepsilon_{def.}$

While the absorbance of all strained samples is less than the unstrained sample, the trend is not monotonic with increasing strain. The largest decrease occurs for the sample with ε_{def}~.159, which is very near the beginning of ε_{pl} formation. After this the absorbance values increase again. This could be an artifact of the decreasing thickness of samples, which reduces absorbance according to the Beer-Lambert Law. The absorbance changes could also be due to the morphological changes associated with increased ΔU_{def} or shear defect nucleation, though no reason is apparent.

4.3.3 In situ emission

Emission data was collected using the method in Chapter 1section 2.2.3.3 using a390nm LED illumination. The emission of DGEBA-DETA with χ=1 is shown in Figure 35. One emission peak is observed, with a maximum emission wavelength of 505nm due to 390nm illumination.

Using the spectrometer with probe tip instead of the fluorimeter setup (compare spectra with Figure 30), the measured emission shows less defined peak structure. The emission covers roughly the same wavelength range.

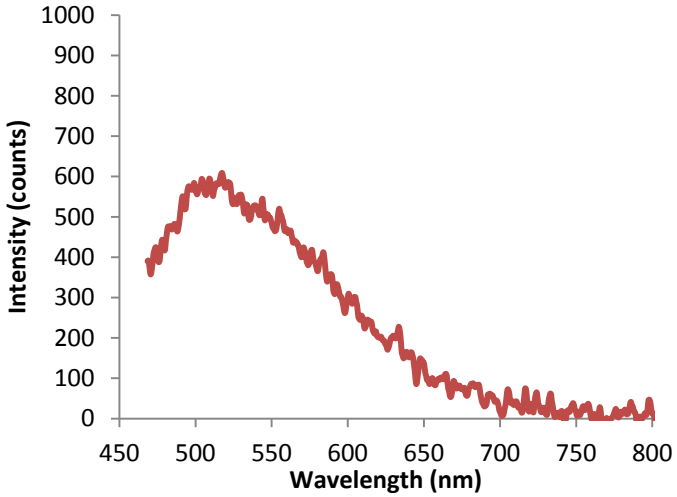

Figure 35: Fluorescent emission of DGEBA-DETA X=1.

4.3.3.1 Effect of stoichiometry on emission

The emission behavior shows a great deal of change with changes in χ, as seen in Figure 36. The emission increases as χ increases, and the peak structure resolves into a dominant peak at ~505nm and a smaller peak at ~437nm. This is consistent with illumination in the higher wavelengths of the excitation spectrum, which would logically excite the lower-energy emission peaks more strongly.

4.3.3.2 Effect of heat on emission

The effect of heat on the emission of DGEBA-DETA when illuminated by 390nm excitation light is shown in Figure 37a, which shows the change in emission due to 100°C exposure, and Figure 37b, which shows the peak emission intensity change due to heat for different χ values.

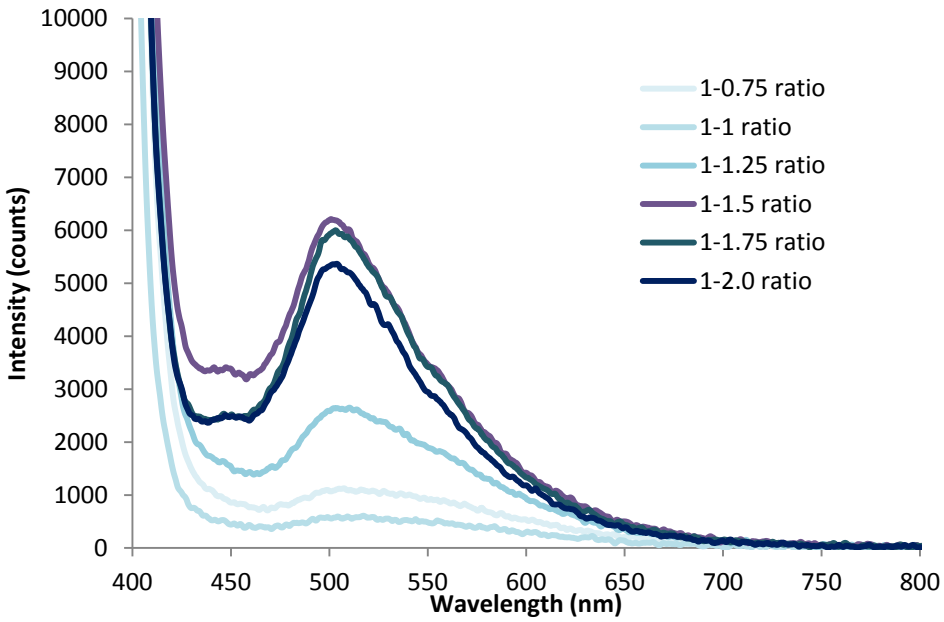

Figure 36: Fluorescent emission of DGEBA-DETA with varying χ.

The change in emission is a uniform increase in peak intensity at the ~505nm peak. The increase becomes stronger as χ increases.

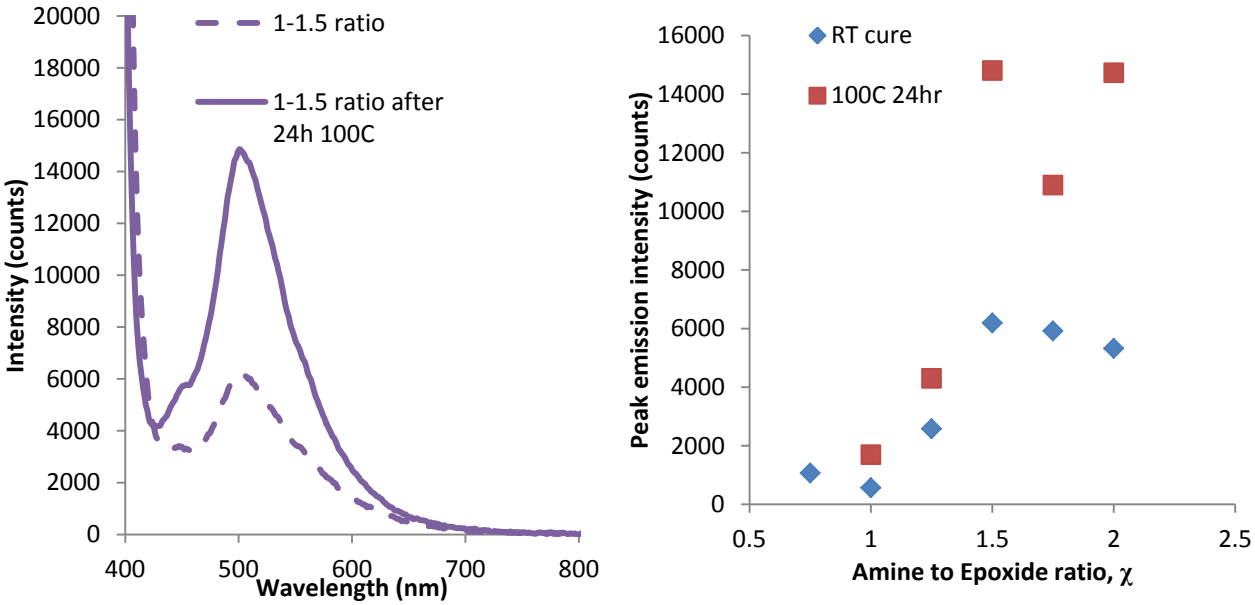

Figure 37: Change in emission due to heating at 100C for 24hr. a) Emission spectra change for X=1.5. b) Peak emission intensity change for varying χ.

4.3.3.3 Effect of uniaxial compression on emission

The change in emission with respect to increasing ε_{def} is shown in Figure 38 for DGEBA-DETA with χ=1. The emission intensity and peak wavelength changes are negligible, within experimental error, due to increasing $\varepsilon_{def.}$ No peak resolution in the emission spectra are observed. While absorbance changes were observed, emission was unchanged with $\varepsilon_{def.}$

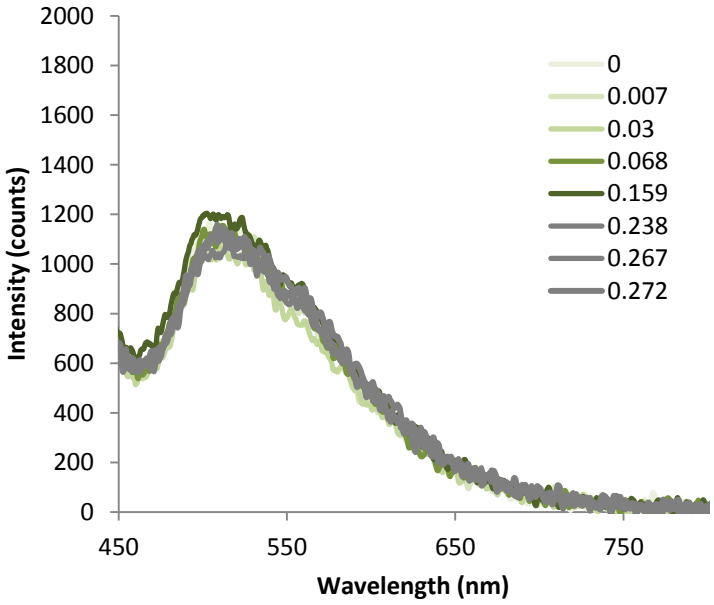

Figure 38: Fluorescent emission of DGEBA-DETA with varying levels of ε_{def}.

4.4 Summary

Table 3 has a summary of the properties characterized in the research presented in this section.

Table 3: Relevant Properties of RT cured DGEBA-DETA, χ=1.

Elastic Modulus, E (GPa)	1.619 ± .17
Yield Strength, σ_{yield} (MPa)	126.7 ± 1.2
Yield Strain, ε_{yield}	.115 ± .012
Degree of Cure, α [DSC], ***[FTIR]***	0.67, ***0.576***
Glass Transition, Tg (°C) [DSC] ***[DMA]***	62.6 ± .754 , ***56.9 ± .689***
Peak Absorbance, nm	375 (χ>1.1)
Peak Emission, nm (390nm excitation)	505

The measured E, ε_{yield} and σ_{yield} are consistent with literature reports of the properties of glassy amorphous polymers and with experiments that suggest the elastic region of the stress-strain curve is determined primarily by stretching of secondary Van der Waals type bonds between chains.

The low values of α_{final} measured by DSC and FTIR suggest that a relatively low crosslink density is to be expected from RT cured DGEBA-DETA compared with other epoxies. When compared with Figure 10 and the surrounding discussion, this confirms that DGEBA-DETA should develop ε_{def} via yielding processes rather than crazing processes.

The values of T_g measured with DSC and DMA suggest that relaxation events should be expected at temperatures of ~40°C and above. DSC measurements of deformed samples

indicated an increase in the exothermic energy release beginning at temperatures ~40°C, and were not observed in samples strained below ε_{def} ~.15. These results are consistent with current theories about epoxy deformation, shear defect formation, and internal energy storage.

Measurements of the recovery of samples heated to 70°C showed the onset of ε_{an} at strains of ε_{def} ~.15.

The absorbance and emission spectra of DGEBA-DETA with χ=1 were collected, and the changes due to variation in χ, heat exposure, and ε_{def} were determined. Table 4 summarizes the changes in absorbance and emission due to these conditions.

Table 4: Summary of changes to absorbance and emission of DGEBA-DETA.

Property	**Increase in χ**	**Heat exposure**	**Increase in ε_{def}**
Absorbance	Increase, 375nm peak develops (χ>1.1)	Increase (χ>1.1)	Decrease
Emission	Increase, peaks resolve	Increase	No Change

This data will help to explore the behavior of the probe molecules AJNDE15 and AJNDE17, which will be explored in Chapter 2.

CHAPTER 2

MECHANOCHROMIC PROBES IN EPOXY

1. INTRODUCTION

In this chapter, mechanochromism in solid polymers will be introduced. The mechanisms reported in literature to date for mechanochromism in solid polymers will be discussed.

A new mechanism for mechanochromism developed by this research project and designed specifically for use in DGEBA-DETA structural epoxy will be presented, and will be compared with the established mechanisms reported thus far.

1.1 Approach # 1 - Aggregation-based mechanisms

If two probe molecules are in very close proximity to one another they may share the energy of an absorbed photon between them in a manner similar to Dexter energy transfer (see Introduction section 2.1) by merging their electron density to form an excimer complex (when two identical molecules are involved, the excimer is commonly called a dimer). The dimer complex absorbs the photon and is promoted to a higher energy state, which then decays as in single molecule fluorescence. The dimer complex usually emits photons of lower energy than the single molecule, called in this context a monomer. This phenomenon is also termed *aggregation*.

The fluorescence behavior of most dye molecules is quenched by aggregation – the dimer formation is much more likely to return to the ground energy state via a non-radiative energy transition than by emitting a photon (49). However, fluorescent emission from aggregate states is exhibited strongly in molecules with an intrinsic dipole moment and highly populated π orbital

structures such as benzene rings and conjugated chains. An illustrative case is pyrene, a molecule with a planar structure of several benzene rings and highly active π structure above and below the molecular plane. Figure 39a shows the absorption spectrum of pyrene as a monomer and as a dimer, with Figure 39b showing the energy levels of pyrene monomer and excimer absorption as a function of distance between molecules. When the distance becomes close enough it is energetically favorable for the dimer state to absorb photons and emit at the longer wavelengths shown in Figure 39a (50; 51).

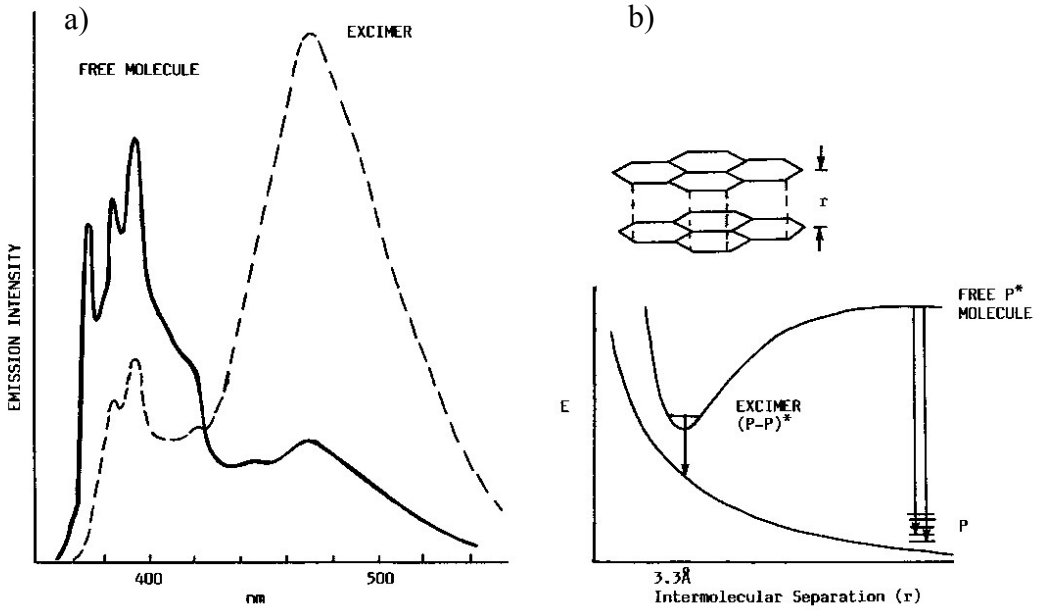

Figure 39: left: emission of pyrene monomer (solid) and excimer (dashed). right: Energy levels of ground to excited state transition of monomer P* and excimer (P-P)* vs intermolecular separation. From (50; 51).

Dimers can only form when two molecules are in very close proximity (1-5Å), so their formation is especially dependent on their local environment. In non-polar liquid solutions which do not interact with the dye molecules, aggregation is strictly a function of concentration, with dimer activity increasing as concentration increases. The lifetime of the excited state is on the order of 10^{-7}s, which dictates that the concentrations in liquid must be on the order of $10^{-4} – 10^{-3}$ mol/L to achieve the necessary proximity (50). The overall aggregation state can be determined for the

solution by comparing the magnitude of activity (whether absorbance or emission) of the monomer state to that of the dimer state, with the dimer state more active when aggregation is highly prevalent.

For probe molecules in solid polymers the overall aggregation state depends on many factors. One of these factors is obviously concentration, but the surrounding polymer network characteristics also play a large part. Most importantly for our research, the aggregation state of some molecules can be influenced by mechanical deformation of the surrounding bulk polymer.

1.1.1 Aggregation-based mechanochromism

Research has demonstrated several molecule types that show deformation induced fluorescence changes in solid polymers based on aggregation. One early example explored copolymers of poly (methyl methacrylate) (PMMA) and 1-naphthyl methyl methacrylate (NMMA) (52). Naphthalene is a molecule with known sensitivity to aggregation; incorporating it into PMMA chains enabled excimer formation between naphthyl units on adjacent chains. When the bulk polymer was elongated, initial excimers were pulled apart during the deformation, while new excimers formed at sites newly in close proximity. Figure 40a has a schematic of the excimer

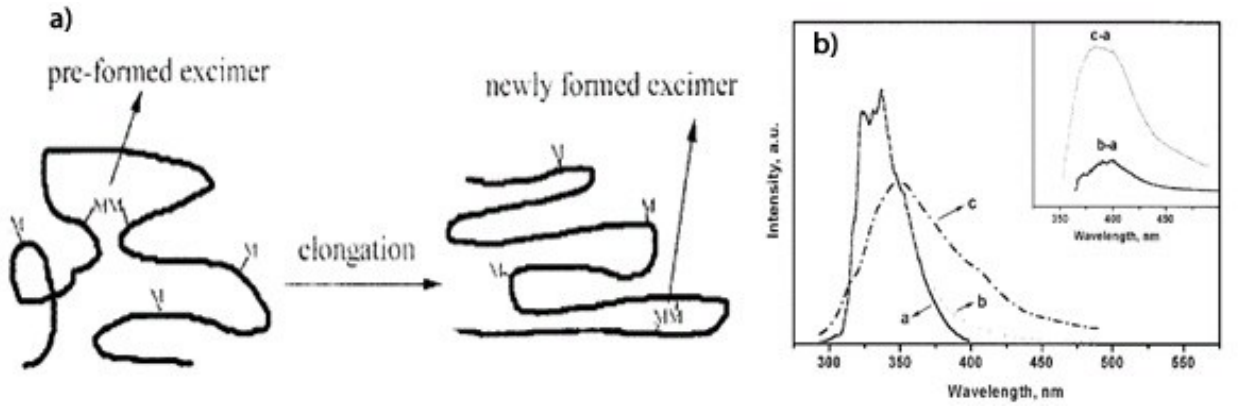

Figure 40: a) Schematic of excimer interaction before and after PMMA elongation. b) a-monomer emission c-excimer emission of naphthalene in PMMA chain. From (52).

interaction before and after elongation, while Figure 40b shows the excimer emission spectrum of naphthalene compared to the monomer spectrum.

PMMA-NMMA copolymer films were uniaxially deformed in tension while fluorescent emission spectra were collected under UV illumination. Figure 41a shows a schematic of the test setup, while Figure 41b shows the collected spectra at several levels of strain. To analyze the

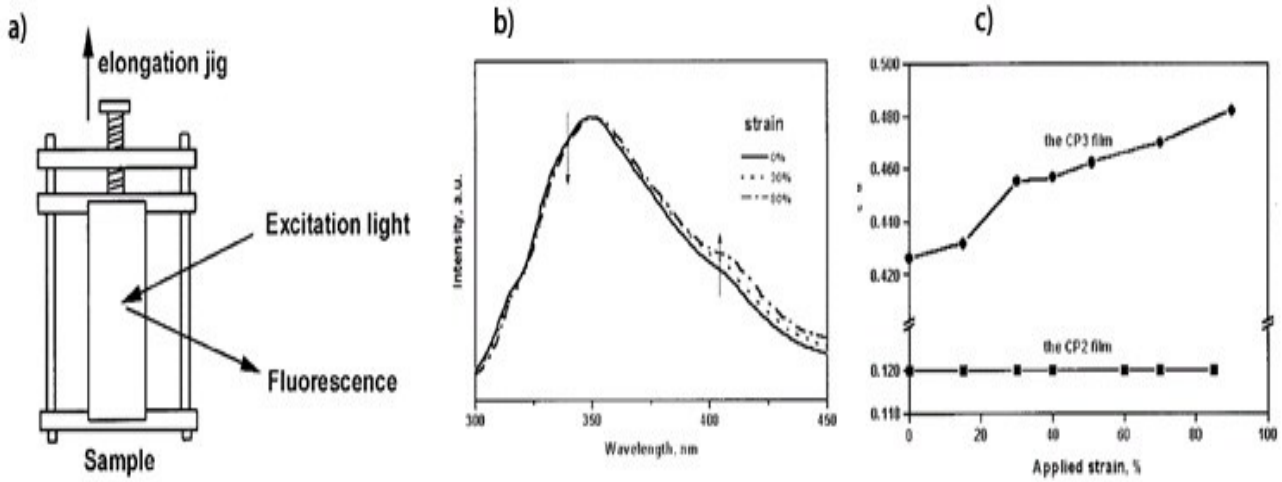

Figure 41: a) Schematic of test setup for elongation of PMMA-naphthalene films. b) emission spectra vs. strain for N-PMMA films. c) Intensity ratio for N-PMMA films. From (52).

excimer to monomer ratio, Yang and co-authors noted that the ratio of the emission intensity of the monomer I_m (for naphthalene Yang et.al. chose 337nm) to the intensity of excimer I_e (447nm) should reflect their relative concentrations. A plot of these ratios for films of two concentrations of NMMA is in Figure 41c. At an appropriate concentration, shown in the data at the top of Figure 41c, this ratio changes with strain, showing increased monomer activity as strain increases.

Of particular note is work done by the Weder group using as fluorescent molecules cyano-modified oligophenyline-vinylidene (cyano-OPVs). The emission wavelengths of cyano-OPVs in the monomer and dimer states are dramatically different, making them very well suited for

optical aggregation studies. These molecules were incorporated into ductile solid polymers via melt processing, with control of the concentration and processing to promote formation of nano-scale aggregate states. As the bulk polymer network deforms, molecular shear mixing as the polymer chains pass by one another breaks up the probe aggregates, causing the overall aggregation state to display more monomeric character (53). Similar results were obtained when probe molecules were bound onto polymer chains, then bulk polymers were deformed in tension. Chain motion moved the bound probes away from one another as tensile strain increased, reducing excimer formation and increasing monomer character.

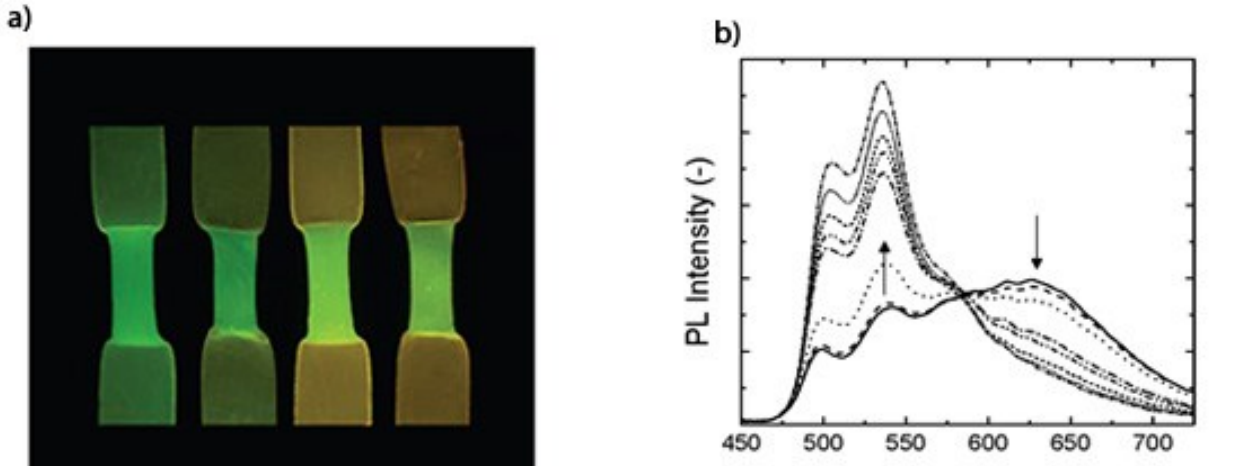

Figure 42: a) tensile LLDPE specimens with cyano-OPVs. b) Emission spectra with arrows showing changes as deformation increases. From (54; 53).

Figure 42a shows an example of a cyano-OPV molecule in a linear low-density polyethylene (LLDPE) tensile specimen under UV excitation, while Figure 42b shows the emission spectra of the necking region of the tensile as stress increases (54). In this case, the cyano-OPV has dimer emission in the red wavelengths and monomer emission in the green. A dramatic shift in emission spectra between the monomer and dimer complexes resulted in red fluorescence from the dimer emission in unstressed areas of the tensile bar, and green emission (monomer fluorescence) in the highly deformed areas. Other research has observed aggregation induced

quenching or increased emission due to local probe proximity changes as the sample with probes incorporated is deformed (53).

This research was conducted using linear low density polyethylene (LLDPE), a semicrystalline thermoplastic polymer of low modulus and high free volume at room temperature. LLDPE is capable of very high elongation in tension, and in this case changes in cyano-OPV fluorescence were reported for values of strain in excess of 300-500%. The aggregation based approach to deformation sensing polymer probes will be dependent on the degree of deformation that a sample has achieved. All indications point to a high degree of deformation required to physically change the aggregation state of a probe molecule.

1.2 Approach #2 – Intramolecular isomer mechanism

The mechanism in this approach is based on the conformational transitions of chemical bonds in response to mechanical force. A diagram of one such transition is in Figure 43. The bond in this figure is a cis-trans rotation around a double bond. The dashed lines outline the volume required for such a transition. Probes based on this type of molecule are often referred to as 'molecular rotor' type probes. Other mechanochromic probes take advantage of twisted intramolecular

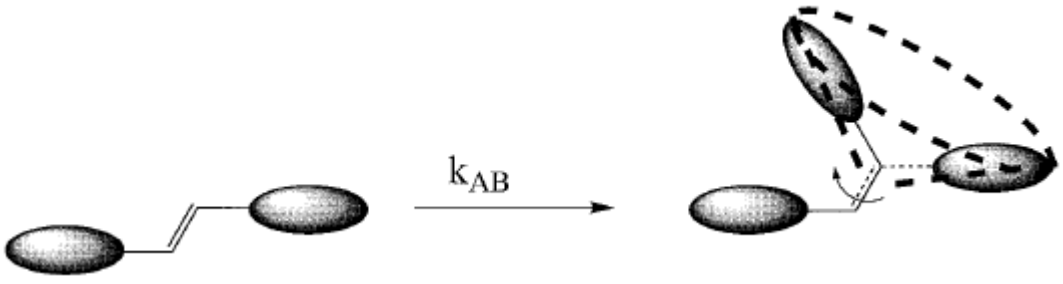

Figure 43: Cis trans transition of a 'molecular rotor' type probe. From (55).

charge transfer (TICT) as a rearrangement method between conformations. To be useful as a mechanochromic probe, the molecule must have different fluorescence characteristics in the two

transition states, and the transition between them must be dependent on the mechanical force or deformation. Free volume in solid polymers is changed by mechanical deformation and therefore a probe sensitive to free volume can be mechanochromic in nature.

Probes using the intramolecular isomer approach have been used to monitor the free volume within epoxy polymers during curing. One such probe is DASPI ((4-dimethylaminostyryl)-2-ethyl-pyridinium oxide), shown in Figure 44a. This probe has excited TICT states which twist

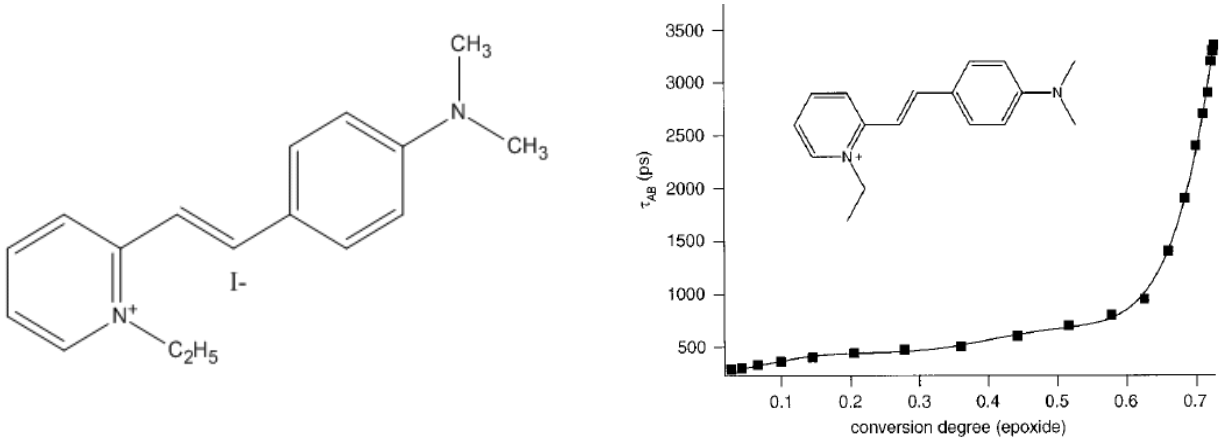

Figure 44: a) Molecular structure of DASPI free volume probe. b) DASPI Fluorescence lifetime vs. degree of cure of epoxy matrix. From (55).

around the single and double bonds between the ring structures. When mixed into epoxy before curing, the transition from one isomer to the other is initially rapid, due to the high free volume in the liquid. As the epoxy cures, free volume is reduced and the transition speed becomes slower. A plot of the transition rate constant vs. degree of conversion of the surrounding network is shown in Figure 44b, showing the transition time slowing as free volume reduced during cure. This measurement of cure behavior correlates very well with other methods such as sol-gel and dynamic mechanical analysis (55).

The characteristic most polymer free volume probes, including DASPI, use is the fluorescence lifetime, or rate of fluorescence decay. This transition occurs faster in polymers of larger free

volume. A version of this probe for the application of mechanical damage would have two configurations, OFF and ON, which have easily identifiable differences in fluorescent emission. The probe molecule would preferentially form the OFF or ON state based on the free volume of its surroundings, and would therefore respond to bulk mechanical deformation due to the deformation's effect on the polymer free volume.

1.2.1 Free volume in polymers

The free volume V_f is defined as the volume in a bulk polymer sample that is not permanently occupied by molecules (56; 57; 58). The free volume can be used to understand many important polymer properties such as freezing - a polymer has large free volume in liquid state and as it cools, free volume decreases until it is small enough to inhibit chain motion, at which point the polymer solidifies. The relationships between free volume and important polymer properties such as chain mobility (V_f increases as chain mobility increases), molecular weight (V_f decreases as molecular weight increases), and crystallinity (V_f decreases as crystallinity increases) are all intuitive and have been studied extensively (56; 57; 58). Other relationships are less intuitive, however, and those that are important to this research will be discussed more thoroughly when necessary.

The free volume concept has several drawbacks. Free volume is difficult to measure directly, with only positron annihilation loss spectroscopy (PALS) claiming to be a direct measurement technique. In this technique, ortho-positronium atoms from a radioactive source are passed through the solid polymer. The positrons exist preferentially in vacuum, and so in a polymer will congregate in the free volume. The positron lifetime is a measure of the size of the free volume hole in which the positron decays, while the intensity of positrons passing through the sample is

a measure of the number of free volume holes. In this manner a profile of the free volume in a solid polymer can be developed, which can be summarized by the average hole radius and the size distribution of the holes. It is difficult to quantify changes across variations in polymer systems because of the mismatch between geometric free volume and the free volume for molecular movement for different molecules. Nonetheless, free volume is a unifying way to discuss the interactions between a fluorescent probe molecule and the solid network polymer around it.

1.2.2 Epoxy free volume

Epoxy free volume has been studied by a variety of methods, but the most direct method is by positron annihilation lifetime spectroscopy (PALS). The average radius of holes in cured epoxy are generally on the order of 1-5Å, with maximum hole volumes reaching as high as 150Å according to some measurements. Free volume also varies as a number of bulk properties of the polymer are changed including plastic deformation and temperature.

1.2.3 Intramolecular isomer probes - mechanochromism

The behavior of an intramolecular isomeric probe in a solid polymer is highly dependent on the polymer's free volume characteristics, as has been demonstrated in many works (55; 59). Mechanical deformation has been shown to cause changes in the free volume characteristics of many solid polymers, which would cause an intramolecular isomer to display mechanochromic behavior changes.

Deviatoric stress on a glassy polymer can cause changes in both the size and density of free volume holes (60). Plastic deformation is thought to occur in glassy polymers through localized shear transformations in areas with high free volume. These transformations increase the free

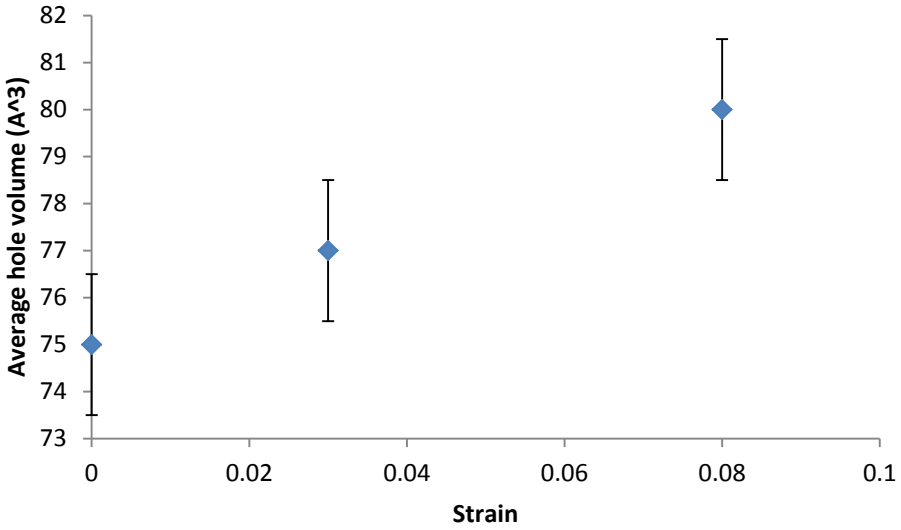

Figure 45: Average free volume hole volume for varying compressive strains in epoxy. From (60; 61).

volume hole size as they occur. The effect of uniaxial compressive loading in particular has been shown to cause an increase in hole volume size. Results of free volume hole sizes collected after plastic deformation of epoxy samples are shown in Figure 45 (60; 61). The effect of hydrostatic compressive pressure cause both a decrease in free volume hole size and a decrease in the number of free volume holes (62).

In this mechanism, the intramolecular isomer's would be affected by the change in free volume hole size brought about by mechanical damage and would therefore display mechanochromic character.

1.3 Approach #3 – Mechanochemical reaction mechanism

Mechanochemical reactions are a type of reaction where mechanical force or stress promotes reactions that would otherwise not readily occur. There are examples of mechanochemical reactions in many fields including biology and metallurgy (63). Two important examples of mechanochemistry in solid polymers are stress-induced homolytic chain scission and photodegradation of polymer films (63; 64). Polymer chains under large amounts of mechanical stress will undergo chain scission, preferentially at the middle bond of the polymer where internal friction stresses are highest. In photooxidation of polymer films, the rate of the photooxidation reaction is greatly increased by mechanical strain on the polymer. Experimental

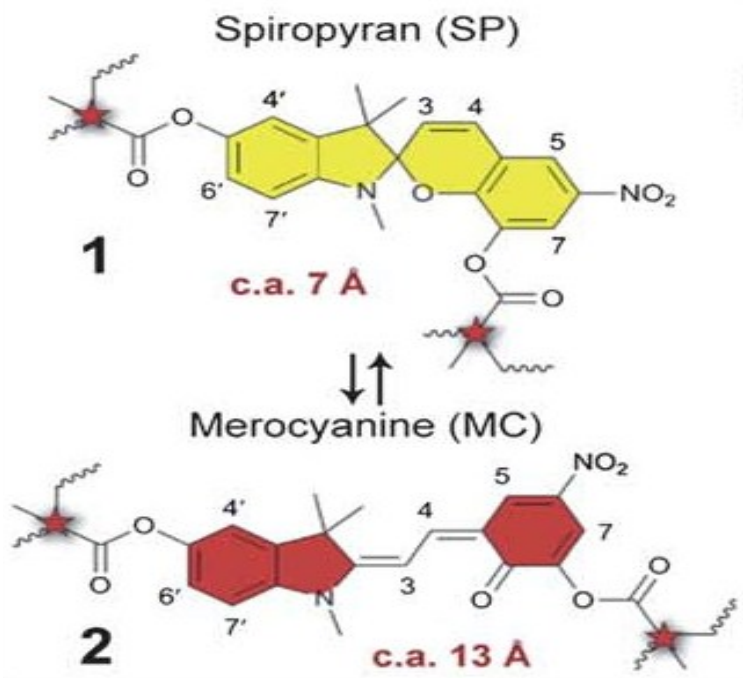

Figure 46: Spiropyran to Merocyanine transition. From (66).

results suggest that the strain on the polymer chains reduces the recombination of radical chain ends after hemolysis of a chain due to UV light exposure (65).

1.3.1 Mechanochemical reaction - mechanochromism

Mechanochemical reactions can cause mechanochromic changes within probe molecules in solid polymers as well. One example of a probe molecule type that has this type of behavior is spiropyran. Mechanical stress can cause the transition around carbons 3 and 4, which changes the molecule into a merocyanine as shown in Figure 46. Spiropyran has yellow color and little fluorescent emission, while merocyanine has purple color and high fluorescent emission (66). Researchers have covalently bound a spiropyran molecule at both ends within chains of poly (methyl acrylate) (PMA) and poly (methyl methacrylate) (PMMA). Solid dogbone specimens of the polymer were then loaded in tension in a creep-like deformation. As polymer chains extended, the molecule transformed from spiropyran to merocyanine form. Figure 47a has a schematic of the approach, while Figure 47b shows images of the spiropyran to merocyanine transition visible as the bulk PMA specimen is deformed. The transition was quantified

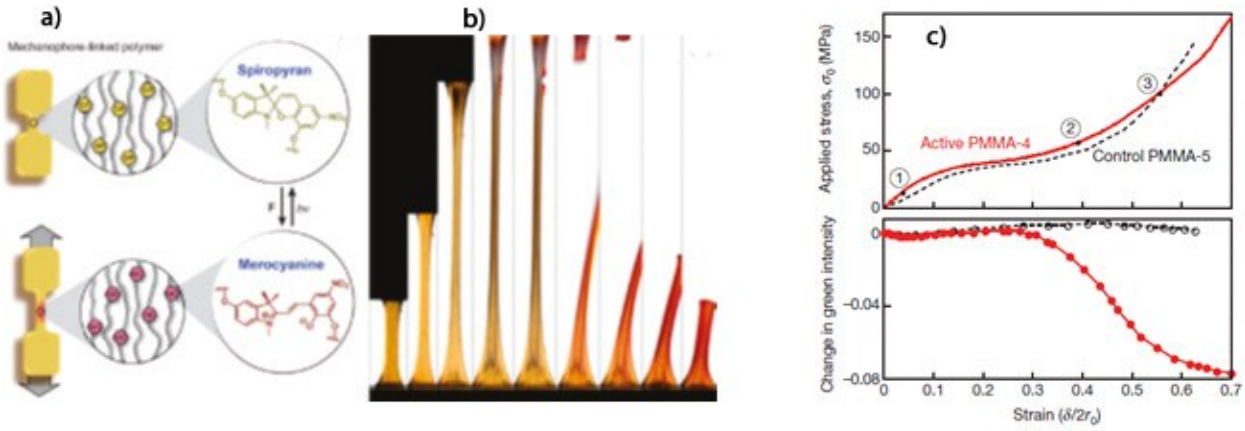

Figure 47: a) Schematic of spiropyran-merocyanine transition in solid polymer tensile specimen. b) Images of tensile specimen under stress showing yellow to red transition. c) Data showing decrease in green intensity for PMMA spheres with probe molecules. From (66).

spectrally by measuring intensity of green-emitting wavelengths – these were observed to decrease as the spiropyran-merocyanine transition advanced in a PMMA specimen. Figure 47c has the stress-strain curves at the top, with the spectral changes shown at the bottom.

Mechanochromic reactions such as spiropyran-merocyanine are influenced by mechanical force. But the reaction must still be favorable from a thermodynamic standpoint to proceed. A recent review described the situation succinctly –

'In general, mechanical force will lower the barrier for a particular reaction…the final transition over the barrier, however, will in general be thermally activated (63).'

Zhurkov described the rate of a mechanochemical reaction with a modified Arrhenius equation

$$K = K_0 e^{\frac{-(E_A - \alpha\sigma)}{RT}} \quad \textbf{9}$$

where K is the reaction rate, K_0 the reaction rate constant, E_A the activation energy for the reaction, σ the mechanical stress, α a constant such that the product $\alpha\sigma$ has units of energy, R the gas constant and T temperature (67). The energy imparted to the molecule by mechanical stress lowers the activation energy for reaction, which will proceed at a rate determined by temperature.

Zhurkov's work described the mechochemical rupture of atomic bonds in polymers, but the mechanochemical equation has been applied to strain-enhanced photodegradation (64), milling-enhanced metal synthesis (68), and grain boundary growth in metal powders (69).

This mechanism would show increasing fluorescent activity in polymers with mechanical force, but would also be activated by elevated temperatures, which would allow the reaction to overcome the activation energy barrier and convert from OFF to ON.

1.4 Approach #4 – Scission based mechanism

In this approach the fracture of a solid polymer is used to cause chain scission within a polymer chain. The bonds that are broken in this scission cause a probe molecule's fluorescence to activate, making the molecule an effective sensor for microcracking and fracture events.

1.4.1 Scission-based mechanism - mechanochromism

Researchers have developed probe molecules which in the aggregated state are not fluorescent active, but are bound together by weak covalent bonds that can be broken by mechanically-driven chain scission. An example of this is in research by the Chung group, which used anthracene - and tricinnamate – based molecules (70; 71).

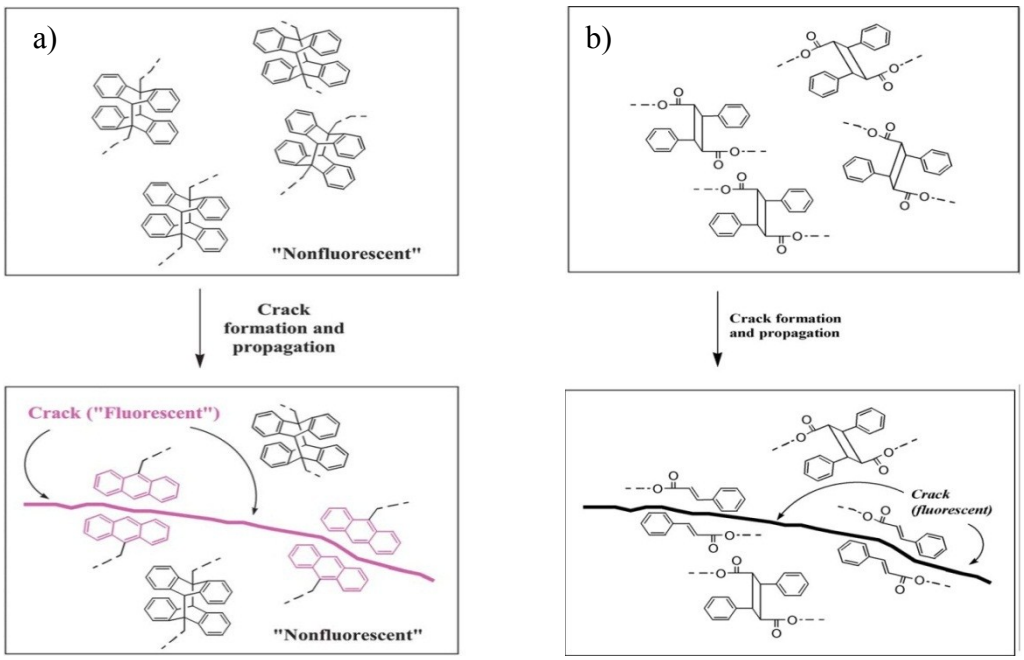

Figure 48: Fluorescent crack sensors based on a) anthracene and b) tricinnamate molecules. From (70; 71).

Figure 48a and b have schematic diagrams of the concept of crack-activated fluorescence in anthracene- and tricinnamate-based molecules.

The molecules initially are in a non-fluorescent state, bound together by cycloaddition into cyclo-octane type dimers. The bond strength of the cyclobutane carbon-carbon bond has been shown to be significantly lower than other C-C or C-O bonds due to the high ring strain. Because of this the cyclobutane bond can be expected to be among the most prevalent bonds broken as a crack propagates through a bulk polymer (71; 72; 73).

To incorporate the molecules into solid polymers for use as crack sensors, the anthracene dimers (AA) were used as crosslinking agents in the polymerization of poly(vinyl alcohol) (PVA) (70). The tricinnamate molecules were photocrosslinked into a polymer, 1,1,1 – tris(cinnamoyloxymethyl)ethane (TCE) (71). Cracks were introduced to the bulk polymers both by grinding (forming many fracture surfaces among the small particles) and by flexing solvent-cast thin films (to produce cracked and uncracked regions for comparison). Fluorescent spectra

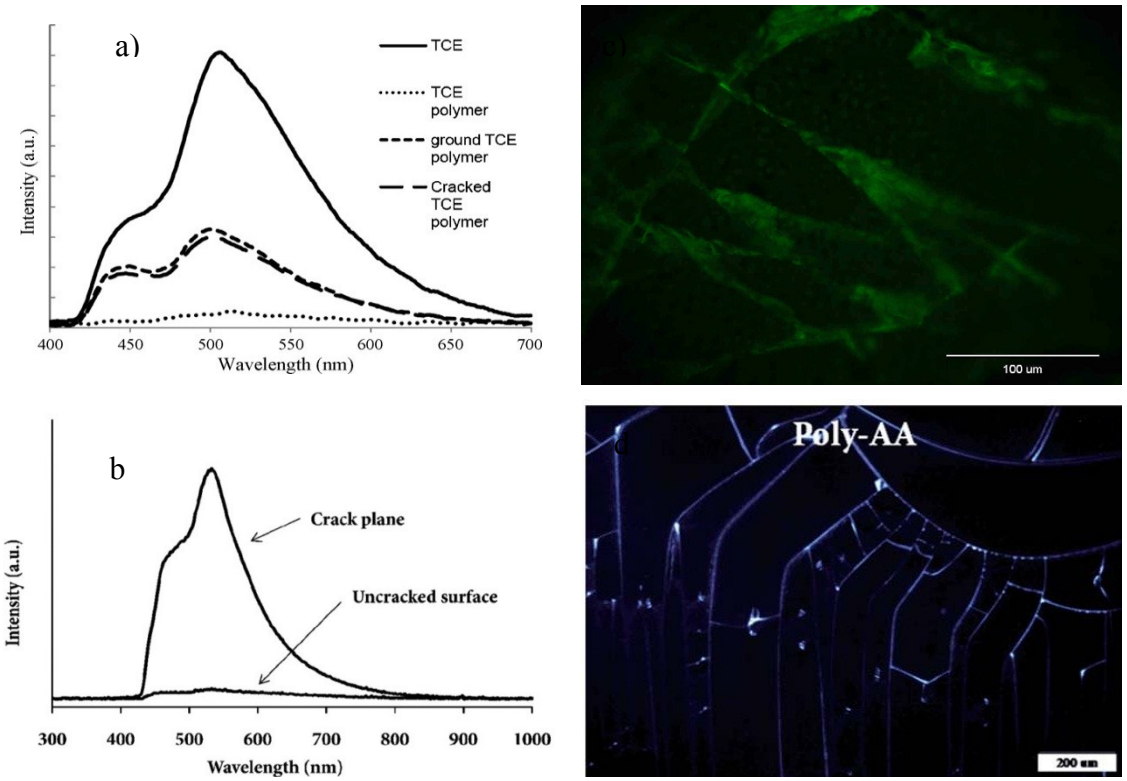

Figure 49: TCE crack sensing polymer a) emission spectra c) thin film crack images. b) PVA-AA emission spectra and d) thin film crack images. From (70; 71).

and thin-film cracked images of TCE are in Figure 49a and c, and of PVA-AA in Figure 49b and d. The images were taken with a fluorescence microscope using UV illumination.

This mechanism would show sensitivity to mechanical deformation only in that it would produce microcracks that cause scission within a molecule or between two molecules, turning the probe from OFF to ON.

1.5 Proposed mechanism – Conjugation pathway interference

This research project has developed what is thought to be a novel mechanochromic mechanism, designed specifically for use in amine-cured epoxies. Probe molecules have been designed with conjugation pathways between an electron donating group and an electron accepting group, allowing for π electron transfer and high fluorescent activity. When in contact with a primary amine group, however, a reaction between the amine and the probe along the conjugation bridge breaks the pathway, inhibits electron transfer, and quenches the fluorescence activity. A schematic of the reaction between probes and amine is shown in Figure 50. These two states are termed the ON (highly fluorescent) and OFF (quenched) states of the probe molecule.

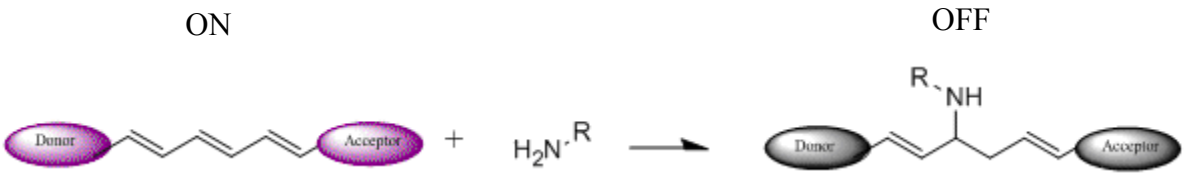

Figure 50: Proposed ON→OFF reaction of probe with amine group.

The proposed mechanochromic response of these probes occurs from the OFF state to the ON state. The application of mechanical force to the OFF molecule while it is in a polymer matrix can dissociate the C-N bond that is interrupting the conjugation pathway. The pathway's

reconnection allows the molecule to fluoresce again. The schematic of this reaction is shown in Figure 51.

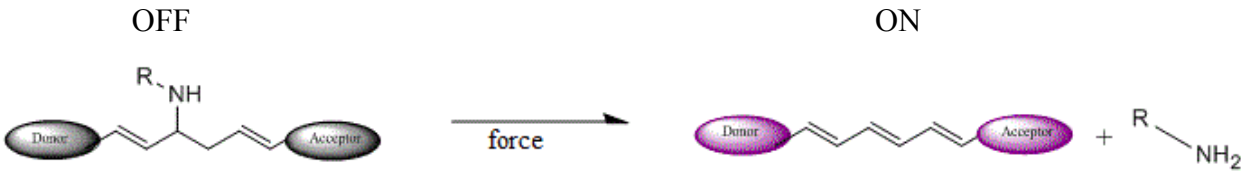

Figure 51: Proposed mechanochromic OFF→ON transition.

The mechanochromic mechanism of the probes depends on the dissociation of the C-N bond preferentially when compared to the other bonds nearby. A preliminary comparison of bond dissociation energies shows that C-N bonds (70 kcal/mol) are weaker than C-C (83 kcal/mol) or C=C (146 kcal/mol) bonds, and would logically be the first bond (apart from the donor and acceptor groups) to dissociate within the molecule (74).

The proposed mechanism of probe molecules suggests a mechanochemical interpretation, where force imparts energy that makes a thermally-activated chemical transition more likely. However, there is also the possibility that AJNDE15 displays some aggregation character since the molecule in the ON state has an intrinsic dipole moment and could form aggregates. The proposed mechanism is not isomeric in nature, but it is still conceivable that this reaction requires free volume to occur and would therefore display similar sensitivity to free volume in the polymer. Finally, the chain scission approach could be appropriate because of the lower dissociation energy of C-N bonds – a crack propagating through a solid polymer would dissociate the C-N bond before the other bonds in the area.

1.6 Summary of mechanochromic mechanisms

The four mechanisms outlined in this review describe how fluorescent probe behavior changes in response to mechanical damage or deformation. A novel mechanism was also proposed, and compared to these four established mechanisms.

In the aggregation approach, mechanical deformation forces the probe molecules closer or farther apart, which promotes or deactivates the aggregation characteristics of the molecules. It is a multimolecular mechanism and as such will be dependent on the probe concentration as well as the degree of mechanical deformation.

In the intramolecular isomer approach, a molecular probe activates when mechanical deformation in the bulk polymer increases the free volume available for isomerization to occur. Transitions that require a larger amount of free volume will occur more often when the free volume increases, and less often when it decreases.

In the mechanochemical reaction approach, a molecular probe is activated when mechanical stress in the bulk polymer causes a chemical reaction in the molecule to occur. This probe type will display sensitivity to mechanical damage when the energy imparted by the damage reduces the reaction's activation energy to the point where it proceeds spontaneously at the environmental temperature.

In the scission-based approach, a molecular probe's fluorescence activates when cracks caused by mechanical deformation break bonds that create an active fluorescent molecule out of an inactive fluorescent molecule. Mechanisms based on the breaking of cyclobutane bonds have been demonstrated in the literature.

In the course of this research project a series of molecules have been developed that display mechanochromic behavior via a proposed novel mechanism involving a reaction between the probe and the amine functional groups in the curing agent of epoxy. Mechanical force promotes the dissociation of this bond, which connects a conjugation pathway within the molecule and activates fluorescence.

The goal of this chapter is to evaluate the proposed mechanism and the the four established mechanisms by comparison with and analysis of experimental results.

2. MECHANOCHROMIC CHARACTERIZATION METHODS

In this section the characterization methods necessary to evaluate the mechanochromic behavior of AJNDE15 and AJNDE17 will be described. In most cases, these will be simple modifications of the methods described in Chapter 1 section 2. Representative spectra will be presented to allow for discussion of the variable R, which is based on characteristics of the fluorescent emission of the probe-epoxy system.

2.1 Materials and sample preparation

In this section the preparation of samples for testing will be described, with differences in the procedures taken for DGEBA-DETA alone highlighted. The two probe molecules AJNDE15 and AJNDE17 will also be described.

2.1.1 AJNDE15

The probe molecule labeled AJNDE15 has the general structure shown in Figure 52. It is

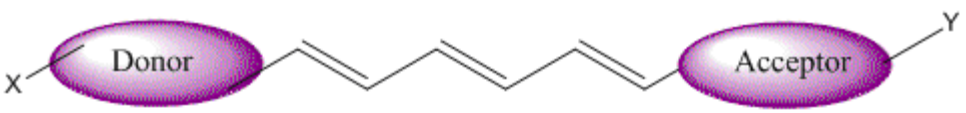

Figure 52: AJNDE15 schematic. X, Y are functional groups.

initially in the ON state. In theory, AJNDE15 will turn OFF during the mixing and curing process by reaction with an unconsumed amine functional group (see Figure 50). After curing, the molecule will be in the OFF state and will be prepared to turn ON when it experiences mechanical deformation or damage (see Figure 51).

2.1.2 AJNDE15 in DGEBA-DETA - Mixing and curing

Probe AJNDE15 was received in powder form. The powder dissolved well in both DGEBA and DETA at room temperatures. Figure 53 shows DGEBA and DETA with AJNDE15 dissolved.

In DGEBA, AJNDE15 is strongly purple in color, while in DETA it shows no color. This is evidence that the probe has turned OFF while in DETA solution via the reaction with DETA amine groups.

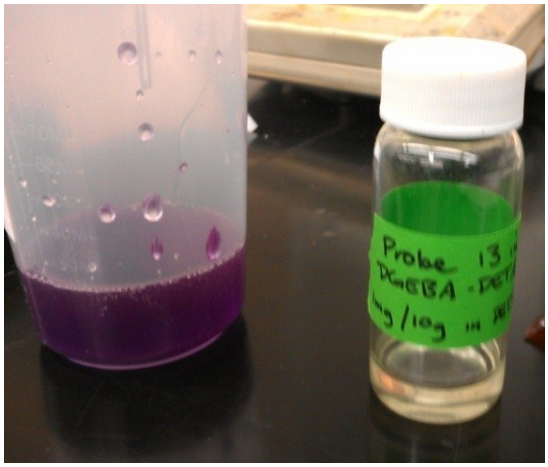

Figure 53: AJNDE15 dissolved in DGEBA (left) and DETA (right).

2.1.3 AJNDE17

Probe AJNDE17 is designed with a similar structure to AJNDE15, but to begin in the OFF state, where AJNDE15 began in the ON state. A schematic of AJNDE17 is shown in Figure 54.

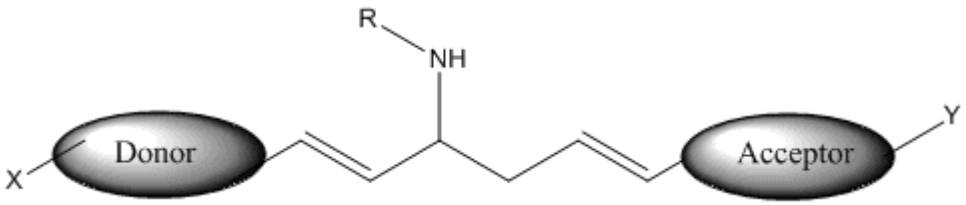

Figure 54: AJNDE17 schematic.

With AJNDE17 beginning in the OFF state, the need for an amine to react with in order to turn the probe OFF is removed. In theory, this should result in a more consistently OFF state after curing, which would allow a more extensive OFF→ON transition due to mechanical deformation.

2.1.4 AJNDE17 in DGEBA-DETA - Mixing and curing

AJNDE17 is received as a liquid in 50wt% solution with DETA. The solution is diluted with DETA to the proper concentration, mixed with DGEBA, and cured as in 2.1.2. The liquid DETA has a yellow color as seen in Figure 55.

Figure 55: AJNDE17 dissolved in DETA.

The curing of DGEBA-DETA-AJNDE15 and DGEBA-DETA-AJNDE17 was accompanied by a color change in the developing solid. Images of the samples before curing and after curing for AJNDE15 are presented in Figure 56.

Figure 56: before (left) and after curing (right) images of DGEBA-DETA-AJNDE15 system.

2.2 Characterization methods

In this section the methods for characterization of the mechanochromism of AJNDE15 and AJNDE17 will be presented, and the differences between these methods and the ones described in Chapter 1 section 2 will be highlighted.

2.2.1 Cure characterization

The cure of DGEBA-DETA-AJNDE15 and AJNDE17 were characterized using absorbance techniques. Samples with varying χ values were allowed to cure in plastic cuvettes as in Chapter 1section 2.1.3.

The cure of AJNDE15 and AJNDE17 was also measured with DSC and FTIR, with no measureable differences at the concentrations studied.

2.2.2 Characterization of solid polymer

The characterization techniques for solid DGEBA-DETA are outlined in this section. Some properties are not changed by the incorporation of probe molecules, and these are mentioned.

2.2.2.1 Glass transition

The glass transition behavior of DGEBA-DETA-AJNDE15 was tested using DMA, and was not found to be measurably different due to the presence of the probe molecules.

2.2.2.2 Mechanical properties

Uniaxial compression tests for modulus and yield strength were conducted as in Chapter 1 section 2.2.2, with no measurable differences in properties due to the presence of the probe molecules.

Tests of probe response to varying ε_{def} were accomplished by first measuring the optical properties of undeformed samples and then conducting the deformation. After deformation, sample optical properties were re-measured as soon as possible after testing. The delay in measurement after deformation was usually on the order of minutes.

2.2.2.3 Optical properties

The absorbance spectra of samples before and after exposure to some stimulus were measured as in Chapter 1 section 2.2.3.1. The samples often had different dimensions before and after testing, which caused absorbance differences that were corrected for by offsetting spectra to 0A at 850nm.

The fluorescent emission and excitation of DGEBA-DETA-AJNDE17 was collected as in Chapter 1 section 2.2.3.2 . The probe was turned ON via exposure to 70°C for 1 minute.

The fluorescent emission of samples was also collected via the spectrometer probe tip setup as in Chapter 1 section 2.2.3.3. Sample spectra were collected before and after some stimulus, whether heat exposure, mechanical deformation, or hydrostatic pressure. Typical spectra collected from the OFF and ON states of the sample are shown in Figure 57.

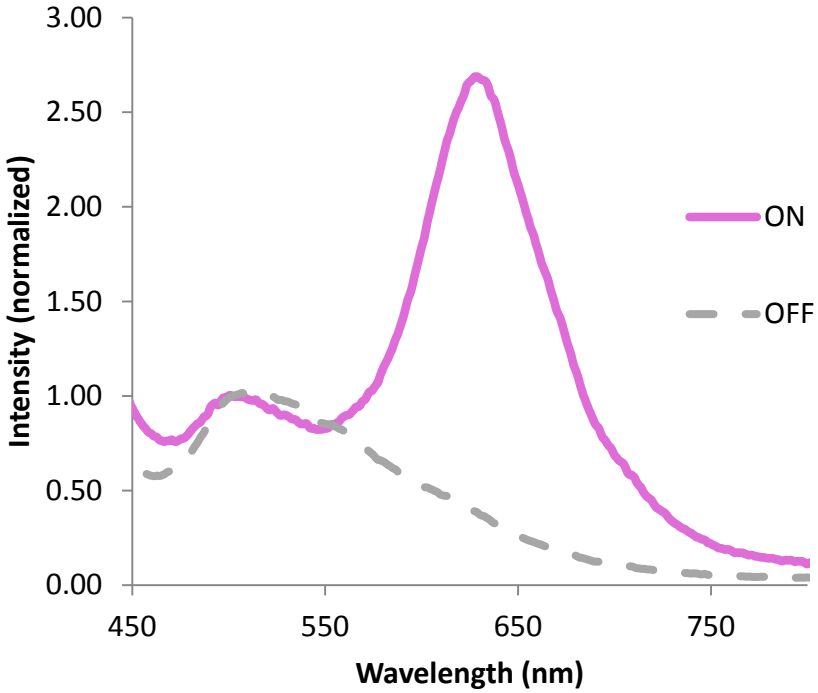

Figure 57: Typical OFF and ON spectra collected via spectrometer probe tip method.

The OFF emission dispays fluorescent emission with a single peak at 505nm which has been identified as the fluorescence peak of DGEBA-DETA (see Chapter 1 section 2.2.3.2). The ON state emission has this epoxy fluorescence as well as a strong fluorescence at 630nm, which we associate with the ON state of the probe molecule.

Direct analysis of the intensities of many of the spectra collected in this work, and comparisons between samples of different sizes or that have undergone physical changes, is not feasible due to the potential for changes in alignment of the portable probe illumination/detection tip of the spectrometer apparatus. To account for this, emission spectra were analyzed by referencing

intensity values to other values within the same spectrum, similar to the ratiometric techniques discussed in the Introduction section 2.2. A method of quantifying the OFF→ON transition of probe molecules has been developed by normalizing the data with respect to the value of the 505nm peak emission which is present in both OFF and ON states. The ratio of the peaks in the OFF state can be compared to the ratio of the peaks in the ON state before and after the transition via the following relation

$$R = \frac{I_{630}/I_{505} - I_{630}^{0}/I_{505}^{0}}{I_{630}^{0}/I_{505}^{0}} * 100 \qquad \textbf{10}$$

where R is defined as the change in OFF→ON ratio in percent, I_{630}^{0} and I_{505}^{0} are the emission intensities of the ON and OFF peaks AJNDE15 before the transition, and I_{630} and I_{505} are the emission intensities of the peaks after the transition. Using this relation the magnitude of the OFF→ON transition can be compared for various external stimuli. This procedure is similar to the one used to quantify changes in the monomer-dimer ratio of naphthalene in PMMA films deformed in tension (52). It is also very closely similar to the modified Stern Volmer relation used to characterize the response of ratiometric probe systems (Eqn.2 Introduction section 2.2).

3. CHARACTERIZATION OF AJNDE15 MECHANOCHROMISM

In this section the results of the characterization of the mechanochromic probe molecule AJNDE15 in DGEBA-DETA will be presented. The results will be discussed in context of the four mechanisms reviewed in section 1 and a mechanism best fitting the observed behavior will be identified.

3.1 Characterization of cure

The cure behavior of DGEBA-DETA-AJNDE15 system was measured using absorbance. An example of the data obtained is shown in Figure 58 for a concentration of .05wt% AJNDE15 with χ=1. Also plotted is data for DGEBA-DETA cured over 24 hours.

3.2 Absorbance

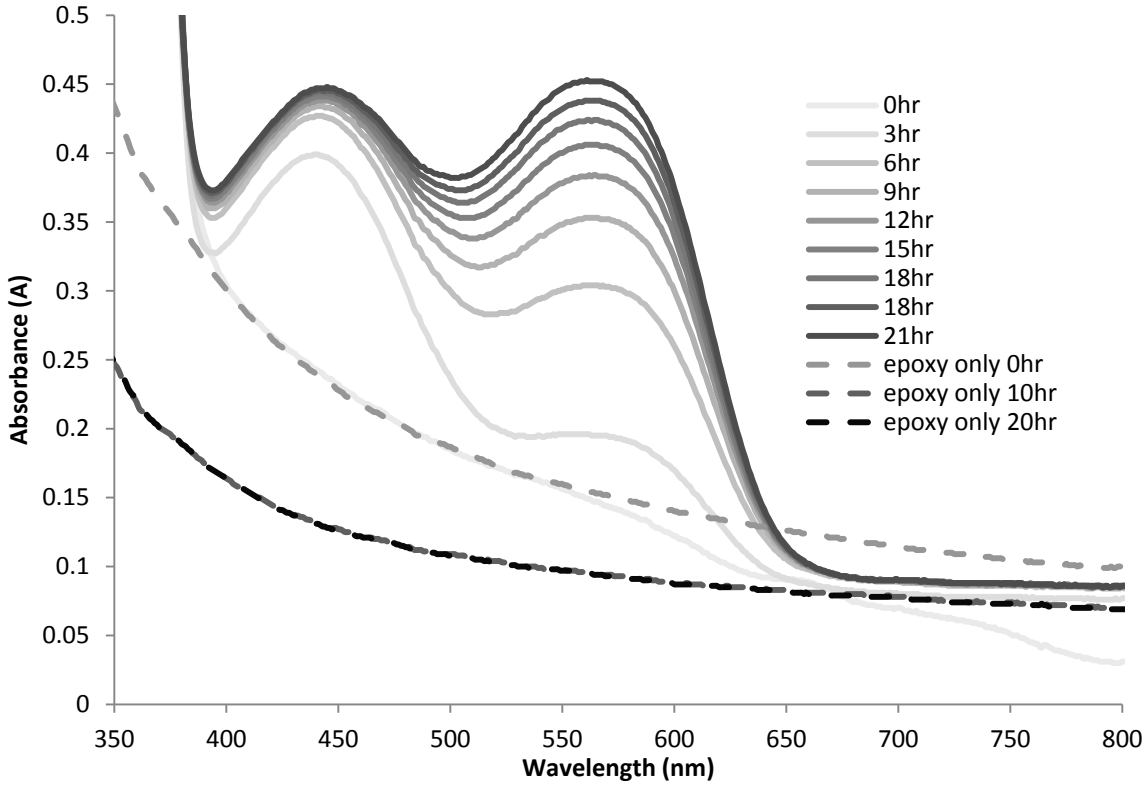

Figure 58: Absorbance of AJNDE15 in DGEBA-DETA during curing. Dashed lines - DGEBA-DETA alone.

It is plain that two absorbance peaks due to AJNDE15 absorbance develop over time – one at 447nm and one at 564nm. Plots of the absorbance values with respect to time for each of these peaks are shown in Figure 59, with absorbance of DGEBA-DETA at 447nm as well (see Figure 25). There is an initial decrease in absorbance which can be attributed to a change in the DGEBA-DETA system since it also occurs in samples with no AJNDE15. The peak at 447nm

grows very quickly and reaches a maximum value after which it remains essentially constant throughout the curing process, while the peak at 564nm grows steadily as the curing progresses. There are several phenomena that could cause this absorbance behavior including a change in the

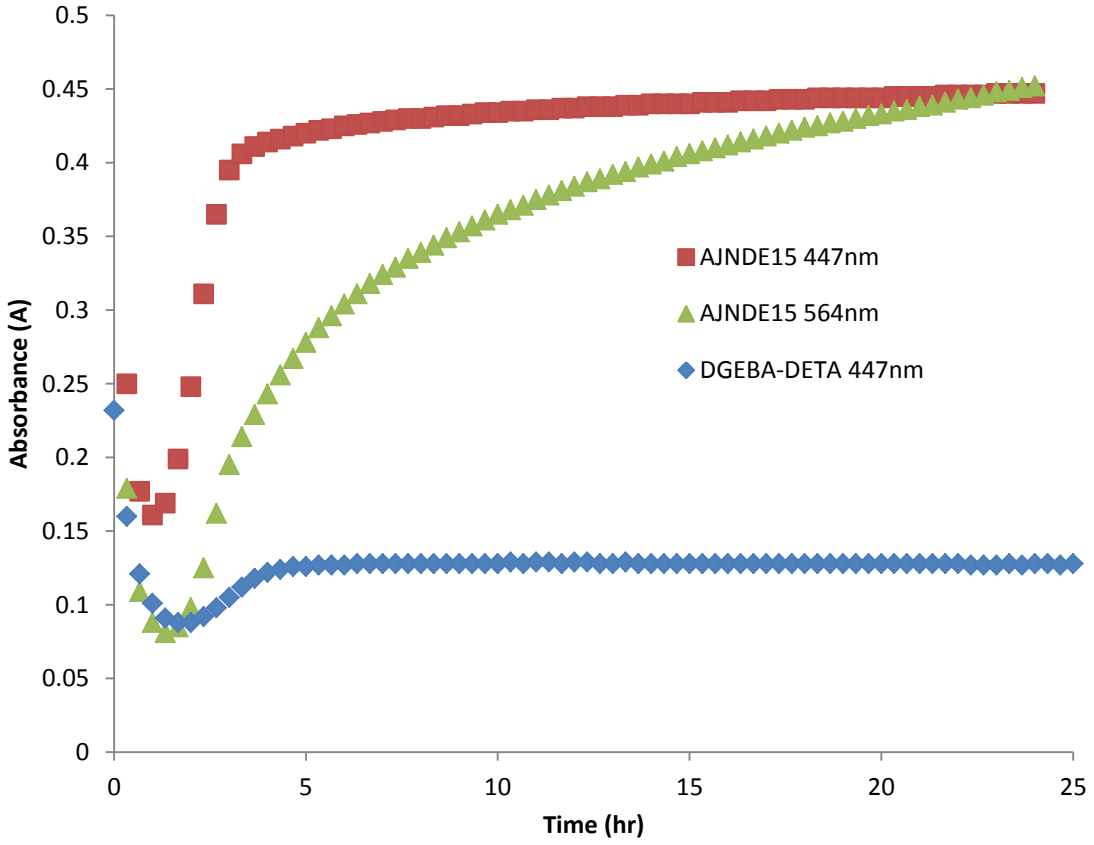

Figure 59: Absorbance values for AJNDE15 peaks in DGEBA-DETA during cure. Blue points are DGEBA-DETA with no AJNDE15.

polarity of the mixture as functional groups are consumed (75), a change in the free volume as liquid epoxy turns to solid (57), or a change in viscosity (59). Based on the proposed mechanism, however, this would suggest that after being turned OFF by reaction with an unbound amine, AJNDE15 is turned ON via a reaction that removes the amine.

The absorbance behavior of AJNDE15 in DGEBA-DETA is highly dependent on the stoichiometry of the initial mixture. While the general behavior of the absorbance peaks of

AJNDE15 over time is similar for each mixture, the absorbance values reached after 24 hours of

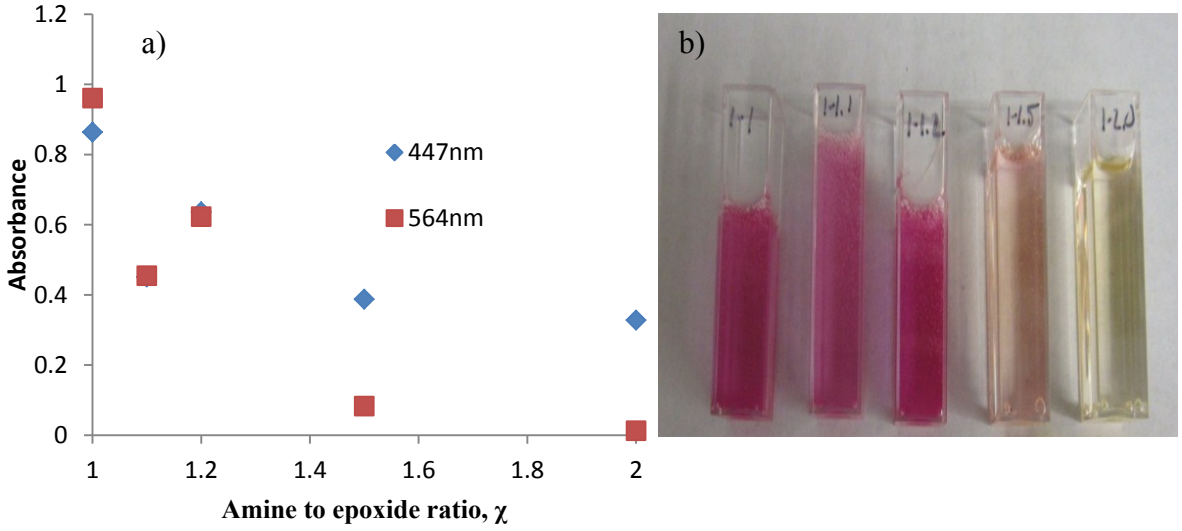

Figure 60: a)Absorbance of peaks at 447 and 564nm of AJNDE15 in DGEBA-DETA after cure for varying stoichiometries. b) Images of cuvettes after cure – left to right: χ=1, 1.1, 1.2, 1.5, 2.0.

curing show a definite correlation with χ. Figure 60a has a plot of the final absorbance values with respect to χ, while Figure 60b has an image of the final cured cuvettes.

It is important to note that changes in DGEBA-DETA itself do not occur in this wavelength region during curing – peak increases in DGEBA-DETA occur due to stoichiometric or temperature changes at 375nm. These absorbance peaks are strictly due to AJNDE15.

It is clear that the final absorbance values of the cured samples changes as χ increases. The 447nm absorbance is still present at the highest χ values, giving the solid bulk polymer a slightly yellow-orange color, but the 564nm peak has all but vanished.

3.3 Characterization of solid polymer

In this section the properties of the DGEBA-DETA-AJNDE15 after curing will be presented. The properties will be compared with DGEBA-DETA with no probe molecules incorporated.

3.3.1 AJNDE15 in DGEBA-DETA – Excitation and emission

The excitation and emission spectra of DGEBA-DETA-AJNDE15 showed no differences from DGEBA-DETA when the probe is in the OFF state. After activation via heat, though, the spectra showed strong emission in the range 600-630nm. The excitation and emission spectra for this particular behavior is shown in Figure 61.

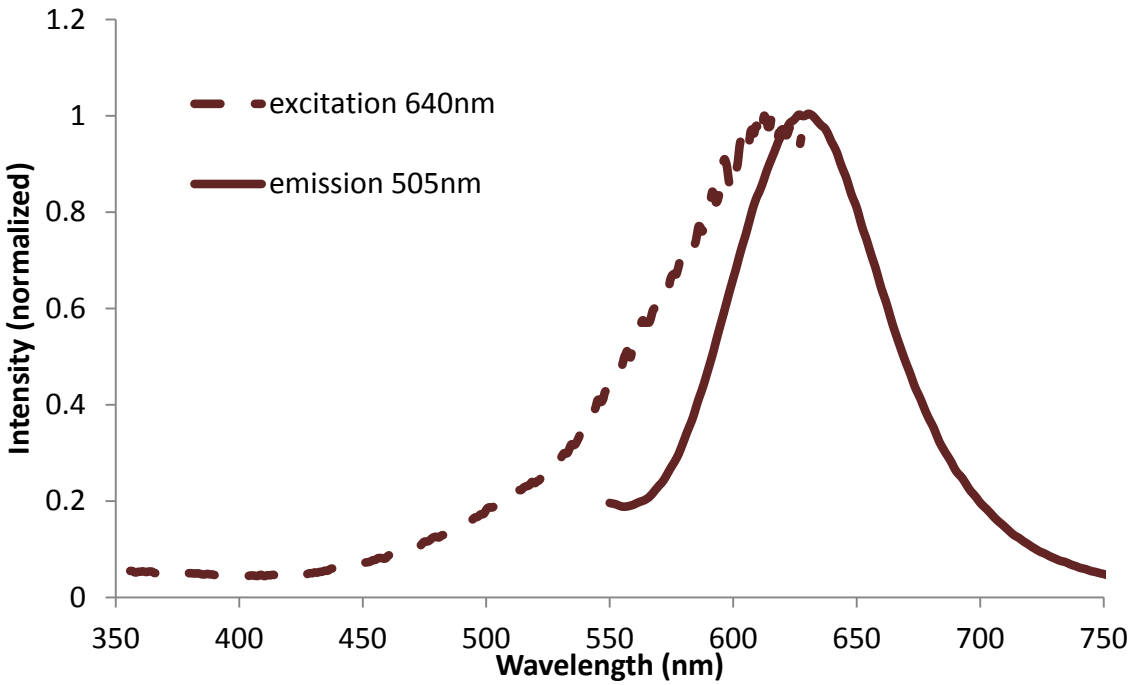

Figure 61: Excitation and emission spectra of AJNDE15 emission peak in DGEBA-DETA-AJNDE15.

The excitation spectrum associated with AJNDE15 emission begins at ~450nm and grows to a peak at ~610nm. The emission caused by excitation at 505nm shows narrow emission beginning at approximately 600nm, with peak emission at ~630nm.

The combined emission of DGEBA-DETA-AJNDE15 is caused by a single 390nm excitation source during in-situ measurements from the spectrometer probe. The emission and excitation spectra for DGEBA-DETA and the AJNDE15 emission in activated DGEBA-DETA-AJNDE15 are shown in Figure 62, with the combined emission spectrum due to 390nm excitation offset

above the spectra. Based on the excitation spectrum shown in Figure 61, it seems unlikely that 390nm excitation can stimulate the 630nm emission observed. However, there is a significant overlap between DGEBA-DETA emission and AJNDE15 excitation, shown in the triangular region in Figure 61. A theory for the excitation of the combined spectra above-offset in Figure 61 is that 390nm excitation stimulates epoxy emission, which in turn excites the AJNDE15 emission at 630nm. Comparing the combined emission spectrum with the DGEBA-DETA emission spectrum supports this conclusion – the emission is significantly decreased in the ~475-525nm wavelengths, where AJNDE15 excitation would take place.

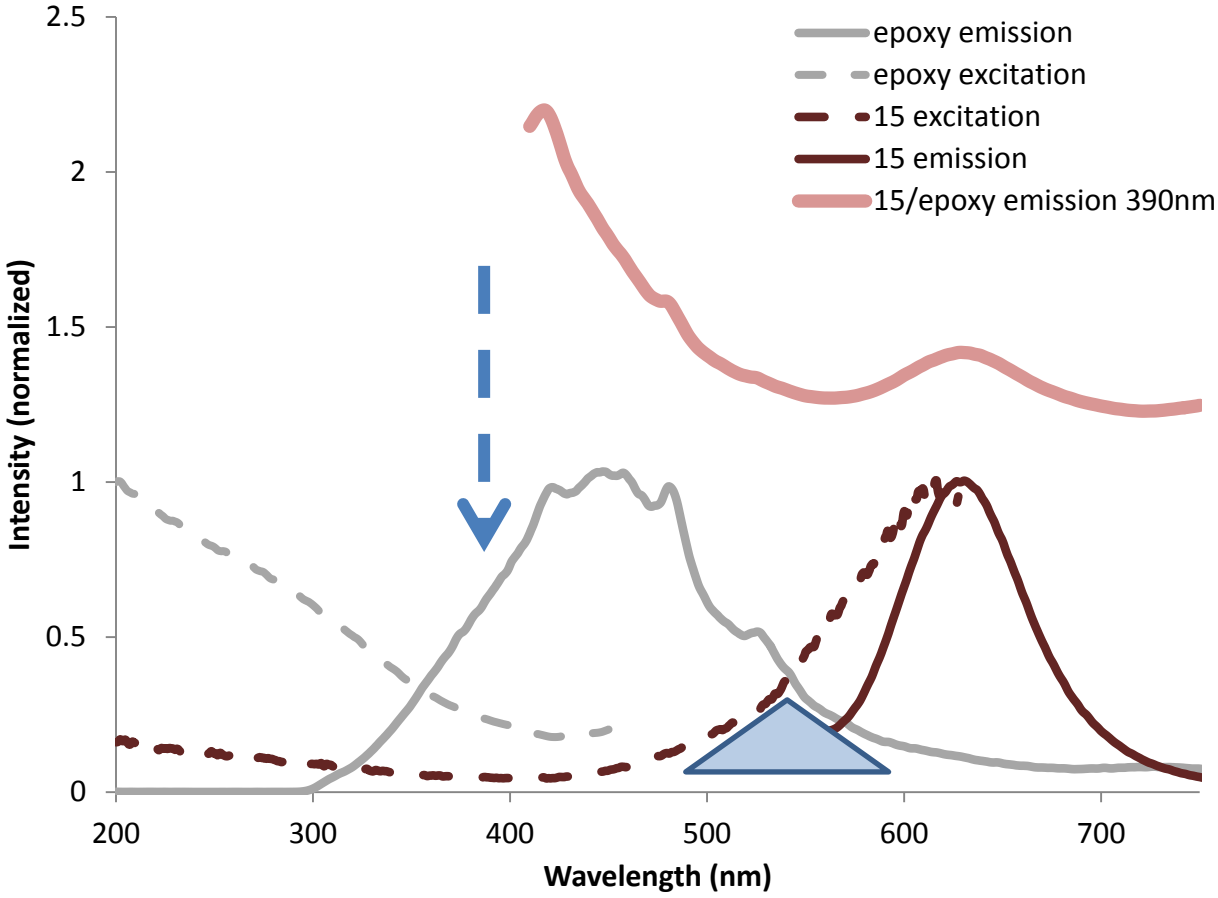

Figure 62: Excitation and emission spectra of epoxy and AJNDE15. Offset above - emission of DGEBA-DETA-AJNDE15 due to excitation at 390nm.

3.3.2 AJNDE15 in DGEBA-DETA – Uniaxial compression

Samples of .05wt% AJNDE15 in cured DGEBA-DETA with χ=1.5 were machined into 8 rectangular plates measuring ~10mmx10mmx1.5mm. Images of the plates were taken under ambient light and in a darkroom under long-wave UV illumination, and spectra were collected using 390nm UV illumination. The plates were then mechanically deformed in compression in load control mode to varying final loads. A typical set of true stress-true strain curves for these measurements is shown in Figure 63.

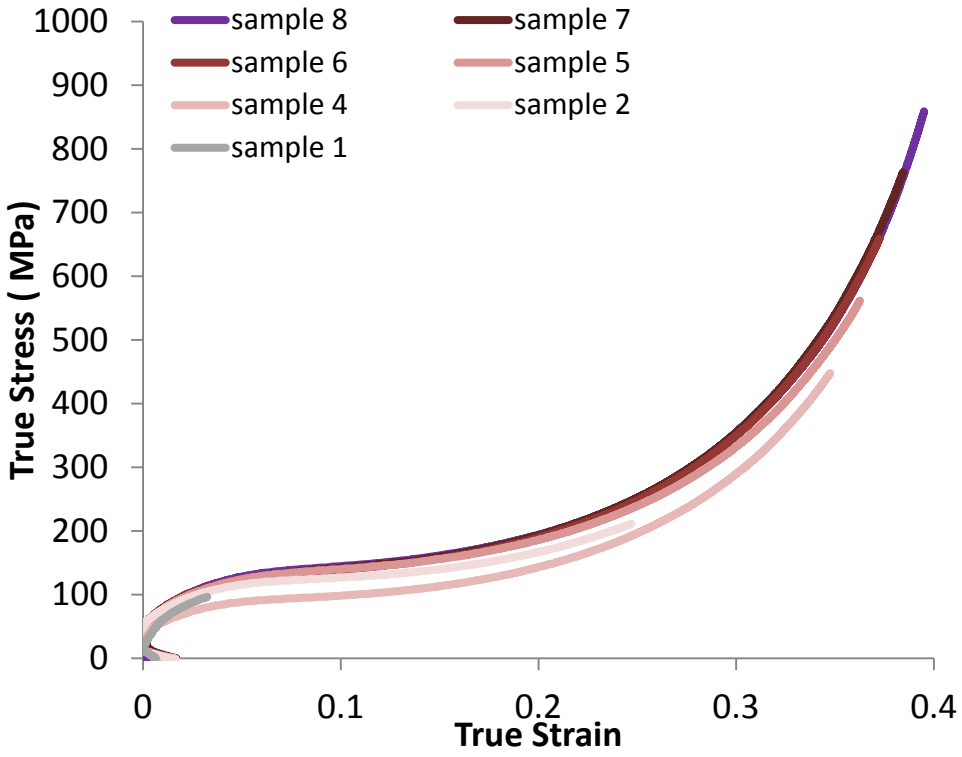

Figure 63: True stress-true strain curves for DGEBA-DETA compression samples.

After deformation, images and spectra were again collected. The before and after images are shown in Figure 64, while the before and after spectra are shown in Figure 65. The dashed black line is DGEBA-DETA fluorescence for reference. The true strain in samples was calculated by measuring sample dimensions after removal from the testing apparatus. Any elastic deformation

Figure 64: AJNDE15 in DGEBA-DETA compression samples. a) Brightfield, before compression. b) UV illuminated, before compression. c) Brightfield, after compression. d) UV illuminated, after compression. left to right: sample 1 – sample 8, increasing ε_{def} 0 to .36. See Figure 63 for stress strain curves.

will have relaxed immediately after the load is removed; this measurement therefore represents the amount of ε_{def} experienced by the samples.

The samples after mechanical deformation show a dramatic color change from clear pink to dark red-purple. The fluorescent emission also changes dramatically from blue-white to red.

The spectra show that initially, AJNDE15 has fluorescent emission with two peaks at ~505nm and ~630nm. After deformation, the emission at 505nm decreases in a general but not monotonic way with increasing strain. The emission of DGEBA-DETA fluorescence does not change greatly due to ε_{def} (see Chapter 1section 4.3.3.3), so changes in this region are attributed to AJNDE15. Based on the excitation and emission spectra results in Figure 61, this is attributed

to AJNDE15's ON state absorbing a fraction of the fluorescence emitted by DGEBA-DETA. The emission at 630nm increases dramatically as ε_{def} increases, which is consistent with the proposed OFF → ON transition with increasing strain.

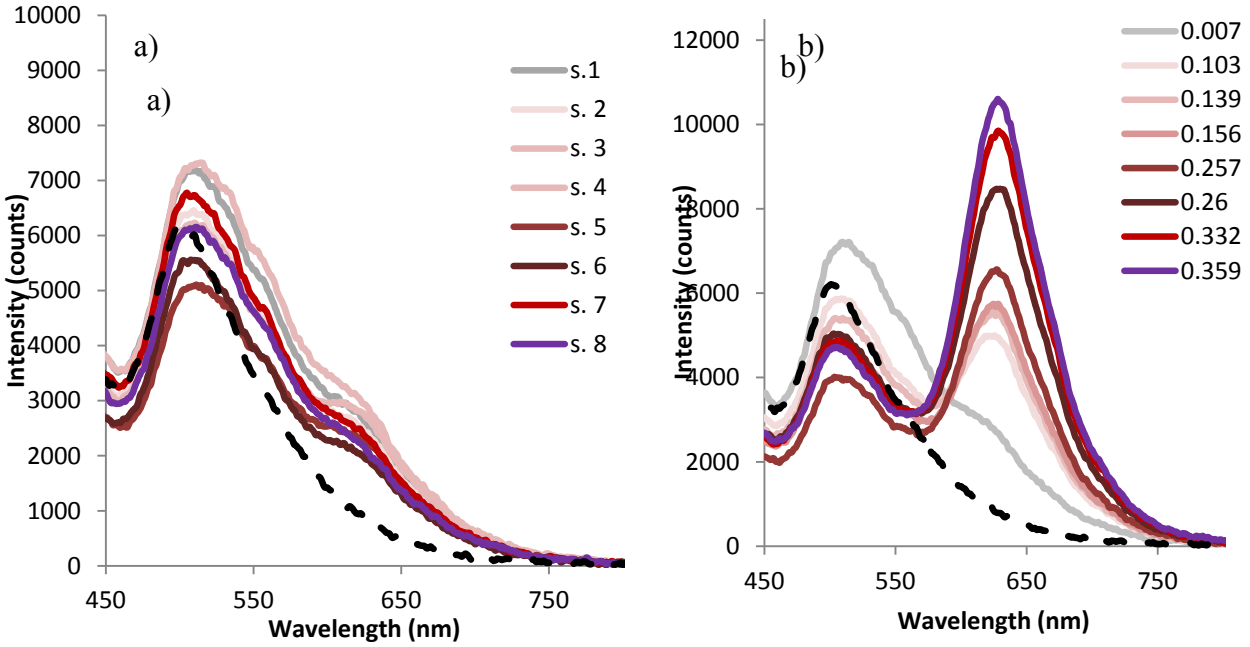

Figure 65: Emission spectra of AJNDE15 in DGEBA-DETA. a) before compression. b) after compression. Legend in b) shows final true strain values.

Figure 66a shows the emission spectra normalized to the peak at 505nm, while Figure 66b shows the R values for increasing ε_{def}. The ratio of intensities at these wavelengths in DGEBA-DETA with no AJNDE15 are also plotted for comparison, showing that very little change in this ratio occurs in DGEBA-DETA as a result of increasing ε_{def}. The increase in R with true strain is, monotonic and one to one, suggesting that this approach is promising as a ratiometric probe for quantitative measures of ε_{def}.

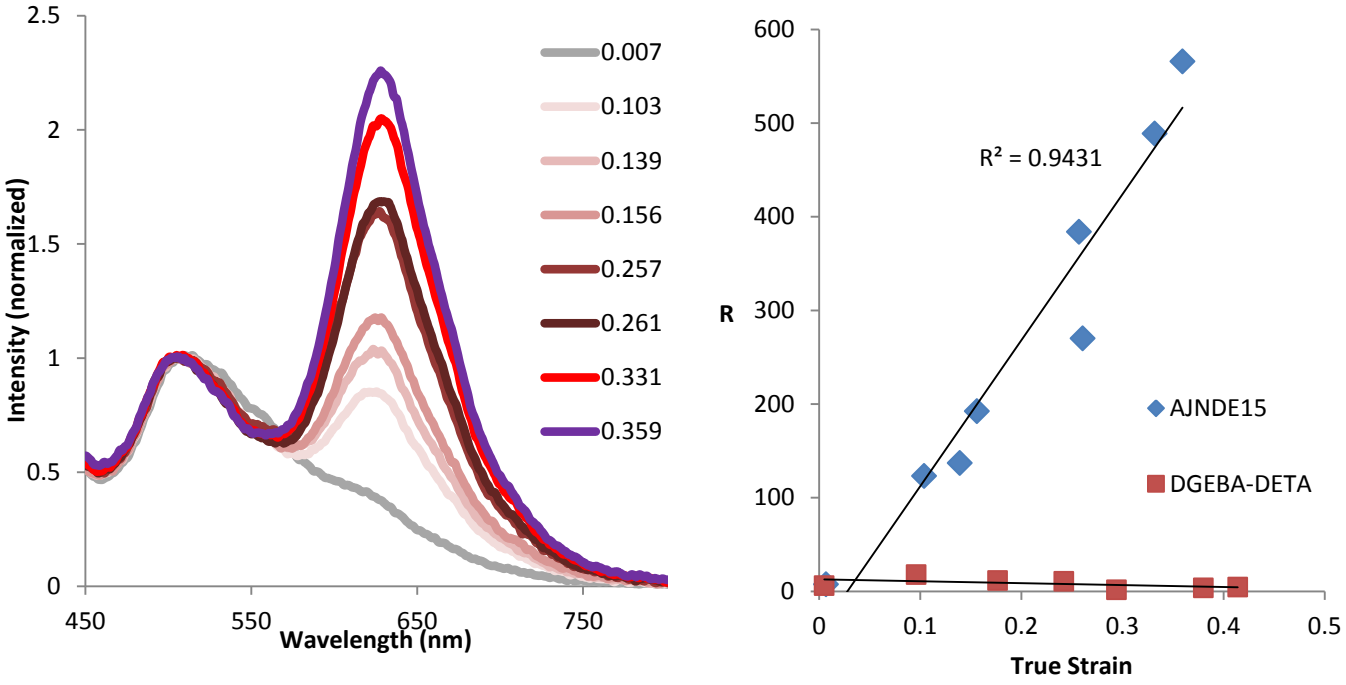

Figure 66: a) Normalized emission of AJNDE15 in DGEBA-DETA χ=1.5 for increasing strains. b) R value for AJNDE15 for increasing strains, with DGEBA-DETA for comparision.

3.3.3 AJNDE15 in DGEBA-DETA - Stoichiometry

Samples of AJNDE15 in DGEBA-DETA with varying stoichiometry were made in the same manner as described in Chapter 1 section 1.2. Absorbance spectra for various χ values were collected via the method in section Chapter 1 section 2.2.3.1. The final absorbance spectra are shown in Figure 67a, with the absorbance of the 564nm peak normalized to the absorbance of the 447nm peak in Figure 67b. The emission spectra collected via the spectrometer probe tip method are shown in Figure 67c, with the absorbance of the 630nm peak normalized to the absorbance of the 505nm peak in Figure 67d.

The emission characteristics with respect to stoichiometry are consistent with the absorption spectra. The relative intensity of the peak at 630nm decreases rapidly as χ increases, just as the relative magnitude of the absorbance peak at 564nm decreases for increasing χ values. These results suggest that the OFF→ON transition occurs during cure, and that increasing χ reduces the extent of the transition.

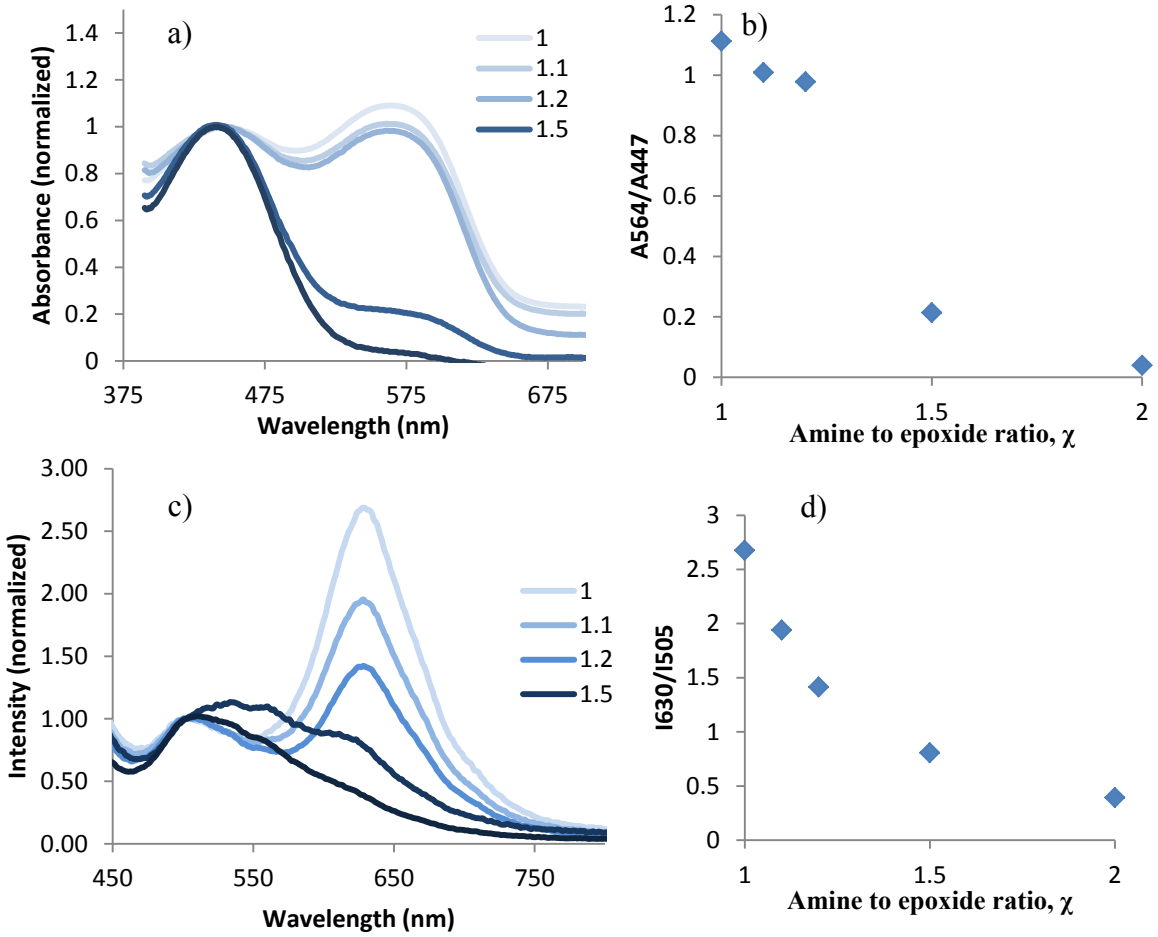

Figure 67: a) Absorbance spectra for AJNDE15 in DGEBA-DETA. b) Ratio of 564nm absorbance to 447nm absorbance for varying χ values. c) Emission spectra for AJNDE15 in DGEBA-DETA. d) ratio of 630nm emission to 505nm emission for varying χ values.

3.3.4 AJNDE15 in DGEBA-DETA - Elevated temperature

It was observed that AJNDE15 samples after room temperature cure in DGEBA-DETA displayed dramatic changes in color and fluorescent emission when exposed to heat. To quantify

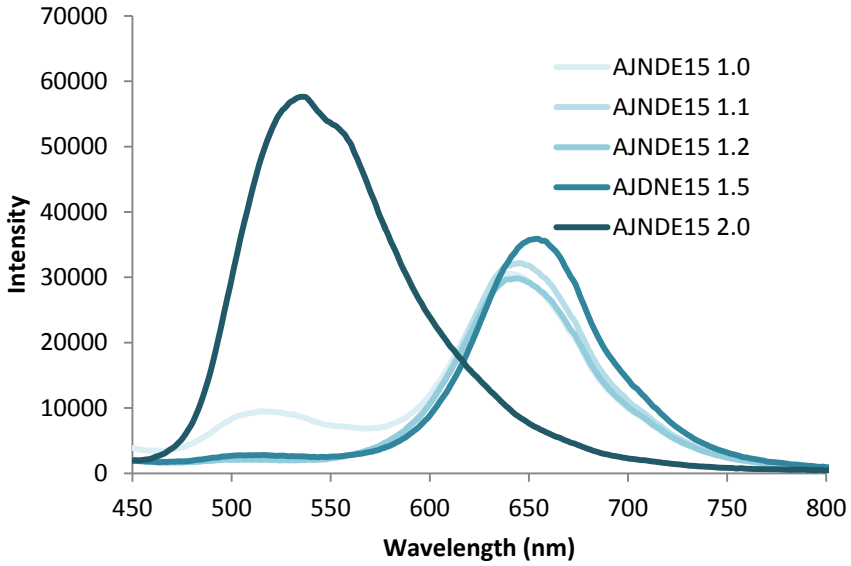

Figure 68: Emission spectra of AJNDE15 in DGEBA-DETA after heating.

this, samples having varying χ values and .05wt% AJNDE15 were placed in a drying oven at 70ºC for 24 hours. Images of the samples were taken before and after exposure in ambient light and in a darkroom under long-wave UV illumination. Spectra were collected with 390nm UV illumination before and after exposure. The spectra of samples after exposure are shown in Figure 68, and before and after images are displayed in Figure 69.

The color of samples clearly changes as a result of the heating from pink or clear to dark red-purple in almost all cases. Fluorescent emission also changes, from mild red or blue emission to strong red emission. The exception is for samples with χ=2.0. These samples change from clear

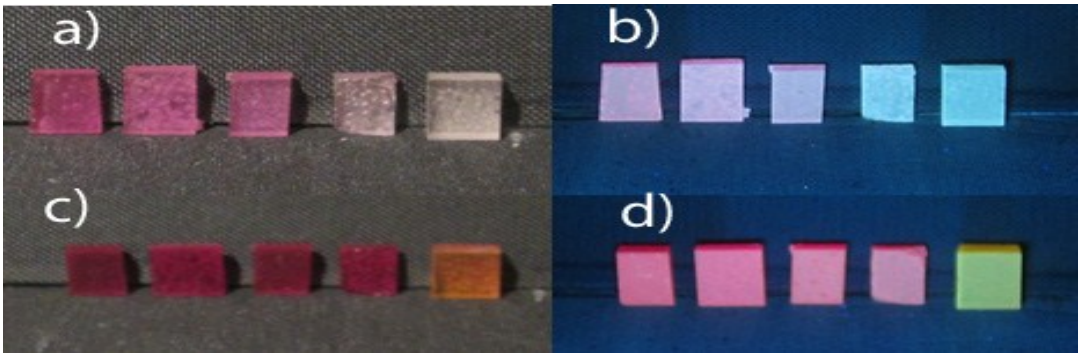

Figure 69: Samples of varying stoichiometry before and after heating. a) brightfield, before heating. b) UV illuminated, before heating. c) Brightfield, after heating. d) UV illuminated, after heating. All images left to right: χ=1, 1.1, 1.2, 1.5, 2.0.

in color, and blue-white emission, to orange color and strong yellow emission. The spectra quantify this observation. The emission spectra of all samples except that of χ=2.0 show a dramatic increase in the emission of the peak at ~630nm. The sample of χ=2.0 shows a very strong emission at ~530nm, which is not attributable to either of the observed AJNDE15 emission peaks, or the epoxy autofluorescence emission. A plot of R as a result of 24h exposure at 70ºC for various stoichiometric ratios is shown in Figure 70. From this analysis it is clear that samples of χ=1.5 shows the greatest magnitude of OFF→ON change as a result of heat at 70°C as the external stimulus.

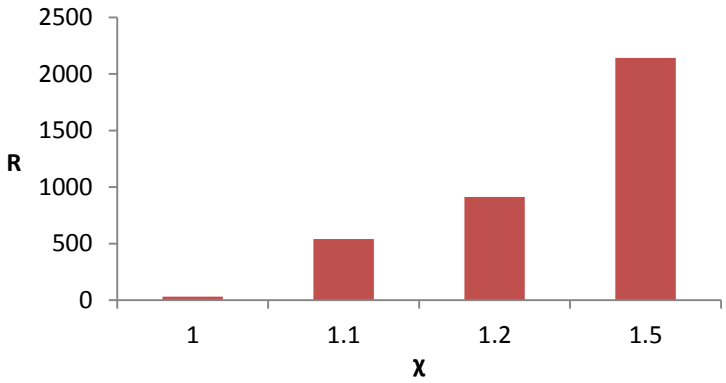

Figure 70: R value for AJNDE15 OFF>ON transition caused by heating.

To begin probing the kinetics of the heat-based OFF→ON transition, a study of AJNDE15 at χ=1.5 for various temperatures and time exposures was conducted. Temperatures from 40°C to 70°C and times from 1 to 10hr were chosen. The samples were imaged in brightfield and fluorescence after exposure, and their spectra were measured before and after exposure. Figure 71a has the images after exposure, while Figure 71b has the R values for the samples for the temperatures and times studied.

There are three important observations that can be made from these measurements. The most important point is that the OFF→ON transition due to temperature progresses further with increasing temperature and increasing exposure times. The second is that temperature values as low as 40ºC cause the transition to occur. And third is that the highest temperature exposures cause initially high R values which are attenuated as exposure increases.

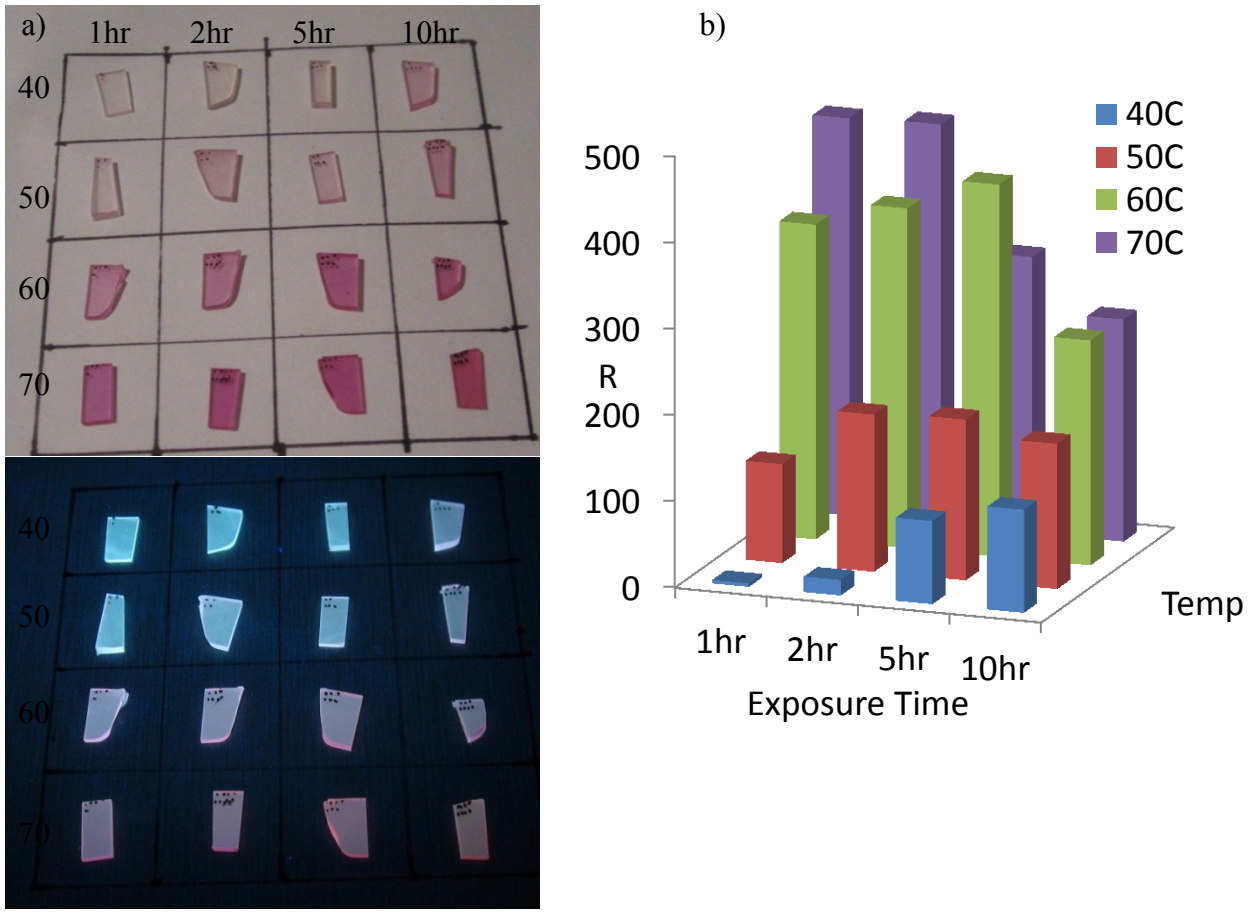

Figure 71: a) top-brightfield images and bottom-fluorescence images of AJNDE15 in DGEBA-DETA χ=1.5 after thermal exposure. b) R values of thermally exposed AJNDE15 in DGEBA-DETA χ=1.5.

3.3.5 AJNDE15 in DGEBA-DETA - Time stability after deformation

It is important for the ultimate application of AJNDE15 as a mechanochromic probe molecule to understand the stability of the OFF→ON transition after deformation. To explore this, a rectangular plate specimen was deformed to strain of ~.40 and spectra were collected from 5 places on the plate. These tests were repeated every 24 hours for 300hr, and again at 500hr. The

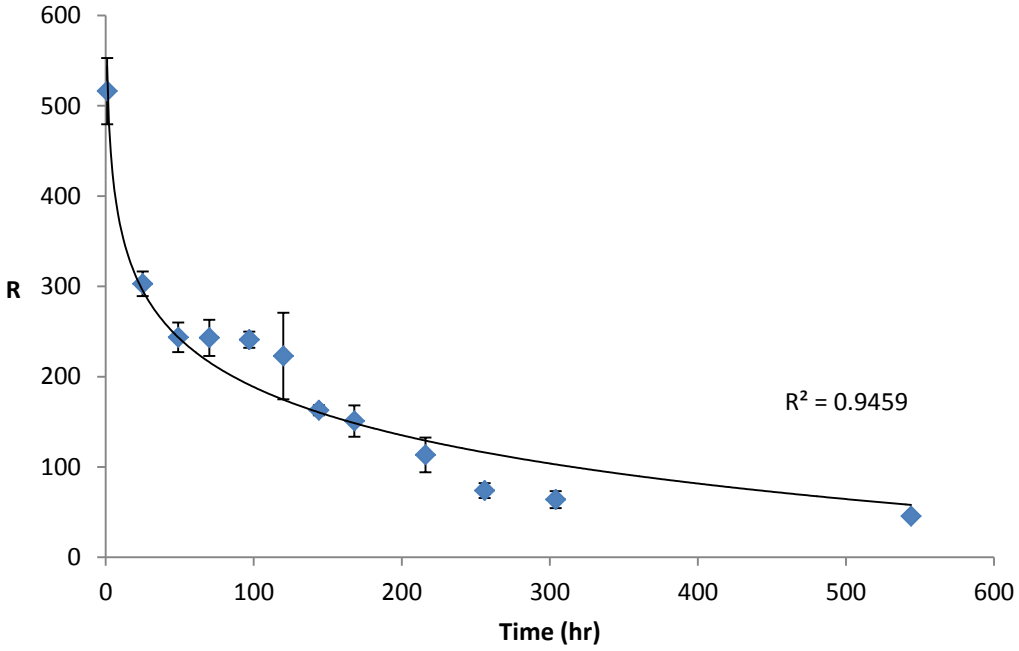

Figure 72: Magnitude of OFF-->ON transition R of AJNDE15 vs. time after deformation.

resulting R values from the spectra are displayed against time in Figure 72.

From Figure 72 it is clear that the OFF→ON transition in AJNDE15 is not permanent – R values decrease dramatically as time increases. A logarithmic model seems to fit the data rather well; an explanation of this trend has yet to be established. Possible explanations include gradual separation of aggregated dye molecules; progression of a degradation or ON→OFF reaction; or relaxation of strain-induced changes in free volume over long time periods.

4. CHARACTERIZATION OF AJNDE17 MECHANOCHROMISM

In this section results gathered from the testing of mechanochromic probe AJNDE17 will be discussed. The general methods are very similar to the discussion of AJNDE15 and so the results will be discussed by comparison with results from AJNDE15.

The probe AJNDE15 is designed to initially start in the ON state, then to react with a primary amine to form the OFF state. This reaction occurred immediately upon mixing into DGEBA-DETA, but during the cure process AJNDE15 returned to the ON state for samples with $\chi \leq 1.5$. Samples with $\chi = 1.5$ stoichiometry were unstable in the ON state after mechanical deformation. As an attempt to stabilize the OFF state in cured DGEBA-DETA at balanced stoichiometries and improve the stability of the ON state after deformation, the probe AJNDE17 was designed.

Probe AJNDE17 is designed with a similar structure to AJNDE15, but to begin in the OFF state, where AJNDE15 began in the ON state. A schematic of AJNDE17 is shown in Figure 73.

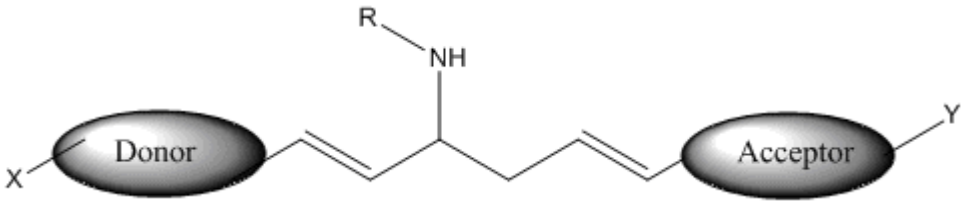

Figure 73: AJNDE17 schematic.

With AJNDE17 beginning in the OFF state, the need for an amine to react with in order to turn the probe OFF is removed. In theory, this should result in a more consistently OFF state after curing, which would allow a more extensive OFF→ON transition due to mechanical deformation.

4.1.1 AJNDE17 in DGEBA-DETA - Mixing and curing

AJNDE17 is received as a liquid in 50wt% solution with DETA. The solution is diluted with DETA to the proper concentration, mixed with DGEBA, and cured as in 2.1.2. The change in absorbance as cure progresses was very similar to AJNDE15 (see Figure 58), with a peak at 447nm that appears very rapidly and a peak at 564nm that develops more slowly. The major difference between AJNDE15 and AJNDE17 in these measurements is the final ratio of peaks. In AJNDE17, the 564nm peak has much lower absorbance after curing at χ=1, 1.1, and 1.2. This suggests that the OFF→ON transition does not progress as far as in AJNDE15 for these stoichiometries. Discussion of this result in more detail will follow in section 4.1.4.

4.1.2 AJNDE17 in DGEBA-DETA – Uniaxial compression

Samples of .05wt% AJNDE17 were mixed with DGEBA-DETA of χ=1. Samples were then cured, machined into plates and tested just as described for AJNDE15. For AJNDE17 however, absorbance spectra were also collected after deformation. The absorbance and emission spectra

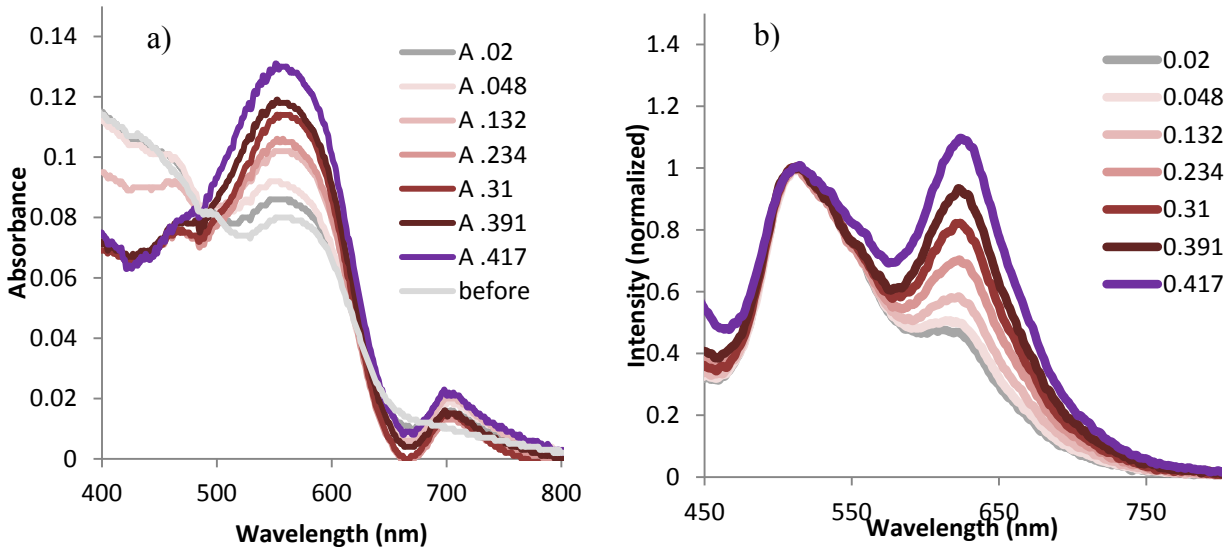

Figure 74: a) Absorbance of .05wt% AJNDE17 after compression. b) Fluorescent Emission of AJNDE17 (390nm illumination).

are shown in Figure 74. Absorbance spectra have been offset to align the background absorbance at 850nm; emission spectra have been normalized to the emission intensity at 505nm.

In Figure 74a, the absorbance peak at 564nm clearly grows stronger as ε_{def} increases. There appears to be an isosbestic point in the visible region of the absorbance spectra, at ~490nm, indicating that a reaction may be occurring between absorbing species in this energy region such as the OFF→ON reaction. The emission spectra in Figure 74b, just as in AJNDE15, show a clear increase in the ratio of emission intensities R (see Eqn. 10) as ε_{def} increases. While the

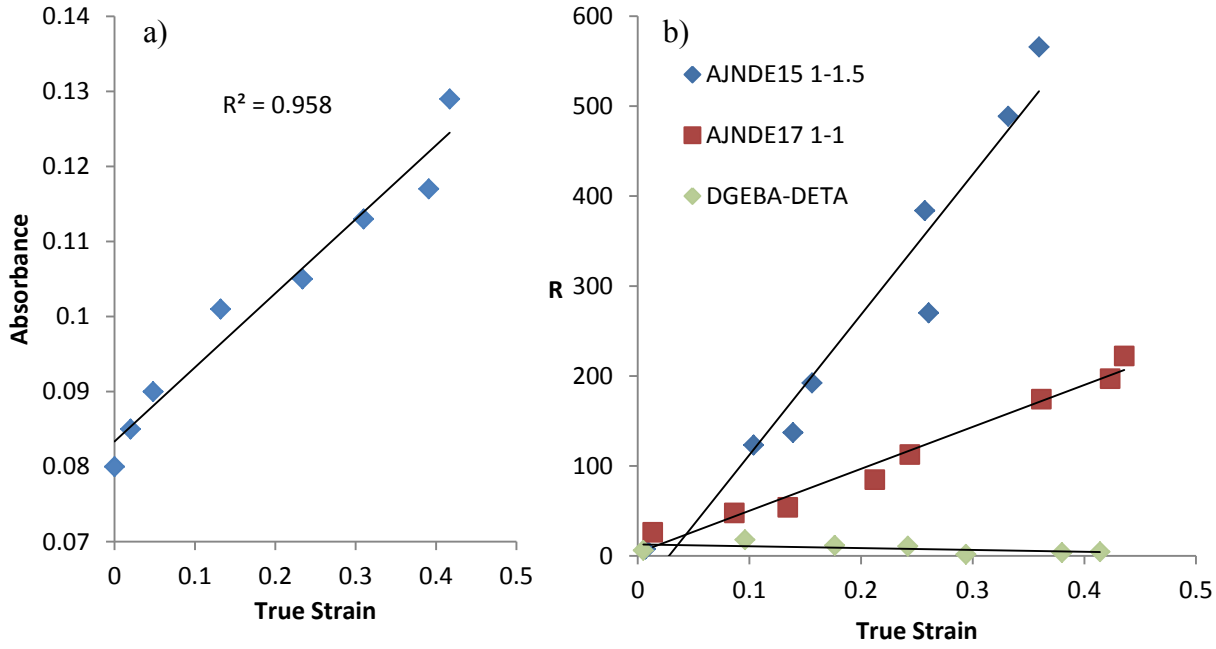

Figure 75: a) absorbance change at 565nm of AJNDE17 .05wt% for changing true strain. b) R value of AJNDE17 χ=1 for increasing true strain compared to AJNDE15 χ=1.5 and DGEBA-DETA χ=1.

maximum R experienced is not as high as in AJNDE15 χ=1.5, the requirement of balanced stoichiometry has been satisfied. Figure 75a has a plot of the change in absorbance value at 565nm, while Figure 75b has a plot of the R ratio change of AJNDE17in DGEBA-DETA χ=1 emission as compared to AJNDE15 in DGEBA-DETA χ=1.5 and DGEBA-DETA χ=1 emission.

The response of both absorbance and emission change with respect to sample true strain is highly linear.

4.1.2.1 AJNDE17 in DGEBA-DETA – Extended study in uniaxial compression

Over the course of the research into AJNDE17, many samples were deformed in uniaxial compression. The simple linear relationship suggested by plots in Figure 72 and Figure 75 may not sufficiently explain the response of DGEBA-DETA-AJNDE17 to ε_{def}.

The data shows a general increase in R (see Eqn. 10) for increasing ε_{def}. A simple linear trendline shows limited correlation with the data. It appears that the fit is too high in the middle range of ε_{def} and too low in the highest range of ε_{def}. An alternative linear fit, dividing the data at $\varepsilon_{def} = .15$, appears to fit the data more closely. Figure 76b shows this alternative fit.

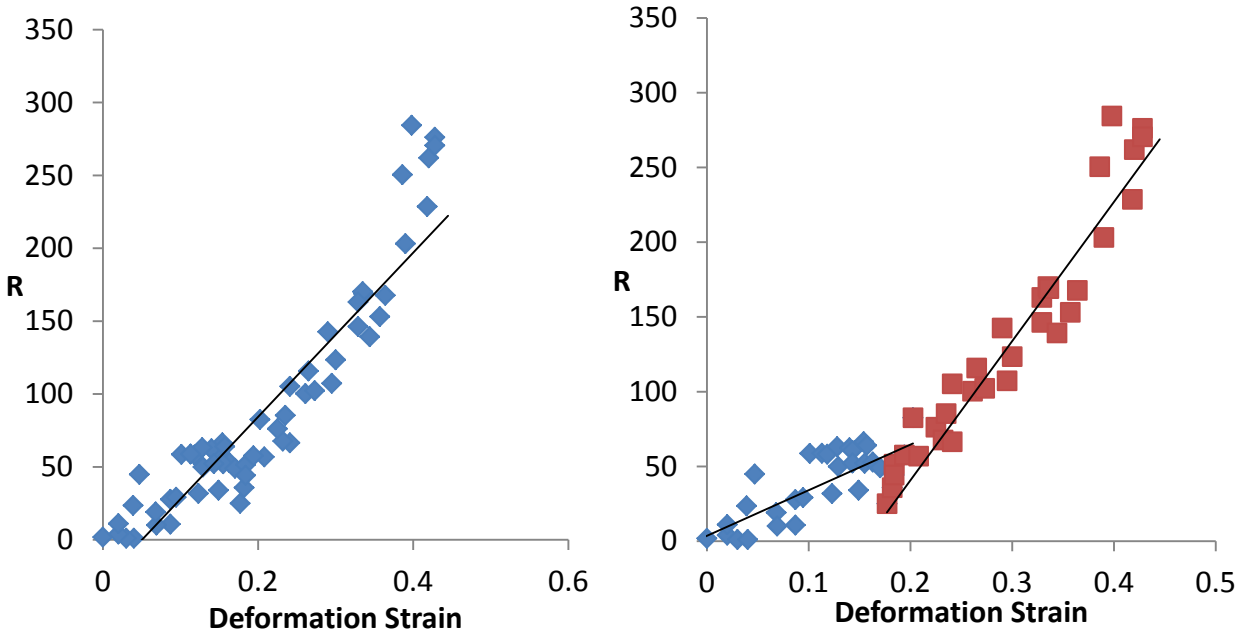

Figure 76: R vs deformation strain for samples of DGEBA-DETA-AJNDE17 - a) simple linar fit. b) two-step linear fit divided at $\varepsilon_{def} \sim .15$.

This result shows the viability of the DGEBA-DETA-AJNDE17 system as a ratiometric fluorescent probe system for deformation. The divided plot in Figure 76b suggests a change in behavior at ε_{def} ~.15, which is consistent with changes in behavior of ε_{an}, ε_{pl}, and $\Delta U_{def.}$

4.1.3 AJNDE17 in DGEBA-DETA – Hydrostatic pressure

The spectra of DGEBA-DETA-AJNDE17 samples loaded in hydrostatic pressure are presented in Figure 77a below. The addition of hydrostatic stress does not activate the OFF→ON reaction, even at stresses well above the σ_{yield} displayed by DGEBA-DETA. Figure 77b shows the R value plotted against the hydrostatic stress experienced by the samples. Uniaxial compression to stresses well below 100MPa causes R values of 100 or more (see Figure 72); hydrostatic

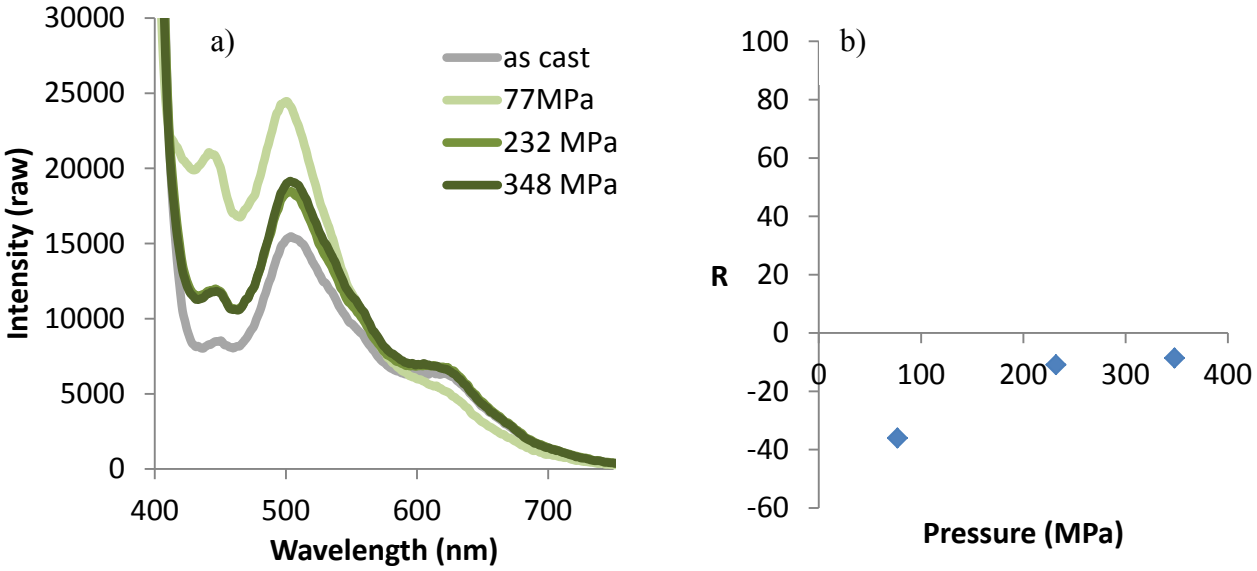

Figure 77: DGEBA -DETA-AJNDE17 response to hydrostatic pressure - a) emission spectra b)R vs pressure.

pressure causes no activation. From literature studies, it has been determined that hydrostatic pressure produces no ε_{def}, causes no intermolecular shear motion, and adds no ΔU_{def} to the internal energy of a glassy polymer (29) (36).

4.1.4 AJNDE17 in DGEBA-DETA - Stoichiometry

An aspect of AJNDE15 that was unsatisfactory for the ultimate application was the requirement that excess amine stoichiometries were required to prevent the probe from turning ON during

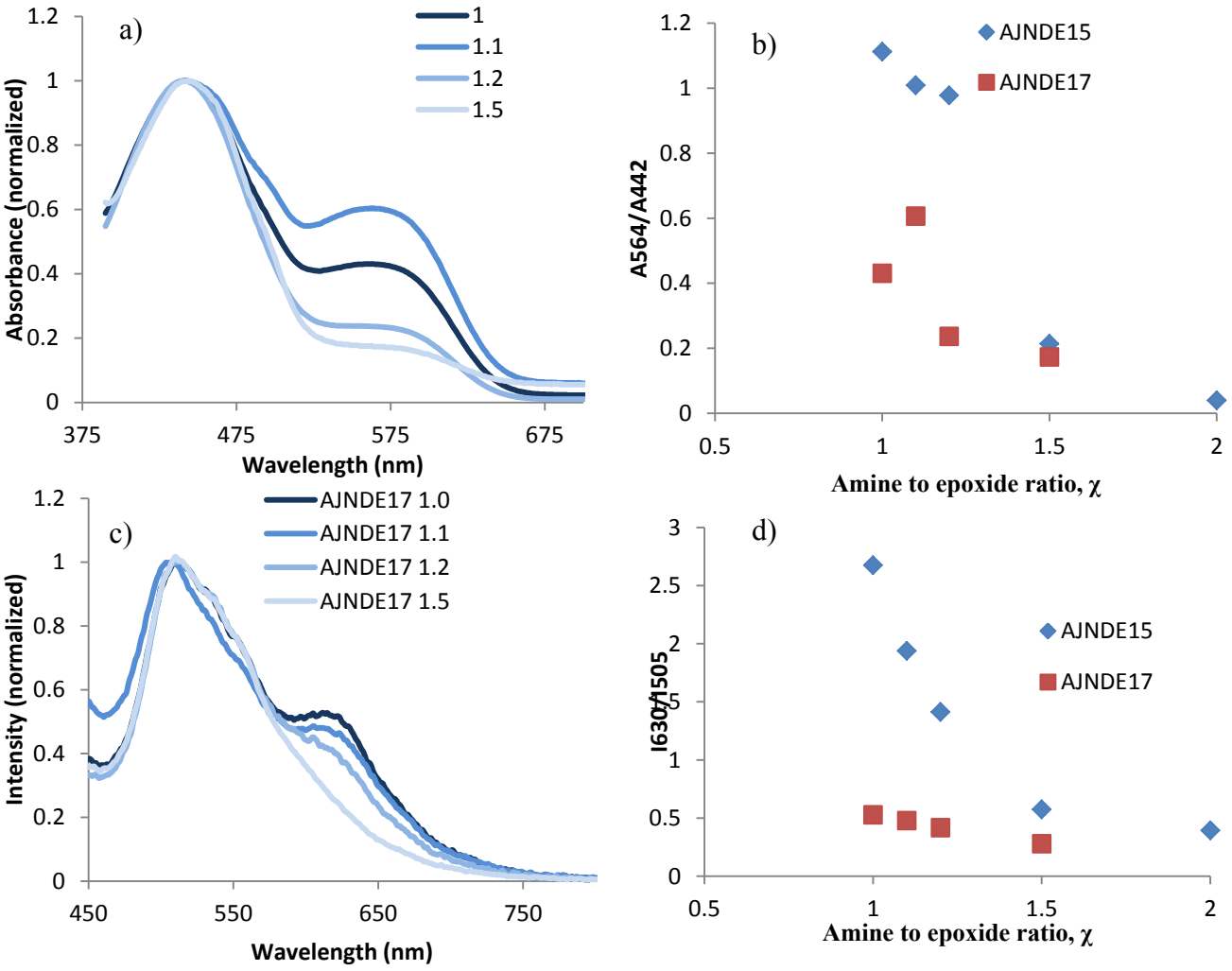

Figure 78: AJNDE17 stoichiometry variation. a) Absorbance after curing. b) ratio of absorbance peaks at 447 and 564nm for AJNDE15 and AJNDE17. c) Emission after curing. d) ratio of emission intensity for peaks at 630 and 505nm for AJNDE17 and AJNDE15.

cure (see Figure 67). The probe AJNDE17 was developed to begin in the OFF state, removing the deactivation step from the AJNDE15 process. In theory, AJNDE17 will remain in the OFF state during and after cure more than AJNDE15.

Figure 78a shows the absorbance data after 24 hours of curing for AJNDE17. Figure 78b shows the ratio of the 564nm peak absorbance to the 447nm peak absorbance for AJNDE17 and AJNDE15 for comparison. Figure 78c shows the emission data for AJNDE17, and Figure 78d shows the ratio of the emission intensity at 630nm compared to the intensity at 505nm for AJNDE17 and AJNDE15 for comparison.

It is clear that AJNDE17 after curing has much lower ON character than AJNDE15 at all χ values, demonstrating the improvement in sensitivity to stoichiometry over AJNDE15. It is especially important to note the large reduction in ON character at χ=1, which is the preferred stoichiometry for aerospace applications.

4.1.5 AJNDE17 in DGEBA-DETA - Elevated temperature

In Figure 68 (Chapter 2, section 3.3.3), the emission spectra of AJNDE15 were presented for temperature exposures of 70°C. A sample of .05wt% AJNDE17 in DGEBA-DETA with χ=1 was exposed to 70°C for 2 hours, and its absorbance and emission spectra were collected before and after exposure. These are shown in Figure 79a and b, with absorbance spectra offset to 0A at 850nm and emission spectra normalized to the 505nm peak intensity. It is clear that AJNDE17 at χ=1 shows some sensitivity to temperature despite the modifications made to improve the temperature stability.

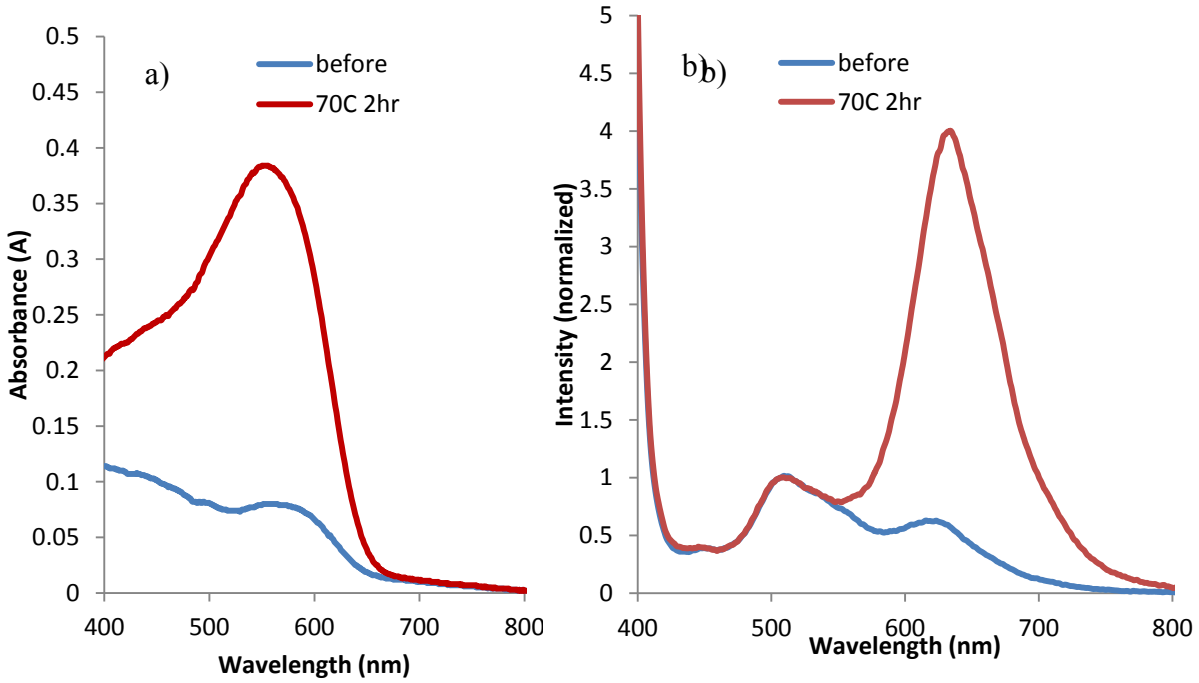

Figure 79: AJNDE17 response to 70°C exposure. a) Absorbance spectra. b) emission spectra.

After 70ºC exposure for 2hr, the R value for the OFF→ON transition is 539, which is comparable to R for AJNDE15 at similar exposures (R=461, see Figure 71).

4.1.6 AJNDE17 in DGEBA-DETA - Time stability after deformation

AJNDE17 was designed to be more stable in the ON state after mechanical deformation. For evaluation, a sample was prepared and tested just as in the AJNDE15 case. The results of AJNDE15 and AJNDE17 R ratio changes with respect to time after deformation are shown in Figure 80. Again, while initial performance of AJNDE15 1-1.5 is much higher, AJNDE17 shows more consistent temporal stability. A line fits the data well instead of a logarithmic decay; as well, after 200hr the AJNDE17 R value is significantly higher than AJNDE15's.

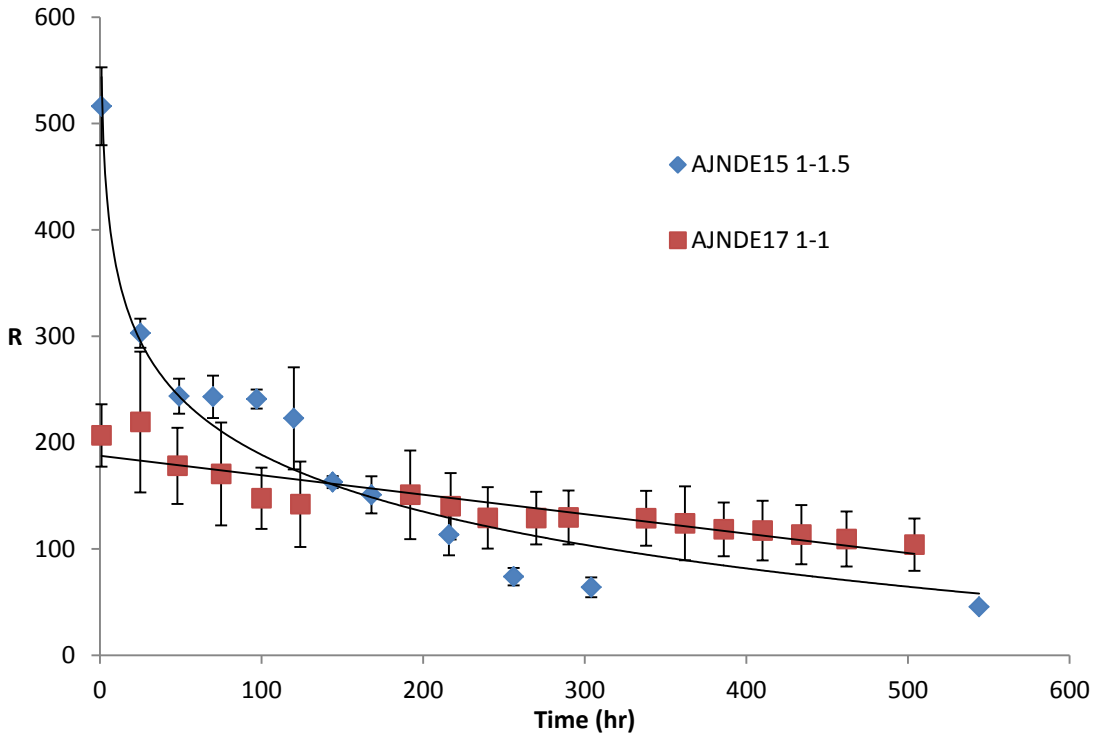

Figure 80: AJNDE15 χ=1.5 and AJNDE17 χ=1 R value vs. time after deformation.

5. EVALUATION OF MECHANOCHROMIC MECHANISMS

In this section the mechanochromic behavior of AJNDE15 and AJNDE17 will be discussed in the context of the four established mechanisms outlined in Chapter 2 section 1.1, along with the proposed mechanism specific to these probes. The results obtained so far will be analyzed to determine whether they support an interpretation of probe behavior based on the mechanisms above. Where necessary, concepts will be reviewed or introduced. Future experiments to provide more evidence in support of each mechanism and the results expected if that mechanism is the governing one will be described.

5.1 Aggregation-based approach

If AJNDE15 and AJNDE17 are mechanochromic through the aggregation-based mechanism, their response is based on molecules' proximity to one another. Deformation of the samples would change this proximity, which would change the fluorescence response by promoting or demoting aggregates.

5.1.1 Curing

Excimer forming molecules can be highly sensitive to the conditions around them, whether liquid or solid. The polarity of the solvent has a large effect on the formation of excimers (76; 77). The viscosity of the surrounding medium can also affect the ability of excimers to form (59). In the case of AJNDE15, the aggregation hypothesis asserts that the dimer species absorbs at 564nm and emits at 630nm. During DGEBA-DETA curing, the dielectric constant decreases (78; 79), while the viscosity initially decreases and then greatly increases (59). Both of these could account for the observed increase in dimer absorbance under the aggregation-based probe hypothesis.

5.1.2 Mechanical deformation & hydrostatic pressure

Aggregation is a process that usually results in emission of lower energy fluorescence from dimers than from monomers. In our case, the emission of AJNDE15 and 17 shows two distinct peaks at 505nm and 630nm. Uniaxial compression causes a decrease of the higher energy emission at 505nm, and an increase of the lower energy emission at 630nm. This is consistent with an aggregation based probe, where compression would force molecules closer together and thus promote dimer formation and emission of the highest-wavelength species. The observation that the OFF→ON transition when quantified by the R value is linear with ε_{def} is also consistent

with aggregation based behavior. An aggregation based probe would be insensitive to the different phases of deformation (elastic, strain-softening, or strain-hardening) and would be expected to respond linearly to permanent deformation ε_{def}. Hydrostatic pressure would cause no ε_{def} and therefore cause no activation of an aggregation-based probe.

5.1.3 Stoichiometry

Based on the mechanical deformation response, the interpretation under consideration is that AJNDE15 and AJNDE17 are aggregation based, and that 630nm emission from the ON state is characteristic of dimer emission. The changing responses of AJNDE15 in DGEBA-DETA of varying stoichiometry suggest that increasing the amine content either inhibits dimer formation or promotes monomer formation. The polymer network in its glassy state becomes denser with increasing χ (see Chapter 2 section 1.2.2) but this would seem to promote dimer formation if it would affect aggregation at all.

An interpretation that may explain this behavior and fit the aggregation hypothesis is the polarity of the network. Aggregation is a phenomenon that is highly affected by polarity, which changes as the DGEBA-DETA network cures (75). It is logical that increasing χ would change the polarity as well.

5.1.4 Elevated temperature

The aggregation-based probe hypothesis is not supported by AJNDE15 and AJNDE17 behavior when exposed to elevated temperature. Exposure to 70ºC is above the glass transition temperature for some stoichiometric ratios of DGEBA-DETA (see Figure 22) and not for others, but the activation of AJNDE15 and AJNDE17 appears to occur strongly for samples independently of T_g. If T_g<70ºC, temperature exposure above T_g could cause cure to progress

further, which according to the absorbance measurements taken during cure might cause more absorbance of dimer characteristics. But this would not agree with the result of section 3.3.3, where increasing χ inhibits dimer formation, because increasing χ also causes the cure reaction to progress further (see Figure 22 and Figure 24).

Other researchers using aggregation based mechanochromic probes in solid polymers have noticed that temperature exposure promoted aggregation (80; 81). They have attributed this to the probe molecules being kinetically trapped in the thermodynamically unstable monomer state when samples were quenched from liquid melts to solids. After annealing above T_g, when molecular chain motion becomes allowed, the molecules were able to approach one another again and form nanoscale aggregates. This behavior was observed to follow Johnson-Mehl-Avrami-Kolmogorov transformation kinetics, and was described by equation 11

$$\frac{I_m}{I_e} = \frac{I_{m\infty}}{I_{e\infty}} + Ae^{-t/\tau} \qquad \textbf{12}$$

where I_m and I_e are the intensities of monomer and dimer emission, $I_{m\infty}$ and $I_{e\infty}$ are the intensities at equilibrium, A is a reaction rate constant, and τ the exponential time constant (80). The exponential time rate constant τ was shown to follow the temperature above T_g ($T-T_g$), however, and annealing below the glass transition caused no change in aggregation (80). This is in contrast with our observations that temperature exposure below T_g causes activation of probes AJNDE15 and AJNDE17.

5.1.5 Time stability

The time stability after deformation of AJNDE15 suggests that in the aggregation hypothesis, molecules that formed dimers when compressed eventually formed monomers over a long time

scale. The formation of dimers is caused by mechanical deformation, which on a macroscopic scale is permanent. The relaxation of anelastic strain ε_{an} could provide the molecular motion possible to break up dimer formation. But based on the OFF→ON transition observed during cure, molecular motion should move the reaction toward the ON state, not OFF state. Based on the hypothesis that aggregation is caused solely by plastic deformation, the decay of AJNDE15 fluorescence after initial deformation cannot be explained adequately. These results are inconsistent with the aggregation based theory.

5.1.6 Summary of aggregation approach

The aggregation based approach is not sufficient to completely explain the response of AJNDE15 and AJNDE17 to all of the conditions the probes have experienced in this study. The changes observed during cure are consistent with the hypothesis, as changing polarity and viscosity could change an aggregation probe's response. The probes' responses to mechanical deformation and hydrostatic pressure are consistent with an aggregation mechanism. Varying the stoichiometry of DGEBA-DETA causes changes in probe behavior that are not explained by aggregation alone, but could be due to changes in polarity affecting the aggregation state. But the probes' temperature exposure response is not consistent with an aggregation-based probe mechanism. The time stability of AJNDE15 over time is also inconsistent with an aggregation based approach.

5.2 Intramolecular approach

If AJNDE15 and AJNDE17 are mechanochromic through an intramolecular mechanism, then their mechanochromic response will be sensitive to the free volume of the polymer and any changes to it. The hypothesis of this interpretation that the OFF→ON transition of AJNDE15

and AJNDE17 is based on a permanent isomerization or TICT transition which requires some finite level of free volume in which to occur. If this is indeed the case, increasing free volume hole sizes will allow more of the probes to transition to the ON state, or for the rate of transition to increase. A discussion of the preliminary results and comparison to previous work characterizing the response of epoxy free volume to various external stimuli will be presented, outlining the results and their support for this hypothesis.

5.2.1 Curing

As a mixture of DGEBA and DETA monomers cures, the free volume decreases from extremely high values to the small volume hole sizes described in literature. Other studies using fluorescent probe molecules using the intramolecular isomer approach have observed this quite extensively in amine-cured epoxies (55; 82). In our results, AJNDE15 turns ON during the cure of DGEBA-DETA. This is inconsistent with the interpretation of our hypothesis based on the mechanical deformation results, which asserted that increasing free volume hole size promoted AJNDE15's ON state.

5.2.2 Mechanical deformation & hydrostatic pressure

Mechanical deformation of AJNDE15 in DGEBA-DETA by uniaxial compression caused the transition from OFF to ON state. Hydrostatic pressure caused no activation. Based on these results, AJNDE15 and AJNDE17 as intramolecular, free-volume sensitive probes, would be expected to turn ON when free volume hole size increases.

Mechanical deformation at different stages of the stress-strain curve and its effect on the free volume has been studies in glassy polymer systems, but not in epoxy to our knowledge. A work that studied PTFE and PE glassy polymers showed an increase in free volume hole size in the

elastic and strain-softening stages, but a slightly decreasing or constant hole size in the strain hardening region (83). Studies in PMMA showed also that hole size linearly increased until the onset of strain hardening, after which hole size remained constant (84). A study in polycarbonate actually reported a decrease in free volume hole size due to compression, but an increase due to tension (85). Hydrostatic pressure caused a decrease in free volume hole size and in the number of free volume holes in epoxy (62).

The results of AJNDE15 and AJNDE17 in DGEBA-DETA in hydrostatic pressure testing are consistent with a free volume interpretation. But in uniaxial compression, samples show a response to increasing ε_{def} that can increases well into the strain hardening region. This is not consistent with free volume measurements in other polymer systems.

5.2.3 Stoichiometry

Several works have shown that free volume in cured epoxy samples varies as the stoichiometric ratio is changed (86; 87). In what may be counterintuitive, the samples with the highest measured overall free volume in the glassy state are samples with balanced stoichiometry (χ=1). This has been attributed to the highest degree of crosslinking and least number of dangling chain ends allowing the least amount of rotation and movement of chain segments between crosslinks (86). However, research directly measuring hole volumes suggests that while samples with the highest crosslink density have the highest *overall* free volume, they also have the lowest free volume *hole size.* In work from reference (87), which took T_g as a measurement of degree of cure and equated degree of cure with crosslink density, samples with the lowest crosslinks had the highest free volume hole sizes. A plot of the average free volume hole radius for varying degrees of conversion is shown in Figure 81, showing a decrease in hole size up to a point after which the hole size remains constant. Samples with increasing χ values showed increasing

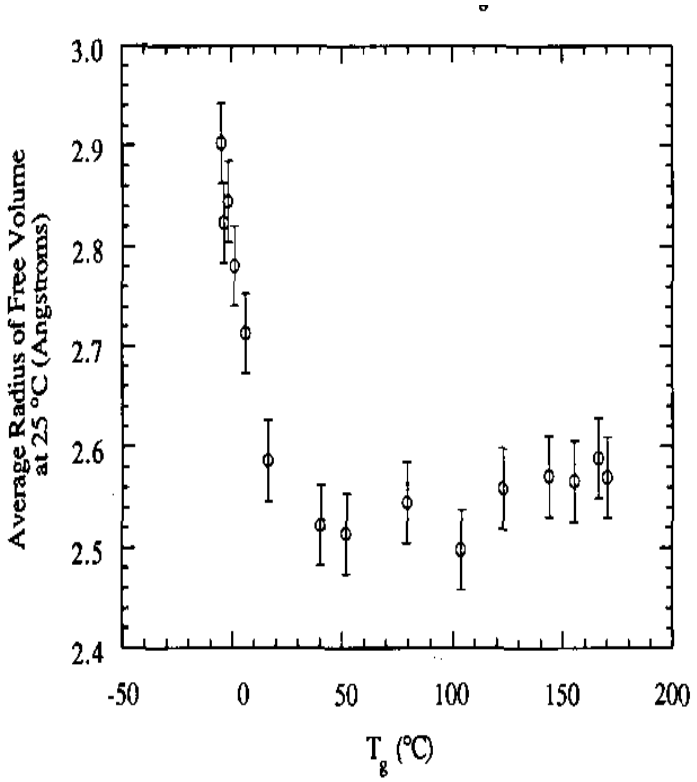

Figure 81: Free volume hole radius in epoxy for varying degree of conversion (see discussion for details). From (86).

degree of cure in DSC measurements (see Chapter 2 sec. 1.2), so would have decreasing hole size. However, increasing χ above 1 will also decrease the crosslink density, which will increase the hole size (86). It is unclear which would be the dominant trend in our system.

The results of AJNDE15 probe behavior in DGEBA-DETA with varying stoichiometric ratios suggests that increasing the amine content drives the probes toward the OFF state. The literature on free volume hole size suggests that increasing degree of cure causes a decrease in hole size, but that decreasing crosslink density causes an increase in hole size. Since increasing amine content causes both increasing degree of cure and decreasing crosslink density, more observations are necessary to evaluate the response of AJNDE15 in samples of varying stoichiometry.

5.2.4 Elevated temperature

The free volume changes with respect to temperature are more complex and are very dependent on whether the sample is in the glassy or rubbery state. If the epoxy is below T_g, increases in temperature causes a small increase in hole radius. If the epoxy is above T_g, the average hole radius increases at a much higher rate, with a broadening of the hole volume distribution towards the highest hole volumes. Figure 82a has the average hole radius plotted against the sample temperature with respect to T_g, showing the two trends above and below the glass transition (data from (88), trendlines added). Figure 82b has the hole volume distribution functions as temperature increases, showing the distributions broadening to higher hole volumes.

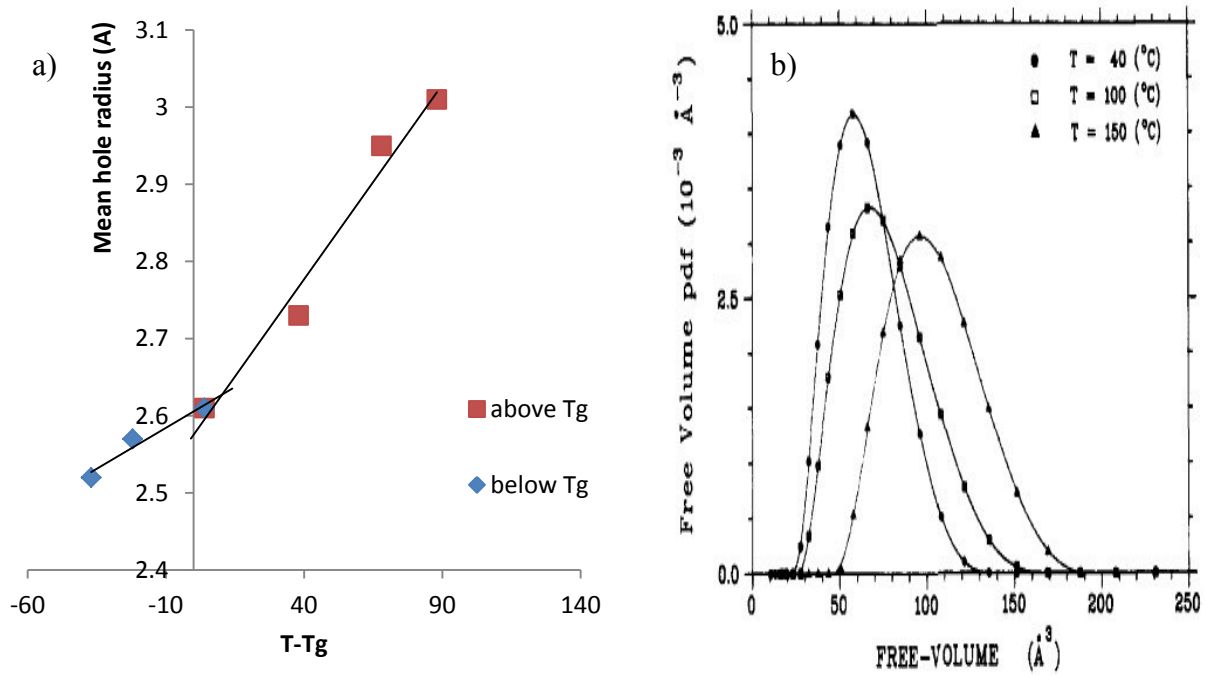

Figure 82: a) Free volume hole radius vs. (T-Tg) in epoxy. b) Free volume hole volume distribution for varying temperatures (Tg=62ºC). Data from (88) – trendlines in a)added by current author.

In Chapter 2 section 3.3.4, heating samples cured at room temperature to 70ºC caused a transition from AJNDE15's OFF state to ON state. Free volume measurements of epoxy showed that above T_g, average hole size increases, which is consistent with our interpretation of

AJNDE15 and AJNDE17 as turning ON with increasing free volume hole size. The kinetic study of AJNDE15 is also consistent with the free volume hole size dependence interpretation, with free volume hole size increasing even below the T_g of the epoxy.

5.2.5 Time stability

Studies have shown that hydrostatic pressure causes a decrease in free volume hole size. When the pressure was removed, holes expanded again to nearly their original sizes over a period of 10 days (62). The increase in hole size due to plastic deformation and its stability over time have to our knowledge not been studied in epoxy. This could serve to explain the decrease in ON state activity over time, if the free volume is also decreasing over time.

At room temperature, the relaxation of ε_{an} over time may help to explain the transition of AJNDE15 and AJNDE17 to the OFF state.

5.2.6 Summary of intramolecular isomer approach

The mechanical deformation of DGEBA-DETA in uniaxial compression causes free volume holes to increase in size according to other researchers' work using PALS. With this in mind, if AJNDE15 and AJNDE17 are isomeric probes, and mechanical deformation has activated them, they are preferentially activated by an increase in the free volume hole size. This interpretation is inconsistent with the observations made during the cure of DGEBA-DETA, which turns AJNDE15 ON while dramatically decreasing the free volume. The hypothesis is consistent with the temperature results, because free volume hole size in epoxy increases with temperature both below and above T_g. It is unclear whether the probes' behavior in DGEBA-DETA of different stoichiometries is consistent or inconsistent with this theory -the convolution of hole size

increase due to increased conversion and hole size decrease due to decreased crosslink density makes drawing a strong conclusion difficult.

5.3 Mechanochemical reaction approach

In this hypothesis, fluorescence in the probes is activated by a chemical reaction which is caused or aided by mechanical energy imparted to the system. The mechanical energy lowers the activation energy barrier required for the reaction to proceed.

5.3.1 Curing

Our hypothesis that AJNDE15 and AJNDE17 are mechanochemical reaction probes suggests that the OFF→ON transition is caused by a reaction similar to spiropyran-merocyanine. Unreacted amines present in DGEBA-DETA during curing could be preventing the reaction from occurring in an effect similar to solvatochromism in the spiropyran-merocyanine reaction, which in liquids is highly sensitive to the polarity of the solvent environment (89; 90). This is supported by our findings that AJNDE15 dissolved in DETA liquid displays no purple color, while in DGEBA it shows strong color. In blends of solvents, in which a solvatochromic molecule is highly active in one and inactive in the other, the fluorescent activity varies with the concentration of solvents (91). This is also consistent with the results gathered for AJNDE15 during curing.

5.3.2 Mechanical deformation & hydrostatic pressure

The activation of AJNDE15 and AJND17 in DGEBA-DETA under uniaxial compression suggests the hypothesis that the energy from compressive deformation to this degree is sufficient to reduce the activation energy to the point that the system has enough thermal energy to activate

at room temperature. This is consistent with the mechanochemical reaction hypothesis. The measurements of hydrostatic pressure are also consistent - hydrostatic pressure has been shown to impart no internal energy to glassy polymer samples and would therefore produce no OFF→ON transition.

The R ratio's linear relationship with ε_{def} suggests that energy is imparted to the system in a monotonic manner with increasing ε_{def}. The ΔU_{def} as measured in DSC is decidedly non-linear with ε_{def} (34). The probe molecule environment may not correspond well with the measurable quantities ε_{def} or $\Delta U_{def,}$ however.

5.3.3 Stoichiometry

The results gathered from stoichiometric variation of the DGEBA-DETA matrix surrounding AJNDE15 are consistent with the mechanochemical reaction hypothesis. Increasing amine content causes AJNDE15 to express more OFF character; in this hypothesis this means that the energy barrier to the ON state is changing as amine content increases. This could be explained by a solvatochromic interaction. The samples of AJNDE15 in DGEBA-DETA with $\chi>1$ have unreacted amines, which could change the overall polarity of the bulk polymer. This could inhibit the OFF→ON reaction, accounting for the decrease in color and fluorescence in cured samples with $\chi>1.5$.

When the samples are exposed to heat, the energy barrier is overcome by the added thermal energy and the reaction is allowed to proceed to completion in this hypothesis. This is consistent with the results we have gathered for thermal exposure of AJNDE15 in different stoichiometries of DGEBA-DETA.

5.3.4 Elevated temperature

The results gathered from exposure to temperature for AJNDE15 and AJNDE17 are consistent with the mechanochemical reaction theory. Exposure to elevated temperatures increases the rate of the OFF→ON reaction, regardless of the glass transition of the material surrounding the probe molecules. The results of the kinetic study of AJNDE15 are also consistent with the mechanochemical reaction theory. Higher temperatures and longer times cause increasing OFF→ON activity, suggesting a reaction rate which obeys Arrhenius laws. Exposure to low temperatures such as 40ºC causes the OFF→ON transition, which suggests that the activation energy barrier is small. This is consistent with the uniaxial compression results, which suggest that the energy imparted by ε_{def} is sufficient to lower the energy barrier to a point where room temperature can activate the reaction.

5.3.5 Time stability

The mechanochemical hypothesis suggests that the OFF→ON transition is caused by a reaction, which mechanical energy makes easier. The time stability of AJNDE15 after the OFF→ON transition suggests that this reaction is not permanent – that over long periods of time there is a reversal of the reaction back to the OFF state, or a further reaction to some non-fluorescent state. The kinetic study of AJNDE15 at the highest temperatures and exposure times shows a decrease in R values from the initial activation. In addition, evidence of a degradation reaction to some product that emits at 530nm for the highest amine content samples was observed for temperature exposures of AJNDE15. Whether the time study is evidence of an ON→OFF transition, or of a degradation of the ON state to the yellow-emitting product is not clear, but both would account for the decreasing R values as time increases. These measurements suggest at the least that the OFF→ON transition is not permanent, which would make the decay of the R value with time

certainly possible under this hypothesis. Further characterization is required, but the current observations are consistent with the mechanochemical hypothesis.

5.3.6 Summary of mechanochemical approach

The hypothesis that a mechanochemical reaction is causing the OFF→ON transition of AJNDE15 and AJNDE17 is consistent with all of the currently observed measurements.

The mechanical deformation of DGEBA-DETA around the probe molecules reduces the activation energy barrier for the OFF→ON reaction, which allows the reaction to proceed at room temperatures. The linearity of the response with ε_{def} is not clearly explained, but the transfer of bulk mechanical strain energy to the probe molecule is also not fully understood .

The behavior of AJNDE15 in the liquid components DGEBA and DETA support the mechanochemical interpretation, as does the observations during curing of the absorbance changes of AJNDE15. The changing polarity of DGEBA-DETA during cure (75; 78) could have a solvatochromic effect, which has been observed for other mechanochemical reactions (89).

The exposure of AJNDE15 and AJNDE17 to elevated temperatures increases the rate at which the OFF→ON reaction proceeds. A kinetic study of AJNDE15 supported this interpretation- increasing temperatures and exposure times causing an increase in the extent of the OFF→ON transition, consistent with Arrhenius-type reaction rate behavior.

Variation of the stoichiometry of DGEBA-DETA around AJNDE15 showed a decrease in ON state character as amine content increased. This is consistent with the mechanochemical reaction theory if the reaction has solvatochromic characteristics, which other mechanochemical reactions like spiropyran-merocyanine have shown (89).

The time stability of AJNDE15 and AJNDE17 after activation is consistent with the mechanochemical hypothesis on the condition that the reaction is either reversible or that another reaction to a degraded state is possible. Evidence for one or both of these possibilities is seen in the kinetic study of AJNDE15, where the highest temperature exposures showed an initial high increase, then a decrease in the R value of the transition as exposure time increased. Evidence for the degradation of AJNDE15's ON state is also seen by the formation of a yellow-emitting product during elevated temperature exposure of AJNDE15 at the highest amine-containing stoichiometry.

5.4 Chain scission approach

In this approach, fluorescence is activated in molecules by chain scission, which is caused by a crack preferentially propagating through a bond that when broken cause the OFF→ON transition. A method in the literature was demonstrated where the broken bond separated two aggregated probes into their fluorescent monomer configuration. If a similar mechanism is causing AJNDE15 and AJNDE17 mechanochromism, crack formation should demonstrably change the fluorescence behavior.

Microcrack formation is observed in DGEBA-DETA samples under compression, so this mechanism is theoretically possible. A detailed investigation of crack formation and its relation to AJNDE15 and AJNDE17 has not been performed, however.

Curing of DGEBA-DETA would not be expected to cause microcracking of the solid polymer. But the mechanism for scission-based mechanochromism has been based on aggregation in other work (70; 71). Aggregation based probes can be highly sensitive to polarity and viscosity, which change dramatically during cure (see Chapter 2 section 5.1.1). So a mechanism dependent on

crack propagation separating excimers into monomers could certainly display the observed behavior of AJNDE15 during cure.

It is conceivable that an elevated temperature exposure could introduce enough thermal energy into the AJNDE15-DGEBA-DETA system to break the bonds that would activate fluorescence in the probe molecule. This scenario would have the same result as the mechanochemical reaction, where elevated temperature causes the OFF→ON transition of AJNDE15.

More research is required to determine what, if any, effect the stoichiometry of a solid polymer might have on the bond strength or scission behavior of a specific bond. Aggregation dependent scission based mechanisms might show sensitivity to stoichiometry based on the polarity of the samples with high χ values.

5.5 Proposed mechanism – Conjugation pathway interference

The proposed mechanism for AJNDE15 and ANDE17mechanochromism is based on a reaction between the probe molecule and an amine functional group. Mechanical force promotes the dissociation of a C-N bond, which when removed connects a conjugation pathway between a donor and acceptor group and activates fluorescence. To review this mechanism, the figures of the OFF→ON and ON→OFF reactions are displayed again in Figure 83.

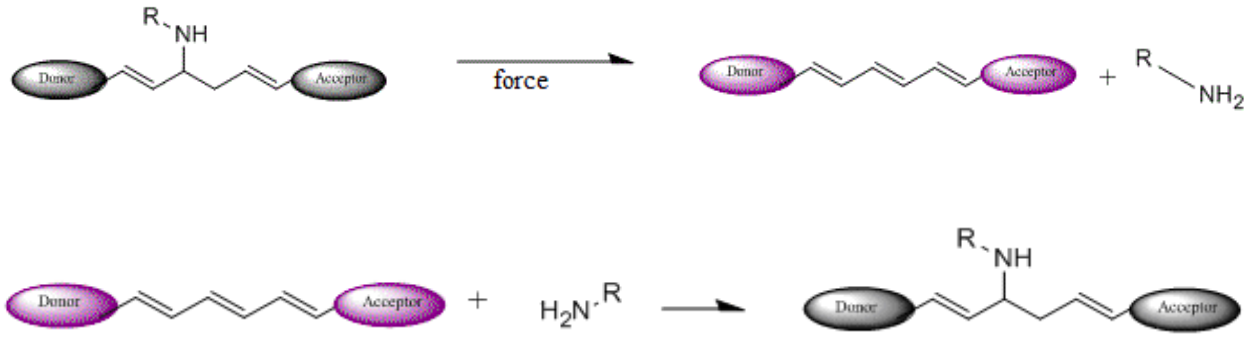

Figure 83: top: proposed OFF-->ON transition for AJNDE15 and AJNDE17. bottom: proposed OFF-->On transition for AJNDE15 and AJNDE17.

5.5.1 Curing

The response of AJNDE15 and AJNDE17 during DGEBA-DETA cure is consistent with the conjugation pathway approach. After mixing, AJNDE15 shows low absorbance from the ON species, indicating that it has been turned OFF during mixing with liquid DGEBA-DETA by the reaction with the primary amine groups of DETA. As curing progresses, these amine groups are consumed by reaction with DGEBA, which is competitive with the ON→OFF reaction. Eventually DGEBA begins to remove the amine groups from AJNDE15, turning it ON. The relative ratio of ON to OFF absorbance and emission after cure shows that AJNDE15 remains OFF in the presence of excess amines, which is consistent with the proposed mechanism.

AJNDE17 shows similar behavior during cure as AJNDE15, with ON absorbance increasing as cure progresses. (see Figure 59). However, the amount of ON character after cure is much lower than AJNDE15 due to the molecule starting in the OFF state instead of the ON state (see Figure 78).

5.5.2 Uniaxial compression & hydrostatic pressure

The response of AJNDE15 and AJNDE17 to uniaxial compression is consistent with the proposed mechanism, where mechanical force encourages the dissociation of the C-N bond that is inhibiting fluorescence. Increasing ε_{def} causes more ON activity in both AJNDE15 and AJNDE17. The bond dissociation process described in the mechanochemical reaction mechanism appears to be appropriate in this situation as well, with the amine-probe bond dissociation being promoted by the addition of mechanical energy, but ultimately being activated by thermal energy. If this is true, mechanical energy added to the bulk polymer must be applied

to the probe molecule efficiently enough to reduce the activation temperature of the C-N dissociation below room temperature. This is conceivable based on the elevated temperature kinetics study of AJNDE15, which shows significant OFF→ON activity at as low as 40°C (see Figure 71).

5.5.3 Stoichiometry

The effect of varying stoichiometries on AJNDE15 and AJNDE17 is consistent with the proposed mechanism. The OFF state of AJNDE15 and AJNDE17 requires the presence of an unreacted amine group, which suggests that increasing amine content would produce more of the OFF state after curing. This is consistent with the results gathered for absorbance and emission of AJNDE15 and AJNDE17 (see Figure 67 and Figure 78).

An alternative interpretation is based on the time that the OFF→ON reaction is allowed to proceed during cure. Increasing χ increases $\frac{d\alpha}{dt}$ (see Figure 24), reducing the time before the onset of gelation and diffusion control. If the reaction is only allowed to proceed during times when some molecular motion is possible, the reduced time before gelation would allow less ON state to form.

5.5.4 Elevated temperature

The response of AJNDE15 and AJNDE17 to elevated temperatures is also consistent with the proposed conjugation pathway mechanism. Increasing temperatures would impart energy to the system which could be used to dissociate bonds. The C-N bond would be the first to dissociate based on its low bond energy, turning the probe molecules ON. The dissociation process appears to follow Arrhenius-type rate law behavior in AJNDE15 kinetics studies at low temperatures, with longer exposures and higher temperatures causing increased OFF→ON transition (see

Figure 71). The kinetics study suggests that at the highest temperatures studied, the OFF→ON transition magnitude decreases as time exposure increases. This study was performed in DGEBA-DETA with χ=1.5, so there are excess amines available which could react with AJNDE15's ON state to turn it back OFF. The high temperatures and excess amines available could promote this transition in this case.

5.5.5 Time stability

The observations of decreasing OFF state over long time periods of AJNDE15 after deformation, and the less prevalent decrease of AJNDE17, are consistent with the proposed mechanism of conjugation pathway interference. After deformation, the probes are in the ON state. Observations from the kinetic temperature study of AJNDE15 suggest the possibility of the ON state reacting with excess unreacted amine to form the OFF state in solid DGEBA-DETA. In these measurements, AJNDE15 samples had χ =1.5, while AJNDE17 had χ=1. After sufficiently long time, it is conceivable that the AJNDE15 ON state turned OFF by reacting with the excess amine, while AJNDE17 samples had much less unreacted amines available for the reaction.

5.5.6 Summary of mechanochromic mechanisms

The mechanochemical reaction mechanism is consistent with all of the observations made at this point. In this mechanism AJNDE15 and AJNDE17's OFF→ON transition is caused by a reaction, which mechanical deformation promotes by lowering the activation energy barrier. The effect of temperature is consistent, along with the effect of amine ratio if some solvatochromic character is postulated for the probes or if the reaction cannot proceed without the freedom for molecular motion.

The aggregation based mechanism is consistent with the observations made for mechanical deformation and for stoichiometric variation. However, temperature should only promote dimer formation at temperatures above T_g, which is inconsistent with the temperature observations made thus far. The time stability of AJNDE15 is also inconsistent with this theory.

The intramolecular isomer approach is consistent with the observation that mechanical deformation increases free volume hole size, which would increase probe fluorescence activity. However, some dependence should be observed on the section of the stress-strain curve in which the deformation takes place. This is either not present or not clearly observable in the data collected thus far. This mechanism is consistent with the temperature measurements – elevated temperatures expand free volume holes both below and above T_g. It is unclear if the stoichiometric variation measurements support or contradict this mechanism. More study is needed to explain the time stability results with respect to this model.

The scission-based approach has not been fully evaluated in this study. Preliminary investigations showed the appearance of microcracking at high ε_{def} but these studies have not been advanced further.

The proposed mechanism of conjugation pathway interference is consistent with all the measurements made thus far. The mechanism has many similarities to the mechanochemical reaction mechanism.

5.6 Summary of mechanochromic mechanism evaluation

A series of fluorescent probe molecules has been synthesized which displays mechanochromic properties in a structural amine-cured epoxy, DGEBA-DETA. To our knowledge, mechanochromism has not before been demonstrated in a structural polymer such as amine-

cured epoxy. This chapter is an attempt to characterize the mechanism by which the probe molecules AJNDE15 and AJNDE17 display mechanochromism. A comprehensive analysis of DGEBA-DETA was performed to separate its response to mechanical deformation, elevated temperature, and stoichiometry variation from the probes' responses. Analysis techniques were developed to quantify the OFF→ON response of the probes due to external stimulus. Four previously reported mechanochromic mechanisms and the proposed mechanism for these probes are evaluated based on their compatibility with the observed probe responses to mechanical deformation, curing, elevated temperature exposure, and time stability of probe fluorescence after deformation. The proposed mechanism and the mechanochemical reaction-based mechanism are identified as being consistent with all of the observations thus far. The results of these discussions have been summarized in Table 5.

Table 5: Summary of Mechanochromic Mechanisms for AJNDE15 and AJNDE17.

	Compression	**Hydrostatic**	**Curing**	**Stoichiometry**	**Temperature**	**Time**
Aggregation	consistent	consistent	consistent	indeterminate	inconsistent	inconsistent
Intramolecular Isomer	consistent/indet.	consistent	inconsistent	inconsistent	consistent	indeterminate
Mechanochemical	consistent	consistent	consistent	consistent	consistent	consistent
Scission Based	consistent	consistent	indeterminate	indeterminate	indeterminate	indeterminate
Conjugation Int.	consistent	consistent	consistent	consistent	consistent	consistent

The combination of conjugation interference and mechanochemical reaction will be the reaction model that is evaluated in Chapter 3.

CHAPTER 3

MODELING AND KINETICS OF MECHANOCHROMISM

1. INTRODUCTION

In this chapter three models relating the OFF→ON reaction of AJNDE17 to the mechanical behavior of DGEBA-DETA described in Chapter 1 will be presented. In addition, the kinetics evaluation techniques used to evaluate the mechanochromic reaction of AJNDE17 will be discussed. The relevant equations and assumptions will be discussed, and theoretical models of the expected behaviors will be presented. The merits of these models will be compared with experimental results in subsequent sections.

To analyze the kinetics of the ON→OFF reaction of probe molecule AJNDE17 in DGEBA-DETA in response to heat and deformation, some assumptions will be required. The validity of these assumptions is of varying degree. After presenting these assumptions, the reaction order equations used to determine various kinetic constants will be discussed.

2. MODEL FRAMEWORK FOR PROBE BEHAVIOR

The discussion of the behavior of probe molecule AJNDE17 in solid DGEBA-DETA must have a grounding in some physical trend, and a model that is able to encapsulate that trend should be applicable. This research will focus on the applicability of one such model - the Zhurkov model for mechanochemical reactions. The model's agreement with observations will be discussed in Chapter 3 section 5.

2.1 Zhurkov model

This section presents a model for probe behavior based on the work of S.N. Zhurkov, who investigated the mechanochemical properties of chain scission in polymers (92). Using techniques such as FTIR and electron spin resonance, he analyzed the byproducts of polymer fracture and their interaction with overall stress on the solid. His work developed a model of bond scission that has been applied to many fracture scenarios in solids, especially mechanochemical processes like stress-activated photochemical degradation in polymer coatings (93; 94). The most important concept in the Zhurkov model is that bond scission is a thermally activated event, with an associated activation energy barrier (95). This activation barrier can be lowered when mechanical work is done on the bond being studied, making the scission of the bond more likely to occur. The Zhurkov equation encapsulates this relationship with a modified Arrhenius rate law:

$$K = K_0 e^{\frac{-(E_A - \alpha\sigma)}{RT}} \quad \textbf{13}$$

Here K is the rate of bond scission, K_0 is a rate constant, E_A is the activation energy for bond scission, α is a constant sometimes called the activation volume, and σ is the applied stress, R is the gas constant, and T the temperature. The term ασ in the exponential is a measure of the mechanical work done on the bond due to the applied stress, and serves to reduce the effective activation energy E_a.

This model may be applicable to our probe behavior by determining conditions for the scission of the C-N bond linking AJNDE17 to the epoxy network, which inhibits the conjugation of the probe and keeps it in the OFF state. The mechanochemical bond scission model was proposed in Chapter 1 of this document as a mechanism for probe activation, and determined to fit all experimental data gathered thus far. The model of thermally activated scission of the C-N bond

creating the ON state agrees with the experimental data of heat exposure-induced activation presented in Chapter 2 section 5.1.4, as well as providing an explanation for the deformation-induced activation of the probe. The increased stress on the bulk polymer is translated to an increased stress on the C-N bond, which lowers the activation energy for scission of the bond to a level where room temperatures provide enough energy to activate bond scission in a significant fraction of the bonds and create a large ON state population.

2.1.1 Hypothesis and experiment

In the Zhurkov model, the exponential term ($E_A - \alpha\sigma$) is the most interesting aspect for this study. The activation energy E_A for scission of the C-N bond should be reduced by increasing stresses in the bond. This should make scission of the bond more likely, and the OFF→ON reaction should happen at a faster rate. A comparison of the OFF→ON reaction at similar temperatures for samples with varying amounts of bond stress should show reaction rates that increase as stress increases. A full Arrhenius activation energy measurement should show decreasing activation energies for the OFF→ON reaction with increasing stresses.

A problem in this model is that the experimental methodology in this study does not simultaneously apply stress and heat. The samples are deformed then heated, or heated then deformed. This study assumes that the measured deformation ε_{def} corresponds to an increase in the bond stress in the C-N bond of AJNDE17, which is by no means assured. The discussion of epoxy deformation in Chapter 1section 1.4 suggests that ε_{def} results in shear defect formation and intermolecular shear motion. The stretching of main-chain bonds is not thought to occur until the strain hardening region at very high ε_{def}, but AJNDE17 is bound to the network via side-chain polymerization rather than main-chain, so intermolecular shear motion may affect the C-N bond more strongly than other bonds.

2.2 Kinetic analysis methods

To evaluate the kinetics of the OFF→ON reaction, a measurement of the change in concentration of the relative species, [OFF] and [ON], with respect to time is necessary. Accepted practices which use the direct measurement of the OFF and ON species via NMR or FTIR are extremely difficult in DGEBA-DETA-AJNDE17 systems because of the low probe concentrations used, the general similarity of the OFF and ON states, and the overwhelming number of C-N bonds involved in the DGEBA-DETA network. Another accepted technique is absorbance, applicable when the species present have distinct absorbance spectra.

During cure, absorbance measurements can be used as a measure of [ON]. The absorbance peak at 564nm was assigned to the activity of the probe molecule AJNDE17 based on the excitation spectra (see Figure 61). Kinetics analysis was performed by using the value of the absorbance at 564nm, A_{564}, as an indicator of [ON]. This technique is widely used to monitor the kinetics of chemical reactions (96). The shape of the curve $A_{564}(t)$ should be a strong indicator of the reaction order of the OFF→ON reaction.

The absorvance technique is impractical for solid samples because it relies on samples having the same absorbance path length throughout testing– this is simple to assure using cuvettes for liquid samples. But solid samples are deforming and relaxing during testing, making the path length for which absorbance can occur shorter or longer. Attempts were made to adjust for this change by normalizing to the new sample dimensions, but did not produce satisfactory data for use in kinetic studies.

Measurements of fluorescence show a very strong and distinct spectral difference between the OFF state and the ON state, suggesting that fluorescent emission may be used to monitor the reaction. This technique has been applied by Carpick et.al. to evaluate the thermochromic

fluorescence of poly(diacetylene) (PDA) thin films, which transform between a non-fluorescent blue state and a highly fluorescent red state when exposed to appropriate heating conditions (97). In this work, the integral of the fluorescence curve associated with PDA's red state was assumed to be proportional to the concentration of the red state. This assumption is less appropriate for DGEBA-DETA-AJNDE17 because of the overlap between epoxy emission and probe emission. For this reason, the intensity of the peak emission of the probe, at ~630nm, will be assumed proportional to the concentration of the ON state. The peak emission intensity of the ON state still varies when the intensity of the entire spectrum changes as in sample realignment between measurements or sample shape change, however, so we must normalize in some way to account for whole-spectrum intensity changes. We can use an approach similar to the ratiometric probe analysis techniques in discussed earlier (see Introduction section 2.2), and assume that the epoxy and ON fluorescences are always proportional in the absence of an OFF→ON transition, to normalize each spectrum and define a quantity *I'*

$$I' = \frac{I_{ON}}{I_{epoxy}} = \frac{I_{630nm}}{I_{505nm}} \quad \textbf{14}$$

that is proportional to the concentration of the ON state

$$I' \propto [ON] \quad \textbf{15}$$

With these assumptions, a measurement of [ON] can be taken from a single fluorescent spectrum. For this approach to be valid, several assumptions must be made. These are presented and discussed in the next section.

2.2.1 Assumptions required for kinetic analysis

The first assumption that is required for kinetic analysis of AJNDE17 in DGEBA-DETA is that the fluorescent spectrum observed is due only to the epoxy, the OFF state of AJNDE17, or the ON state of AJNDE17 – that is, no other fluorescent species are contributing to the emission. We can further modify this assumption by observing from the excitation and emission data (see Figure 62 that the OFF state is non-fluorescent so that the fluorescence observed comes only from DGEBA-DETA or the ON state:

$$f_{total} = f_{epoxy} + f_{ON} \quad \textbf{16}$$

Some attributes of the OFF→ON reaction are assumed as well. The reaction is assumed to occur in one step, with no byproducts, so that the total concentration of OFF and ON molecules is constant. This is normalized to the initial concentration so that

$$[OFF] + [ON] = 1 \quad \textbf{17}$$

Where [OFF] is the relative concentration of OFF molecules and [ON] is the relative concentration of ON molecules.

Another assumption about the OFF→ON reaction is that the back reaction ON→OFF does not occur quickly at room temperature. The results in section Chapter 2 section 3.3.5 show that the back-reaction is possible over long time periods and in the presence of excess amine molecules, but we assume that testing in this analysis is completed quickly enough after deformation or heating that the back-reaction can be disregarded. Efforts were made to minimize the time between heat exposure or deformation and subsequent spectra collection; the delay was on the order of minutes in most cases.

The most important assumption requires that the ratio of epoxy fluorescence to ON state fluorescence is unchanging if the OFF→ON reaction is not occurring:

$$\frac{f_{epoxy}}{f_{ON}} = constant\Big]_{\frac{d[ON]}{dt}=0} \quad \textbf{18}$$

This assumption may not be perfectly valid for a number of reasons. The first reason is the changes in shape of the epoxy due to deformation and heat-induced recovery of deformation. The excitation LED source is not a perfect single-wavelength source, and some of the excitation source is always reflected back to the detector even in perfect 45° alignment. Any overlap between the excitation source bell curve distribution and the epoxy fluorescence will be magnified when the sample is moved closer to the probe tip, as is the case when samples expand. The opposite effect is expected when samples are deformed. The epoxy fluorescence signal will therefore be increased when samples are expanding, and decreased when samples are contracting. The overlap between excitation and fluorescence is relevant only for the epoxy fluorescence, which occurs at wavelengths adjacent to the excitation.

Another reason why Eqn. 18 may not be valid is the effects quantified in Chapter 1 and summarized in Table 4 – the changes in DGEBA-DETA fluorescence due to varying environmental conditions. The fluorescence of DGEBA-DETA does not change significantly with ε_{def}. But it does increase with elevated temperature exposure, which is crucial to our kinetics analysis procedure. The effect of elevated temperature on the DGEBA-DETA fluorescence is a small increase in intensity at 505nm for samples with χ=1. This will cause I' values to be smaller than a true measurement of [ON] would report.

Another problem with Eqn. 18 is that the fluorescence of DGEBA-DETA occurs at wavelengths which overlap with the excitation spectrum of AJNDE17. If AJNDE17 absorbs any of the

fluorescence emission from DGEBA-DETA, the decrease in I_{505nm} will cause I' to be larger than a true measurement of [ON] would report.

These assumptions must be considered when evaluating the validity of Eqn. 18. It is hoped that the reduction in I' due to increased DGEBA-DETA fluorescence due to elevated temperature exposure, and the increase in I' due to DGEBA-DETA fluorescence being absorbed by AJNDE17's ON state, will combine to leave I' an adequate measure of [ON].

2.2.2 Order of reaction

No attempt has been made to study the kinetics of the OFF→ON reaction before this work, so the order of the reaction is not known. Based on the proposed mechanism for the conversion from OFF to ON, the reaction is most likely either 0^{th} or 1^{st} order. For a 0^{th} order reaction, the change in concentration of a reactant [OFF] is independent of the concentration. Written in terms of the concentration of the product [ON] in combination with Eqn. 17, this change is expressed as

$$\frac{d[ON]}{dt} = -k \quad \textbf{19}$$

Or, integrated,

$$[ON] \propto -kt \quad \textbf{20}$$

Where k is the reaction rate constant.

If the reaction is 1^{st} order, the change in concentration of the reactant [OFF] is proportional to the remaining quantity of OFF molecules. Written in terms of the product [ON] in combination with equation x, this is expressed as

$$\frac{d[OFF]}{dt} = -k[OFF] = -k(1 - [ON]) \quad \textbf{21}$$

Or, integrated,

$$[ON] \propto 1 - e^{-kt} \quad \textbf{22}$$

Figure 84 shows a simplified plot of the behavior that the concentration of [ON] molecules should exhibit over time if the reaction is of 0th order or 1st order. One of the major goals of this work is to identify the order of reaction of the OFF→ON reaction in DGEBA-DETA-AJNDE17.

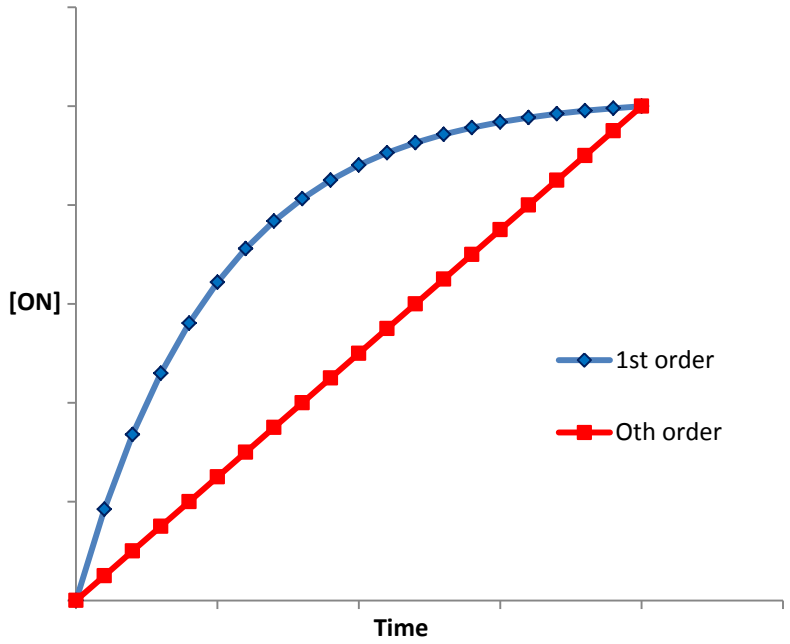

Figure 84: simplified plot of [ON] vs. time theoretical behavior if reaction is 0th order or 1st order.

2.2.3 Activation energy calculation

Using the models described in section 2.2, a reaction rate constant k can be extracted from plots of I' vs. time. The reaction rate constant varies with temperature according to the Arrhenius reaction rate law

$$k = Ae^{-\frac{E_a}{RT}} \quad (23)$$

Where k is the reaction rate, A is the pre-exponential factor, E_a is the reaction's activation

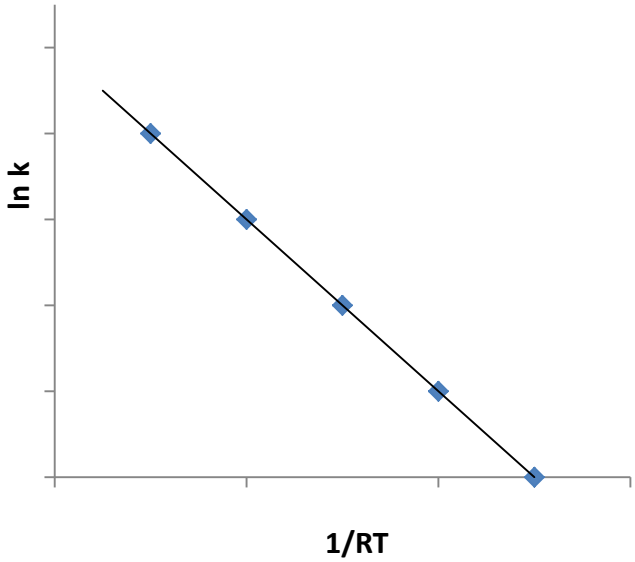

Figure 85: Example Arrhenius plot.

energy, R is the gas constant and T the temperature. Gathering reaction rates at several temperatures, an Arrhenius plot of ln k vs. (1/RT) can be constructed, the slope of which is the activation energy of the reaction. Figure 85 has a sample Arrhenius plot.

3. KINETIC ANALYSIS MEASUREMENT TECHNIQUES

In this section the measurement techniques used to perform the kinetic analysis of DGEBA-DETA-AJNDE17 will be presented. In Chapter 2, large OFF→ON reactions were observed under 3 conditions – during cure, during elevated temperature exposure, and after uniaxial compression. These three conditions can contribute to our understanding of the OFF→ON reaction and provide data that can allow the kinetic analysis described in Chapter 3 section 2.2.

3.1 Kinetic analysis during cure

Plastic cuvettes containing uncured DGEBA-DETA-AJNDE17 mixture were placed in the UV-Vis absorbance beam path and allowed to cure. Absorbance spectra were collected at appropriate time intervals (every 30 minutes for most mixtures) for the duration of the cure process (24hr for most mixtures). Baseline absorbance was taken on an identical plastic cuvette filled with unmixed DGEBA.

3.2 Kinetics of cured samples

The kinetics of cured samples were evaluated using combinations of elevated temperature and mechanical deformation. It was not possible to develop an in-situ measurement technique for the OFF→ON reaction during uniaxial compression, but the effects of ε_{def} can be measured indirectly by observing how ε_{def} affects the OFF→ON response to heat.

3.2.1 Kinetics of heat exposure

Two methods of quantifiably measuring the OFF→ON reaction response of DGEBA-DETA-AJNDE17 samples to elevated temperatures were used. The first is an incremental annealing method, where samples were tested after successive cycles of exposure to heat in a water bath, then quenching in ice water to return the sample rapidly to room temperature. Background spectra were taken before each measurement to account for changes in signal intensity due to any sample shape change. Water bath temperatures were 35, 40, 45, and 50°C. Annealing increments were 15 seconds for each exposure except for 35°C measurements where the exposures were in 30 second increments.

The second method is an *in-situ* heating method, where samples are placed on a digitally controlled heated stage (part of a GladiATR FTIR fixture, Pike Technologies, Madison, WI)

while aligned with the spectrometer probe tip as in Figure 20. The stage was brought to the exposure temperature, and a thin layer of heat transfer paste (Uniweld CoolBLUE) was used to ensure good thermal contact between the sample and the stage. After quickly attaching the sample to the stage using the heat transfer paste, spectra were collected continuously every 10 seconds beginning immediately after sample mounting. Temperatures were again 35, 40, 45, and 50ºC.

The two measurements are designed to measure the same phenomenon, the OFF→ON reaction of the probe molecule in the solid epoxy at different temperatures. In the incremental method, data collection is time consuming and difficult, samples must be re-aligned in the spectrometer after heating, and error in sample exposure temperature and time are more of a factor. But the ability to re-take background spectra between each spectra collection means that measurements are corrected for any changes in spectra associated with shape change of the sample during heat exposure. Spectra taken in the *in-situ* method are not corrected for sample shape change, and so care must be taken in interpreting the spectral results to avoid times when large sample changes are taking place due to recovery of ε_{an}.

3.3 Kinetics of heat-deformation combined exposure

In Chapter 2, fluorescence changes due to the OFF→ON reaction in DGEBA-DETA-AJNDE17 were observed in samples in response to both heat and deformation. In order to explore the interplay of these two effects, experiments combining temperature exposure and ε_{def} were designed. The temperature exposures were carried out via the methods described in Chapter 3 section **Error! Reference source not found.**, with the same temperatures and exposure times. our samples were deformed to the same ε_{def} increment, approximately every .05 ε_{def} up to .40,

and exposed to the four temperatures. Another set of four samples was loaded in the elastic region of the stress-strain curve and unloaded, then tested for heat exposure changes.

4. KINETIC ANALYSIS OF MECHANOCHROMISM

This section presents the data gathered using the methods described in Chapter 3 section 3. The kinetic analysis techniques discussed in Chapter 3 section 2.2 are applied, and the results are presented.

4.1 Kinetics during cure

Figure 86 is a plot of the absorbance of AJNDE17 at 564nm, A_{564}, as cure time increases in a RT cure of DGEBA-DETA-AJNDE17. The red line shows the fitting curve developed from eqns. **21** and **22**, the 1st order reaction models. The fit is extremely accurate up to times ~1000min, with R^2 =.9977. After this time the absorbance values increase away from the first order prediction.

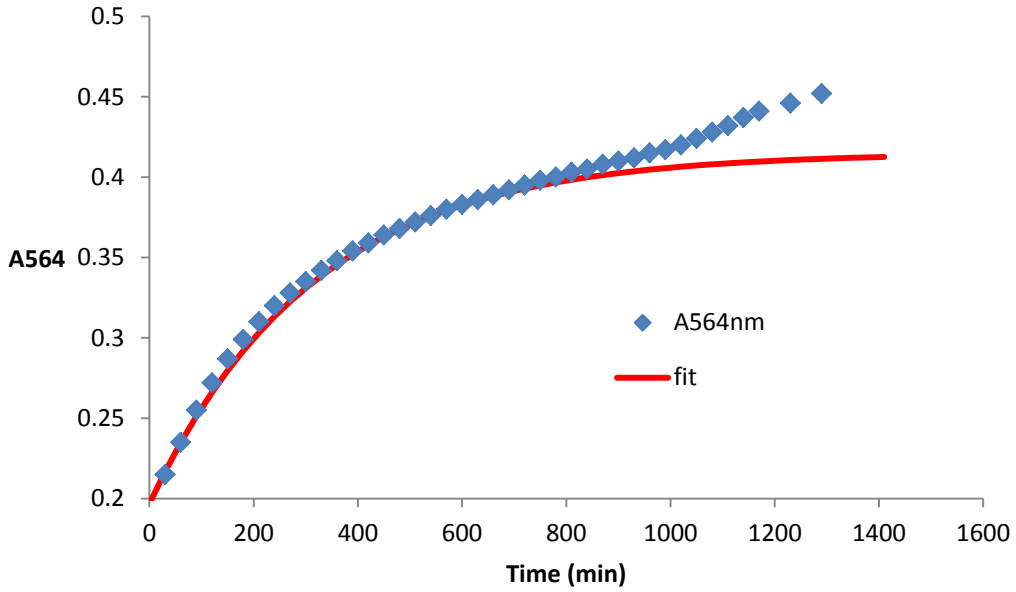

Figure 86: Absorbance of AJDNE17 during DGEBA-DETA cure and fit line based on 1st order model.

This result is strong evidence that before curing, AJNDE17's OFF→ON reaction is of 1st order. The reaction deviates from 1st order behavior after 1000min (16.6hr), which by comparison with the α(t) plot in Figure 23 is well past the time when chain motion would be prevented by the vitrification of DGEBA-DETA. The combined conclusion is that the OFF→ON reaction displays 1st order kinetics when intermolecular chain motion is not prevented.

4.2 Kinetics in solid polymer

The kinetics of DGEBA-DETA-AJNDE17 were explored first as a function of heat alone, to establish baseline levels of activity for the OFF→ON reaction. Both the water bath method and the in-situ method were used. Results will first be presented for the water bath method, after which the in-situ method's results will be discussed.

4.2.1 Heat exposure via water bath

Figure 87 shows the raw emission spectra collected from a sample of DGEBA-DETA-AJNDE17 after several heat exposure-quench cycles. The spectra here are collected using the spectrometer setup described in Chapter 1 section 2.2.3.3, and the water bath heat exposure method described in Chapter 3 section 3.2.1.

The spectra show that the emission peak at 505nm gradually decreases as heat exposure increases, while the emission peak at 630nm dramatically increases. This is consistent with the theory proposed in Chapter 2 section 3.3.1 where emission from DGEBA-DETA excites AJNDE17 emission. This behavior was typical of all temperatures tested and all methods used, whether in-situ heating or water bath heat-quench cycles were the source of heat.

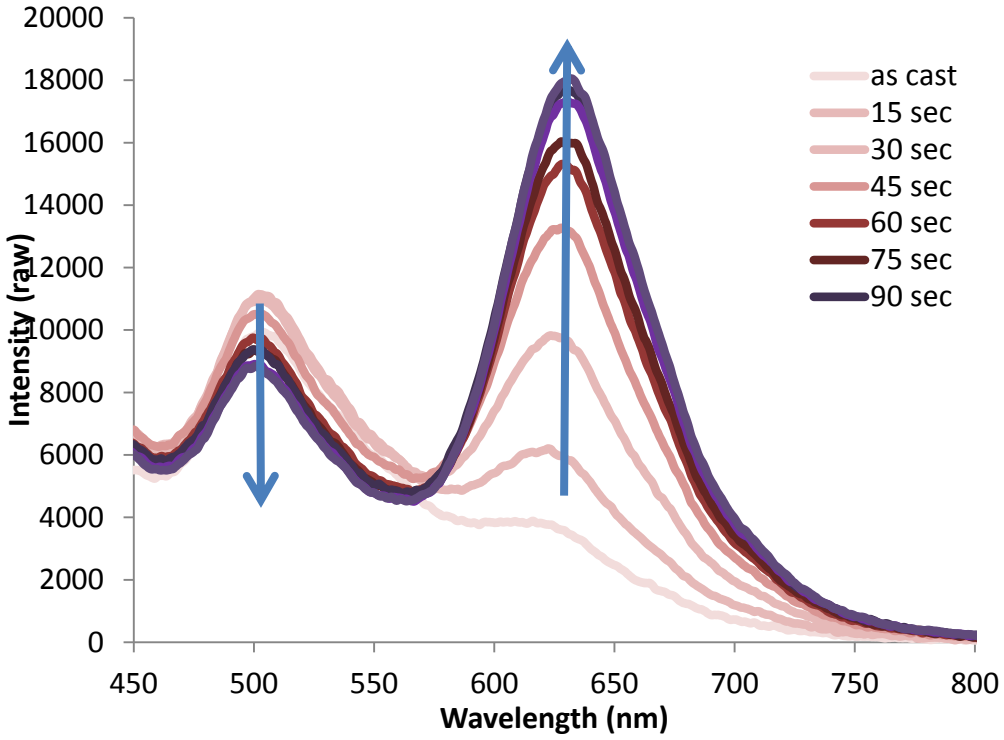

Figure 87: Emission spectra of DGEBA-DETA-AJNDE17 after successive heat exposures in 45C water bath. Arrows indicate spectral intensity changes with increasing heat exposure.

Figure 88 shows a plot of I'(t) for the four temperatures used, collected from the water bath-quench method. It is clear that increasing temperature exposures cause an increase in both the

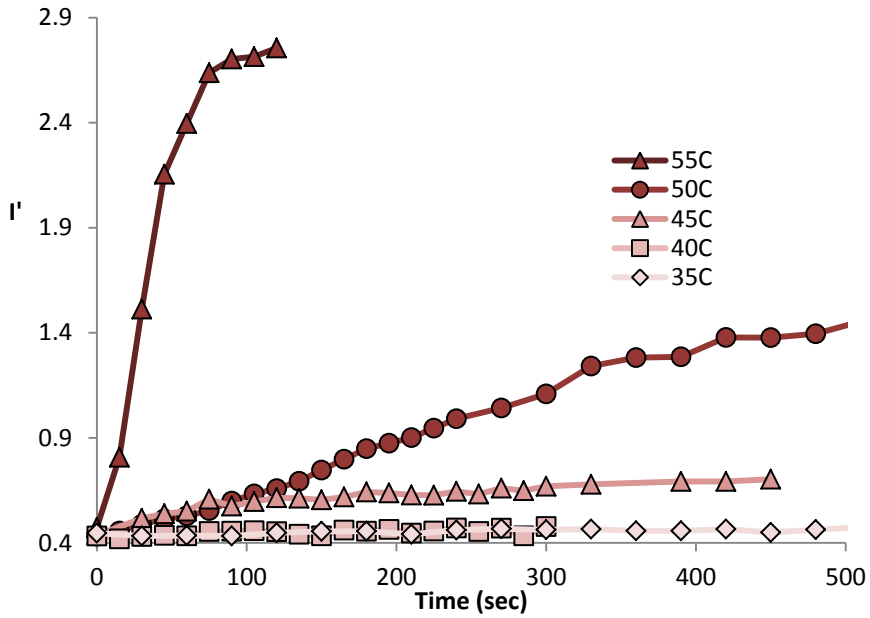

Figure 88: I' vs time for DGEBA-DETA-AJNDE17 samples experiencing different heat exposure temperatures.

magnitude of the maximum value of I'(t), $I'_{max,}$ and the rate of change $\frac{dI'}{dt}$. These observations are consistent with Arrhenius type reactions. Samples below 40°C (~T_g - 20°C) show little activation.

4.2.2 Heat exposure after strain – water bath method

Figure 89 shows the change in I' with time for samples initially strained to various ε_{def} and subsequently heated at 50°C via water bath method. Note the initial change in I' with no elapsed time due to strain.

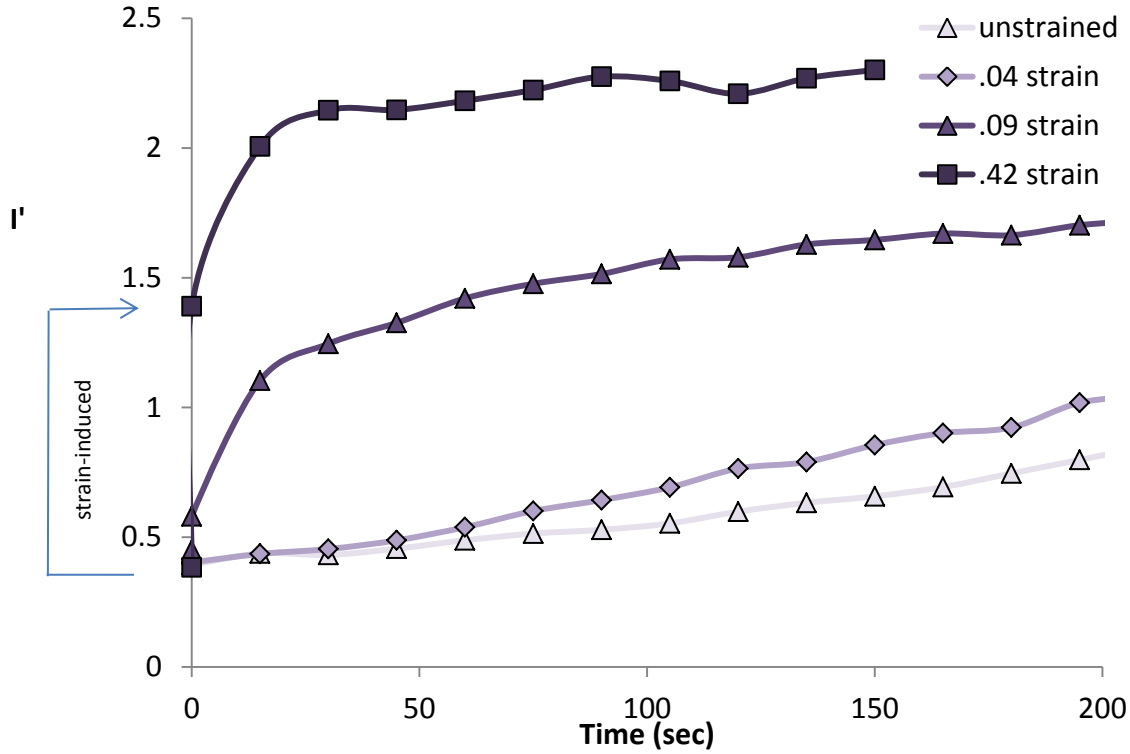

Figure 89: I' vs time for 50°C heat exposures of DGEBA-DETA-AJNDE17 after varying ε_{def}, listed in legend. Note strain induced change at t=0.

The rate of change in I' appears generally to increase as ε_{def} increases. There also appears to be a change in the shape of the curve, from a linear increase with time for low ε_{def} to a curve that appears exponential at high ε_{def}. It is possible that $\frac{dI\prime}{dt}$ is exponential for all ε_{def}, but with such low exponential terms that the behavior appears linear.

4.2.3 Water bath method – kinetic analysis

The representative data shown in Figure 89 for 50ºC exposure in the water bath method, when compared with the theoretical data for 0^{th} order and 1^{st} order reaction, does not allow a strong conclusion to be reached about the OFF→ON reaction order. The reaction appears to be linear at low ε_{def}, suggesting 0^{th} order, but exponential at high ε_{def}, suggesting 1^{st} order. For this reason, data was analyzed considering the reaction as both 0^{th} order and 1^{st} order.

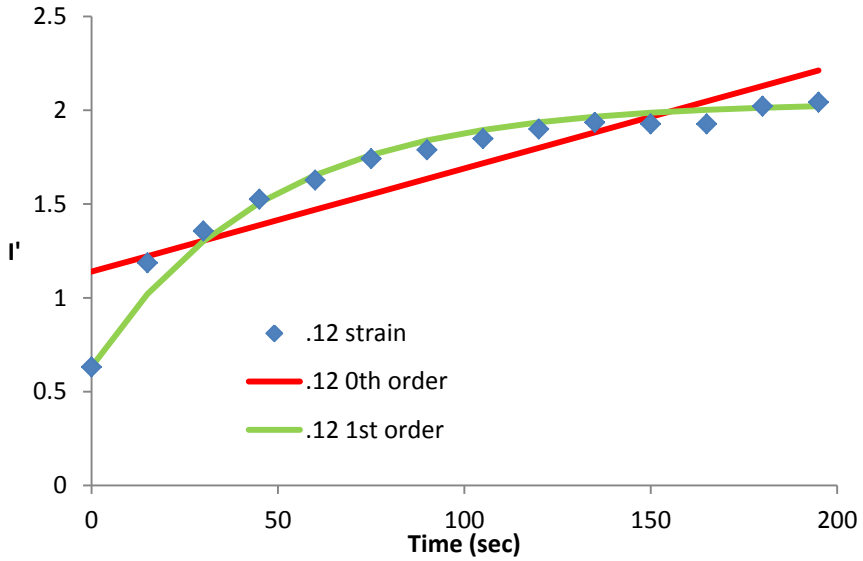

Figure 90: comparison of models for sample of ε_{def}=.12 heated at 50°C with water bath method.

A representative data set showing the models' respective fitting curves for a sample of DGEBA-DETA-AJNDE17 having ε_{def}=.12 is shown in Figure 90. As expected, the 0^{th} order fitting is not appropriate for samples of high ε_{def}, but the analysis was carried out for comparison.

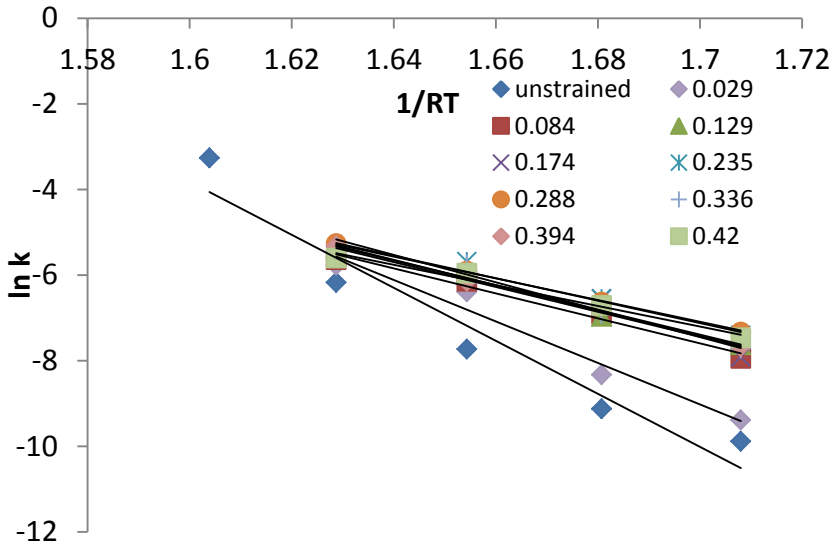

Figure 91: Arrhenius plot for 0th order fit of OFF-->ON reaction data collected using water bath method.

The Arrhenius activation energy calculations were carried out using the reaction rate constants calculated for 0^{th} order and 1^{st} order fits of I'(t) curves, using the procedure described in Chapter 3 section 2.2.3. The Arrhenius plot of the 0^{th} order fit is displayed in Figure 91. The lines of best fit drawn through the four data points represent the activation energy of the OFF→ON reaction at the ε_{def} of the samples, listed in the legend.

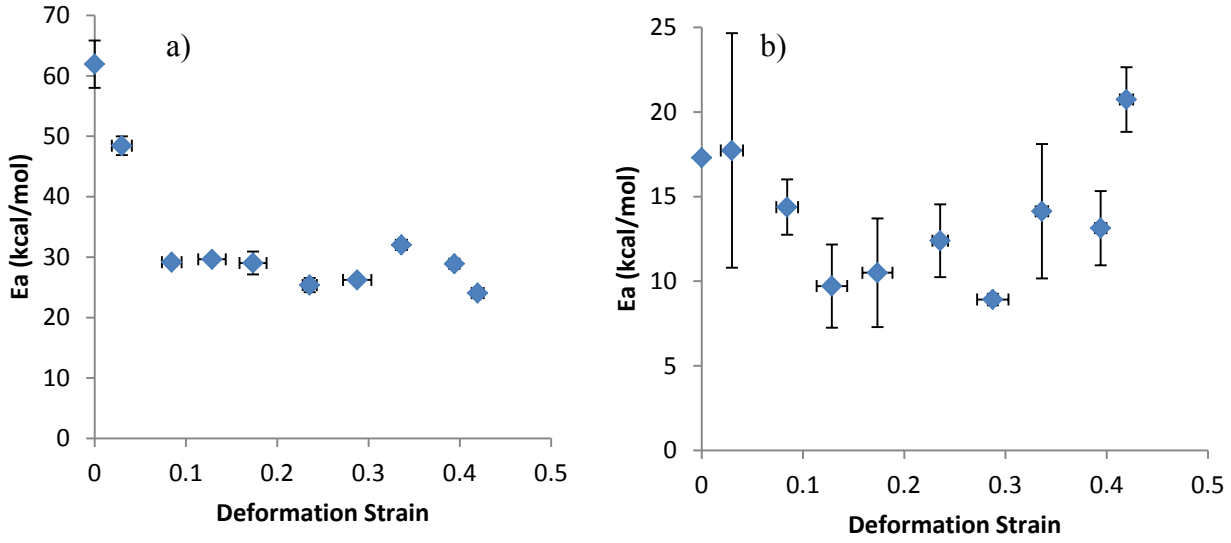

Figure 92: Activation energies for OFF-->ON reaction calculated using a) 0th order and b) 1st order kinetics models.

Plots of E_a measured for varying levels of ε_{def} are displayed in Figure 92a for 0^{th} order and Figure 92b for 1^{st} order. The error bars in the x-direction represent the standard deviation of the ε_{def} of the four samples used to calculate E_a. the error bars in the y-direction are a measure of the coefficient of linearity of the best fit line through the four values in the Arrhenius plot (see Figure 91). The activation energy results show a significant decrease in magnitude as ε_{def} increases from 0 to ~.15, after which E_a remains nearly constant until after ε_{def}~.30. The reaction order models differ in their evaluation of activation energy change at high ε_{def} – the 0^{th} order model has E_a remaining essentially constant at the decreased values, while the 1^{st} order model has E_a rising to pre-deformation values and above after ε_{def} ~.30.

The results differ in magnitude as well (E_a = 61.9 kcal/mol for 0th order, unstrained vs 17.3 kcal/mol for 1st order, unstrained). The 1st order result is more closely matched to literature values for thermally activated fluorescence reactions in literature (97).

4.2.4 Kinetics of heat exposure – in-situ method

Figure 93 shows representative data gathered from the in-situ method at 50°C for samples of various ε_{def}. This plot has been corrected to allow for comparison between unstrained and strained samples by offsetting the curves to begin at (t=0, I'=0). It is clear from this data that samples with higher strains show an elevated reaction rate compared to unstrained samples, and that 1st order kinetics is a more appropriate model for evaluating the reaction kinetics.

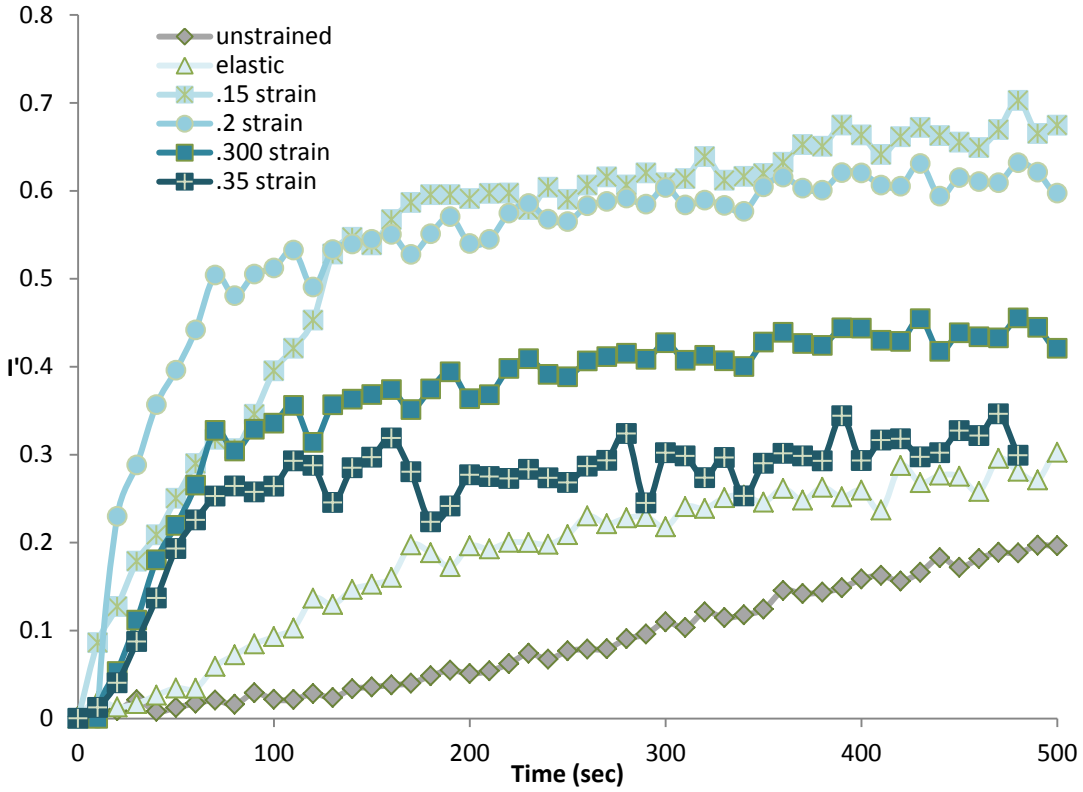

Figure 93: I' vs time data for samples heated at 50C after varying ε_{def}, collected by in situ heating method.

Figure 94 shows the results of E_a calculations for the OFF→ON reaction based on 1st order kinetics fitting of the I'(t) curves collected from DGEBA-DETA-AJNDE17 samples using the in-situ method.

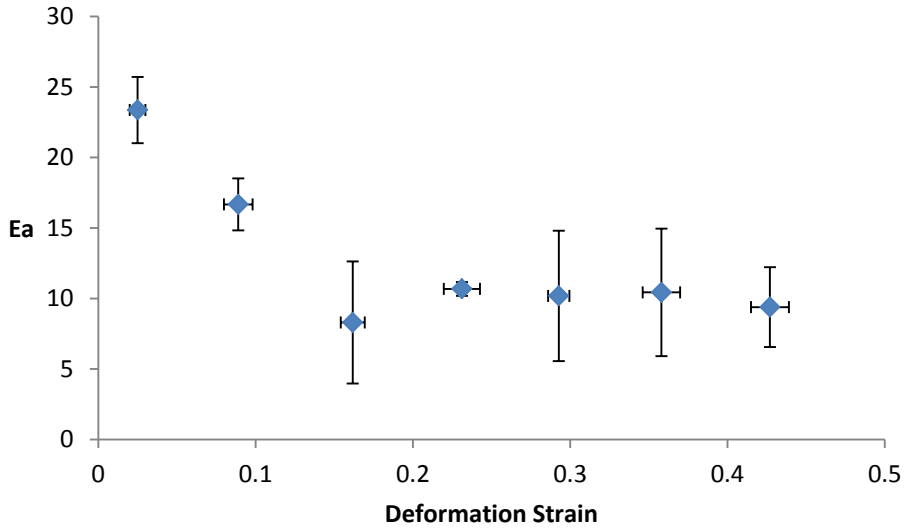

Figure 94: Activation energy of OFF-->ON reaction for varying deformation trains - 1st order fit of in-situ heating method

The results agree generally with data collected from the water bath method – E_a decreases with increasing ε_{def} until approx. ε_{def}=.15, after which it remains nearly constant for increasing ε_{def}. The magnitude of E_a calculated with this method also agree well with the 1st order kinetics measurements done via water bath, and with literature values for thermally activated reactions measured by fluorescence (97).

5. DISCUSSION OF EXPERIMENTAL RESULTS

In this section, the results gathered from kinetic studies of the OFF→ON reaction of DGEBA-DETA-AJNDE17 during cure and during exposure to heat will be discussed.

5.1 Kinetics during cure

The results in Figure 86 strongly support the conclustion that the OFF→ON reaction of AJNDE17 during cure of DGEBA-DETA obeys 1st order kinetics. This kinetic model predicts the slowing of the reaction as time increases. However, it cannot fully explain the variation in magnitude of A_{564} at the end of cure with χ (see Figure 78). One possible explanation may lie in the changing rate of cure $\frac{d\alpha}{dt}$. As χ increases, $\frac{d\alpha}{dt}$ increases, so the sample reaches the gelation point more quickly. The OFF→ON reaction would not progress as far if the 1st order reaction was limited to activity below the gel point.

5.2 Kinetics in solid DGEBA-DETA

A comparison of the change in E_a with the quantities ΔU_{def}, ε_{an} and ε_{pl} can help identify the most important aspects of the epoxy molecular environment that influence the OFF→ON reaction of AJNDE17. The data from the in-situ heat/strain testing method will be compared in detail with these quantities, and the other kinetic methods' results will be compared with these results.

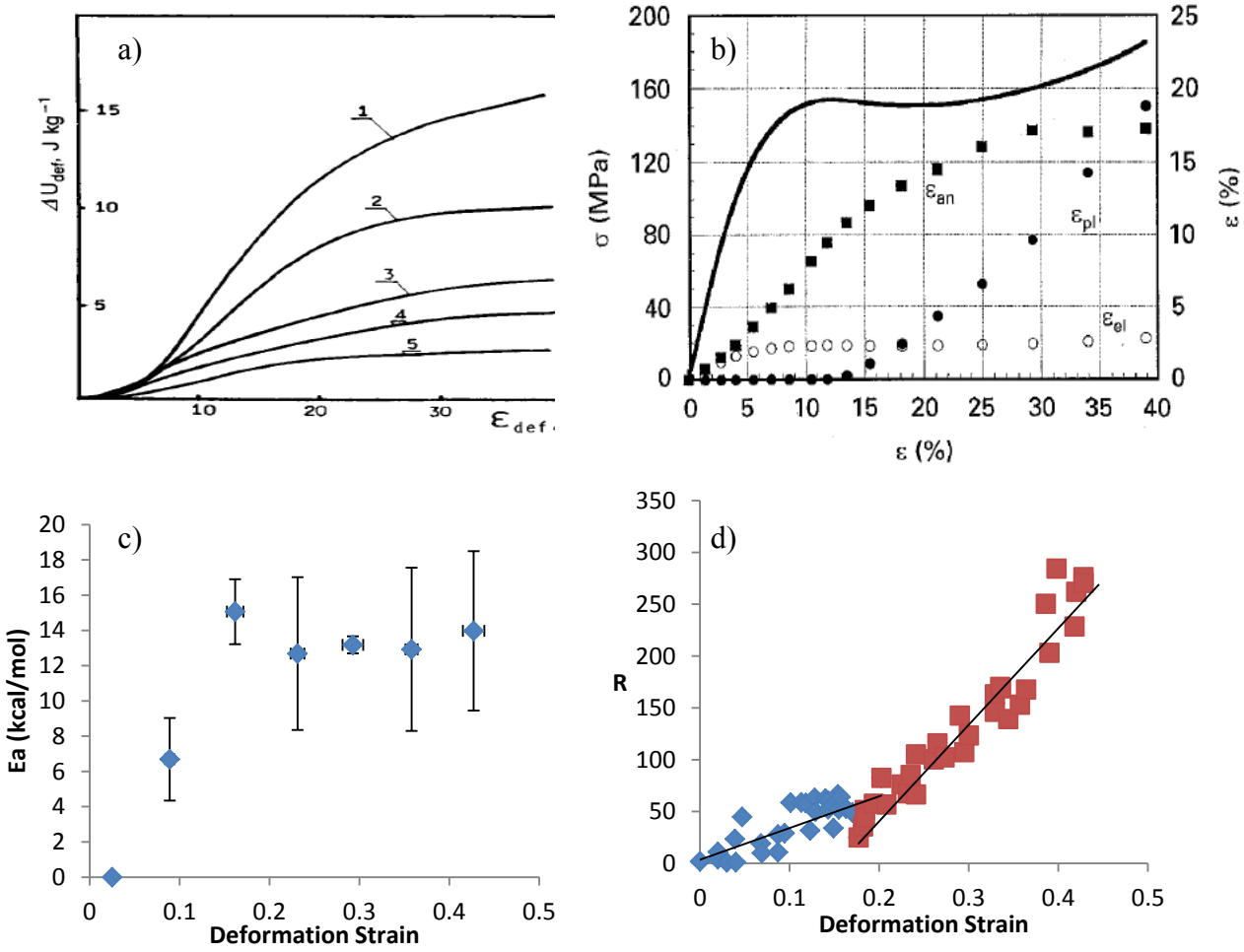

Figure 95: comparison of stored internal energy of epoxy with reduction in activation energy for OFF-->ON reaction of DGEBA-DETA-AJNDE17. A) curve 1 b) in situ heating method. Figures from (36) and (38).

Figure 95a shows the quantity ΔU_{def} for amine-cured epoxy for increasing ε_{def} (curve 1, ref. (36)) side-by-side with Figure 95b, the values of ε_{an} and ε_{pl} for increasing ε_{def} (38). Figure 95c shows the change in E_a measured by the in-situ heating method with 1st order fit, while Figure 95d shows the change in R with increasing ε_{def}.

The ΔU_{def} curve for epoxy shows little or no increase until ~ε_{def} ~.10, after which a strong rise is observed followed by a slower rise or plateau-type region above ε_{def} ~.25. The measured change in E_a for the OFF→ON reaction of AJNDE17 in DGEBA-DETA approximately mirrors this trend. Based strictly on the on the magnitudes of energy involved that the ΔU_{def} cannot be

directly responsible for the reduction in E_a of the reaction – the highest measured ΔU_{def} is only .00121 kcal/mol of DGEBA, far below the ~12 kcal/mol change recorded in this study. However, it is the molecular changes associated with the increase in ΔU_{def} that are interesting.

Comparing Figure 95b with Figure 95c shows a similar correlation between the change in E_a and the change in ε_{an}, with increasing values at lower ε_{def} and a plateau region above ε_{def}~.25. There is ambiguity in the measured E_a data about where the onset of E_a reduction begins, but the plateau region is clear.

The increase-plateau behavior in ΔU_{def} and ε_{an} with respect to ε_{def} has been associated with the nucleation and growth of shear defects and intermolecular shear motion. The activation energy decrease for heat-induced activation of the OFF→ON reaction of AJNDE17 in DGEBA-DETA also shows increase-plateau behavior with respect to ε_{def}, which is suggests an important correlation between shear defects and intermolecular shear motion and the OFF→ON reaction.

Figure 95d shows the activation of the OFF→ON reaction induced only by mechanical deformation, plotted against ε_{def}. When compared with Figure 95a and b, this behavior correlates more closely with the behavior of ε_{pl} than with ε_{an} and ΔU_{def} – it grows slowly before ε_{def} ~ .15, then more rapidly for higher values of ε_{def}.

5.3 Comparison with Zhurkov model

The Zhurkov model's modified Arrhenius equation (Eqn. 13) predicts a reduction in E_a for the breaking of a bond as the stress on the bond σ is increased. The OFF→ON reaction of AJNDE17 involves the breaking of the C-N bond that attaches AJNDE17 to the DGEBA-DETA network, so the model has some physical relevance. The relevant results gathered in Chapter 2 and Chapter 3 will be discussed here in relation to the Zhurkov model.

5.3.1 Kinetics during cure and stoichometric dependence

The observed OFF→ON reaction kinetics of AJNDE17 during cure, and the dependence of the reaction progress on χ, suggest that the molecule AJNDE17 is being turned ON during the period before gelation. The source of the stress on the C-N bond during this period is difficult to quantify, but may come from competing reactions for the amine from epoxide groups, or from intermolecular shear mixing motions that are possible while DGEBA-DETA is still a liquid. In any case, if the reaction is allowed to proceed during the time before gelation, the OFF→ON reaction's varying progress with respect to χ can be explained by the increased rate of cure lowering the time allowed for the reaction.

5.3.2 Mechanical deformation and hydrostatic stress

The C-N bond cannot be part of the DGEBA-DETA network, since it has only one reactive site, and so AJNDE17 must be a side-chain addition to the network. A main-chain bond would begin to be stressed only during strain hardening after chains begin to align and stretch (see Chapter 1 section 1.4.5). But a side chain bond would more logically be stressed during intermolecular shear motion.

The activation of the OFF→ON reaction due to ε_{def}, measured by the variable R and plotted in Figure 76, shows a two-step increase – a slow region below ε_{def}~.15, and a more rapid region above ε_{def} ~.15. The correlation between the change in R with ε_{def} and the plateau in ε_{an} should be noted. Below this plateau, the nucleation and growth of shear defects and the intermolecular shear motion associated with their appearance is low but increasing, just as the slope of R is increasing. At this plateau intermolecular shear motion reaches its maximum, so the stress on the C-N bond should reach its maximum as well. The value of R continues to increase beyond

this plateau, constantly and at its fastest rate. The time spent under load in uniaxial compression increases during this time, allowing the OFF→ON reaction to continue to progress while intermolecular motion is allowed, leading to increased R values.

Hydrostatic pressure causes no ε_{def}, therefore no intermolecular shear motion is produced and no stress on the proposed C-N side chain bond is produced. The OFF→ON reaction does not occur at room temperature, therefore, because the energy barrier is prohibitive.

5.3.3 Activation energy

A side chain bond would more logically be stressed during intermolecular shear motions such as those associated with ε_{an} and ΔU_{def}. These properties show a plateau around ε_{def}~.15, just as the decrease in E_a plateaus. This result is consistent with the Zhurkov model.

5.4 Summary

If the assumption is made that the side-chain bond attaching AJNDE17 to DGEBA-DETA is stressed predominantly during intermolecular shear motion, the data observed during cure, during heat exposures, and after ε_{def} strongly supports the Zhurkov model. This work does not evaluate the fitness of that assumption, but it is logical based on the molecular structure and design of AJNDE17 in DGEBA-DETA.

CONCLUSIONS

- Fluorescent probe molecules AJNDE15 and AJNDE17 were characterized in DGEBA-DETA, and found to be mechanochromic.
- Techniques similar to those used in ratiometric fluorescent sensors were applied to evaluate the mechanochromic response, using the ratio of DGEBA-DETA fluorescent emission to probe molecule emission. The response of the probes was found to be monotonic and one-to-one with the deformation strain ε_{def}.
- The mechanism by which the probe molecules display mechanochromism was evaluated by comparison with mechanochromic mechanisms reported in the literature. A mechanochemical reaction which interrupts the conjugation of the probe molecules was consistent with observed probe responses during cure, and responses after cure to uniaxial compression, hydrostatic pressure, elevated temperature exposure, and variation in stoichiometry.
- The kinetic behavior of AJNDE17's OFF→ reaction was investigated. The probe was determined to turn ON via 1st order kinetics under conditions where intermolecular shear motion occurs, such as during cure; during uniaxial compressive deformation beyond the yield point; and at temperatures within 20°C of T_g.
- The activation energy of AJNDE17's activation reaction was compared with the amount of deformation strain using 3 methods of combined heat-strain testing. The activation energy decreases then plateaus in a manner consistent with the nucleation, growth, and motion of shear defects and intermolecular shear motion.

- If the side-chain bond attaching AJNDE17 to the DGEBA-DETA network is assumed to be stressed by intermolecular shear motion but not by hydrostatic pressure or main-chain alignment, the Zhurkov model is consistent with the observations made in this study.

ACKNOWLEDGEMENTS

This project was funded by the Boeing Company's University Research Program, under project #BL8DL (Witness Surface Coatings Project).

The author would like to thank PhD Advisor and project Principal Investigator Dr. Brian Flinn; project co-Principal Investigator Dr. Alex Jen, project co-workers Dr. Sei-Hum Jang, Dr. Zhengwei Shi, Tucker Howie; project contributors Aaron Capps, Natalie Larson, Nathan Lowman, A.J. Singh, Jeffrey Yang; Flinn Group co-workers especially Gary Weber, Ashley Tracey, Curtis Hickmott, Dana Rosenbladt; Jen Group co-workers Dr. Cody Youngbull; PhD Committee members Dr. Christine Luscombe, Dr. Santosh Devasia, Dr. Gary Georgeson.

The author would like to thank personally his family and friends for their continued support and patience.

WORKS CITED

1. **Liber, T., Daniel, I.M., Schraum, S.W.** *ASTM STP 696 - Ultrasonic Techniques for Inspecting Flat and Cylindrical Composite Parts.* Conshocken, PA : ASTM International, 1979.

2. **Cantwell, W.J., Curtis, P.T., Morton, J.** 1986, Comp. Sci. & Tech., Vol. 25, pp. 133-48.

3. **Kumar, P., Rai, B.** 1993, Comp. Struct., Vol. 23, pp. 313-18.

4. **Morton, J., Godwin, E.W.** 1989, Comp. Struct., Vol. 13, pp. 1-19.

5. **Messner, D.** Presentation at ASM Non Destructive Testing Tutorial. Seattle, WA : s.n., 2004.

6. **Henneke, E.** *Non Destructive Testing of Fiber Reinforced Plastics Composites.* [ed.] J. Summerscales. New York : Elsevier Applied Science, 1990. Vol. II.

7. **Stone, D.E.W, Clarke, B.** 1975, Non-Destr. Test., Vol. 8, pp. 137-145.

8. **Dean, G.D., Lockett, F.J.** *ASTM STP 521: High Modulus Fibers and Composites.* Conshocken : ASTM International, 1973. pp. 326-46.

9. **Prakash, R.** October 1980, Composites, pp. 217-224.

10. **Scott, I.G., Scala, C.M.** April 1982, NDT Int'l, pp. 75-85.

11. **Durr, Heinz and Bouas-Laurent, Henri, [ed.].** *Photochromism: Molecules and Systems.* New York : Elsevier, 1990. pp. 15-25.

12. **Victoria, University of.** epi-fluorescence techniques. [Online] http://web.uvic.ca/ail/techniques/epi-fluorescence.html.

13. **Valeur, B and Berberan-Santos, M.** *Molecular Fluorescence - Principles and Applications.* New York : Wiley-VCH, 2002.

14. **Van Keuren, E., Littlejohn, D. and Schrof, W.** 2004, J. Phys. D: Appl. Phys., Vol. 37, pp. 2938-43.

15. **Drickamer, H G and et al.** 2001, Ind. Eng. Chem. Res., Vol. 40, pp. 3038-41.

16. **Woo, H Y and et al.** 2005, J. Am. Chem. Soc. , Vol. 127, pp. 14721-14729.

17. **Itakagi, H, Horie, K and Mita, I.** 1990, Prog. Polym. Sci., Vol. 15, pp. 361-424.

18. **Hu, J and Liu, S.** 2010, Macromolecules, Vol. 43, pp. 8315-30.

19. **Grynkiewicz, G, Peonie, M and Tsien, R Y.** 6, 1985, Journal of Biological Chemistry, Vol. 260, p. 3440.

20. **Life Technologies.** Indo-1 Calcium Indicator. *www.invitrogen.com.* [Online] [Cited: 3 6, 2013.] http://www.invitrogen.com/site/us/en/home/Products-and-Services/Applications/Drug-Discovery/Target-and-Lead-Identification-and-Validation/g-protein_coupled_html/cell-based-second-messenger-assays/indo-1-calcium-indicator.html.

21. **Charier, Sandrine, et al., et al.** 2004, Angewandte Chemie International Edition, Vol. 43, pp. 4785-4788.

22. **Zhu, Houjuan, et al., et al.** 2012, Nanotechnology, Vol. 23, p. 315502.

23. **Kostov, Yordan, et al., et al.** 6, 2000, Applied Spectroscopy, Vol. 54, p. 864.

24. **Bamfield, Peter and Hutchings, Michael G.** *Chromic Phenomena: The technological applications of colour chemistry.* Cambridge, UK : Royal Society of Chemistry, 2010. pp. 104-5.

25. **Beckham, H W and Rubner, Michael F.** 5, 1989, Macromolecules, Vol. 22, p. 2130.

26. **Yoshino, Katsumi, Sawada, Keiji and Onoda, Mitsuyoshi.** 1989, Japanese Journal of Applied Physics, Vol. 28, p. L1029.

27. **Crist, B.** Yield Processes in Glassy Polymers - Ch. 4. [ed.] R N Haward and R J Young. *The Physics of Glassy Polymers.* 2nd. New York : Chapman & Hall, 1997.

28. **Yamini, S and Young, R J.** 1980, Journal of Materials Science, Vol. 15, pp. 1814-22.

29. **Oleinik, E F.** 1986, Advances in Polymer Science, Vol. 80, pp. 49-99.

30. **Haward, R N and Young, R J.** Introduction - Chapter 1. *The Physics of Glassy Polymers.* 2nd. New York : Chapman & Hall, 1997, pp. 1-30.

31. **Rackley, F A, et al., et al.** 1974, Journal of Polymer Science, Polymer Physics Edition, Vol. 12, p. 1355.

32. **Berger, Larry L and Kramer, Edward J.** 1988, Journal of Materials Science, Vol. 23, pp. 3536-3543.

33. **Donald, A M.** Crazing, Ch. 6. [ed.] R N Haward and R J Young. *The Physics of Glassy Polymers.* 2nd. New York : Chapman & Hall, 1997, p. 296.

34. **Oleinik, E F, Rudnev, S N and Salamatina, O B.** 12, 2007, Polymer Science A, Vol. 49, pp. 1302-1327.

35. **Kargin, V A and Slonimskii, G L.** *Short Essays on Physical Chemistry of Polymers.* Moscow : Khimiya, 1967.

36. **Oleynik, E.** 1989, Progress in Colloid & Polymer Science, Vol. 80, pp. 140-150.

37. **Callister, William D.** *Materials Science and Engineering - An Introduction.* 6th. New York : John Wiley & Sons, 2003.

38. **Quinson, R, et al., et al.** 1996, Journal of Materials Science , Vol. 31, pp. 4387-4394.

39. **Boyce, M C and Haward, R N.** The post-yield deformation of glassy polymers - Ch. 5. [ed.] R N Haward and R J Young . *The Physics of Glassy Polymers.* New York : Chapman & Hall, 1997, p. 213.

40. **Treloar, L R.** *The Physics of Rubber Plasticity.* 3rd. Oxford : Clarendon Press, 1975.

41. **Arruda, E M and Boyce, M C.** J. Mech. Phys. Solids, Vol. 41, p. 389.

42. **Arruda, E M and Boyce, M C.** International Journal of Plasticity, Vol. 9, p. 697.

43. **Lohse, F, et al., et al.** 1969, British Polymer Journal, Vol. 1, pp. 110-14.

44. **Prime, R B.** Characterization of Thermoset Resins. [ed.] Edith A Turi. *Thermal Characterization of Polymeric Materials.* San Diego : Academic Press, 1997.

45. **Ye, Q, et al., et al.** 2, 2007, Journal of Biomedical Research, Vol. 80, pp. 440-6.

46. **Vatanprast, R and Lemmetyinen, H.** 2000, Polymer, Vol. 41, pp. 5571-6.

47. **George, G A, Cash, G A and Rintroul, L.** 1996, Polymer International, Vol. 41, pp. 169-182.

48. **International, ASTM.** *ASTM E1640.* West Conshocken, PA : ASTM International , 1997.

49. **Birks, J B.** 1975, Rep. Prog. Phys. , Vol. 38, pp. 903-974.

50. **Zlatkevich, Lev, [ed.].** *Luminescence Techniques in Solid State Polymer Research.* New York : Marcel Dekker, 1989.

51. **Barltrop, J A and Coyle, J D.** *Principles of Photochemistry.* London : John Wiley and Sons, 1978.

52. **Yang, J, et al., et al.** 2000, J. Appl. Polym Sci., Vol. 82, pp. 2347-2351.

53. **Crenshaw, B R and Weder, C.** 2003, Chem Mater, Vol. 15, pp. 4717-4724.

54. **Lowe, C and Weder, C.** 22, 2002, Adv. Mater., Vol. 14, p. 1625.

55. **Strehmel, B, Strehmel, V and Younes, M.** 13, 1999, J. Polym. Sci. B, Vol. 37, pp. 1367-86.

56. **Treloar, L R. G.** *The Physics of Rubber Elasticity.* New York : Oxford University Press, 1975.

57. **Godovsky, Yuli K.** *Thermophysical Properties of Polymers.* New York : Springer-Verlag, 1992.

58. **Nielsen, L E and Landel, R F.** *Mechanical Properties of Polymers and Composites.* 2nd. New York : Marcel Dekker, Inc, 1994.

59. *Polymer.* **Wang, Francis W, Lowry, Robert E and Fanconi, Bruno M.** 1986, Vol. 27, pp. 1529-32.

60. —. **Goyanes, S, et al., et al.** 2005, Vol. 46, pp. 9081-7.

61. —. **Goyanes, S, et al., et al.** 2003, Vol. 44, pp. 3193-9.

62. **Deng, Q and Jean, W C.** 1993, Macromolecules, Vol. 26, pp. 30-34.

63. *Chemical Reviews.* **Beyer, Martin K and Clausen-Schaumann, Hauke.** 8, 2005, Vol. 105, pp. 2921-44.

64. **Benachour, Djafer and Rogers, C E.** Strain-Enhanced Photodegradataion of Polyethylene. [ed.] S Peter Pappas and F H Winslow. *Photodegradation and Photostabilizaton of Coatings: ACS Symposium Series 151.* s.l. : American Chemical Society, 1981, pp. 263-274.

65. *Journal of Macromolecular Science C: Polymer Reviews.* **Tyler, David R.** 4, 2004, Vol. 44, pp. 351-388.

66. **Davis, D A.** 2009, Nature, Vol. 459, pp. 68-72.

67. *Journal of Polymer Science B: Polymer Physics.* **Zhurkov, S N and Korsukov, V E.** 2, 1974, Vol. 12, pp. 385-98.

68. *Physics of the Solid State.* **Butyagin, P Yu and Streletskii, A N.** 5, 2005, Vol. 47, pp. 830-836.

69. *Treatment of Dispersed Materials and Media.* **Borunova, A B, Zhernovenkova, Yu V and Streletskii, A N.** Odessa : s.n., 1999, Vol. 9, p. 158.

70. *Journal of Materials Chemistry.* **Song, Young-Soo, et al., et al.** 2012, Vol. 22, pp. 1380-1386.

71. *Sensors and Actuators B: Chemical.* **Cho, Sung-Youl, Kim, Joong-Gon and Chung, Chan-Moon.** Vol. 134, pp. 822-25.

72. **Smith, M B and March, J.** *March's Advanced Organic Chemistry, Reactions, Mechanisms, and Structures.* 5th. New York : John Wiley and Sons, 2001.

73. *Journal of the American Chemical Society.* **Cremer, J and Gauss, J.** 1986, Vol. 108, pp. 7467-7477.

74. **Brown, Theodore L, LeMay, H Eugene and Bursten, Bruce E.** *Chemistry: The Central Science.* 8th. Upper Saddle River, New Jersey : Prentice-Hall, 2000.

75. *Polymer.* **Lin, King-Fu and Wang, Francis W.** 4, 1994, Vol. 35, pp. 687-91.

76. *Accounts of Chemical Research.* **Lewis, Frederick D.** 4, 1979, Vol. 12, pp. 152-8.

77. *Journal of Chemical Physics.* **Masuhara, H, Hino, T and Mataga, N.** 1975, Vol. 79, p. 994.

78. *Polymer Engineering Science.* **Nass, K A and Seferis, J C.** 5, 1989, Vol. 29, p. 315.

79. *Bulletins of the Korean Chemical Society.* **Kim, Hongkyeong and Char, Kookheon.** 11, 1999, Vol. 20, p. 1329.

80. *Chemical Materials.* **Kinami, Maki, Crenshaw, Brent R and Weder, Christoph.** Vol. 18, pp. 946-955.

81. *Macromolecular Rapid Communications.* **Kunzelmann, Jill, et al., et al.** Vol. 227, pp. 1981-7.

82. **Law, K Y and Loutfy, R O.** 1981, Macromolecules, Vol. 14, p. 587.

83. *Journal de Physique IV.* **Wang, S J, Wang, C L and Wang, B.** Colloque C4, 1993, Vol. 3, pp. 275-9.

84. *Journal of Polymer Science B: Polymer Physics.* **Hasan, O A, et al., et al.** 1993, Vol. 31, pp. 198-197.

85. —. **Xie, L, et al., et al.** 1995, Vol. 33, pp. 77-84.

86. *Polymer.* **Gupta, V B and Brahatheeswaran, C.** 10, 1991, Vol. 32, pp. 1875-84.

87. **Venditti, R A, et al., et al.** 1995, J. Appl. Polym. Sci., Vol. 56, pp. 1207-20.

88. **Deng, Q, Zandiehnadem, F and Jean, W C.** 1992, Macromolecules, Vol. 25, pp. 1090-1095.

89. *Journal of Physical Chemistry A.* **Wojtyk, J T C, et al., et al.** 39, 2000, Vol. 104, pp. 9046-55.

90. —. **Chibisov, A K and Gorner, H.** 24, 1997, Vol. 101, pp. 4305-4312.

91. *Pure and Applied Chemistry.* **Wetzler, Diana E, et al., et al.** 3, 2001, Vol. 73, pp. 405-9.

92. **Physics of the Solid State Editorial Board.** 5, 2005, Physics of the Solid State, Vol. 47, pp. 771-6.

93. **Beyer, Martin K and Clausen-Schaumann, Hauke.** 8, 2005, Chemical Reviews, Vol. 105, p. 2921.

94. **Tyler, David R.** 4, 2004, Journal of Macromolecular Science Part C - Polymer Reviews, Vol. 44, p. 351.

95. **Zhurkov, S N and Korsukov, V E.** 2, 1974, Journal of Polymer Science - Polymer Physics Edition, Vol. 12, p. 385.

96. **Treinin, A and Hayon, E.** 20, 1970, Journal of the American Chemical Society, Vol. 92, p. 5821.

97. **Carpick, R W, et al., et al.** 2000, Langmuir, Vol. 16, pp. 4639-4647.

98. **Schultz, J M.** *Polymer Materials Science.* s.l. : Prentice-Hall, Inc, 1974. pp. 500-1.

99. **Treloar, L R.** *The Physics of Rubber Plasticity.* 3rd. Oxford : Clarendon Press, 1975.

100. **Poon, C. et. al.** 1990, Theor. & Appl. Fract. Mech., Vol. 13, pp. 81-97.

101. **Wu, W-C. et.al.** 2010, Adv. Funct. Mater., Vol. 20, pp. 1413-23.

102. **Luo, J.** 2001, Chem. Commun., pp. 1740-1.

103. **Bokobza, L.** 1981, Polymer, Vol. 22, pp. 1309-1311.

104. **Younes, M, Wartewig, S and Lelliger, D.** 1994, Polymer, Vol. 35, pp. 5269-78.

105. **Rettig, W, Fritz, W and Springer, J.** *Photochemical Processes in Organized Molecular Systems.* [ed.] K Honda. Amsterdam : Elsevier Science, 1991. p. 61.

106. **Strehmel, B, et al., et al.** 1992, Eur. Polym. J., Vol. 25, p. 325.

107. **Royal, J S, Victor, J G and Torkelson, J M.** 1992, Macromolecules, Vol. 25, pp. 729-34.

108. **Royal, J S and Torkelson, J M.** 1992, Macromolecules, Vol. 25, pp. 4792-4796.

109. **Loutfy, R O and Arnold, B A.** 1982, J. Phys. Chem., Vol. 86, pp. 4205-4211.

110. **Technologies, Agilent.** *Basics of Measuring the Dielectric Properties of Materials.* s.l. : Agilent Technologies, 2006.

111. *Journal of Physical Chemistry.* **Abdel-Halim, Shakir T, Abdel-Kader, Mahmoud H and Steiner, Ulrich E.** 1988, Vol. 15, pp. 4324-8.